Spring 2017

A Predictor Analysis Framework for Surface Radiation Budget Reprocessing Using Design of Experiments

Patricia Allison Quigley
Old Dominion University

A PREDICTOR ANALYSIS FRAMEWORK FOR SURFACE RADIATION BUDGET REPROCESSING USING DESIGN OF EXPERIMENTS

by

Patricia Allison Quigley
B.S. April 2007, Strayer University
M.S. August 2012, Old Dominion University

A Dissertation Submitted to the Faculty of
Old Dominion University in Partial Fulfillment of the
Requirements for the Degree of

DOCTOR OF PHILOSOPHY

ENGINEERING MANAGEMENT

OLD DOMINION UNIVERSITY
May 2017

Committee Members:

Dr. Resit Unal (Director)

Dr. Steven T. Cotter (Member)

Dr. C.B. Daniels (Member)

Dr. Paul W. Stackhouse, Jr. (Member)

Dr. Stephen J. Cox (Member)

ABSTRACT

A PREDICTOR ANALYSIS FRAMEWORK FOR SURFACE RADIATION BUDGET REPROCESSING USING DESIGN OF EXPERIMENTS

Patricia Quigley
Old Dominion University, 2017
Director: Dr. Resit Unal

Earth's Radiation Budget (ERB) is an accounting of all incoming energy from the sun and outgoing energy reflected and radiated to space by earth's surface and atmosphere. The National Aeronautics and Space Administration (NASA)/Global Energy and Water Cycle Experiment (GEWEX) Surface Radiation Budget (SRB) project produces and archives long-term datasets representative of this energy exchange system on a global scale. The data are comprised of the longwave and shortwave radiative components of the system and is algorithmically derived from satellite and atmospheric assimilation products, and acquired atmospheric data. It is stored as 3-hourly, daily, monthly/3-hourly, and monthly averages of 1°x1° grid cells.

Input parameters used by the algorithms are a key source of variability in the resulting output data sets. Sensitivity studies have been conducted to estimate the effects this variability has on the output data sets using linear techniques. This entails varying one input parameter at a time while keeping all others constant or by increasing all input parameters by equal random percentages, in effect changing input values for every cell for every three hour period and for every day in each month. This equates to almost 11 million independent changes without ever taking into consideration the interactions or dependencies among the input parameters. A more comprehensive method is proposed here for the evaluating the shortwave algorithm to identify both the input parameters and parameter interactions that most significantly affect the output

data. This research utilized designed experiments that systematically and simultaneously varied all of the input parameters of the shortwave algorithm. A D-Optimal design of experiments (DOE) was chosen to accommodate the 14 types of atmospheric properties computed by the algorithm and to reduce the number of trials required by a full factorial study from millions to 128.

A modified version of the algorithm was made available for testing such that global calculations of the algorithm were tuned to accept information for a single temporal and spatial point and for one month of averaged data. The points were from each of four atmospherically distinct regions to include the Amazon Rainforest, Sahara Desert, Indian Ocean and Mt. Everest. The same design was used for all of the regions. Least squares multiple regression analysis of the results of the modified algorithm identified those parameters and parameter interactions that most significantly affected the output products.

It was found that Cosine solar zenith angle was the strongest influence on the output data in all four regions. The interaction of Cosine Solar Zenith Angle and Cloud Fraction had the strongest influence on the output data in the Amazon, Sahara Desert and Mt. Everest Regions, while the interaction of Cloud Fraction and Cloudy Shortwave Radiance most significantly affected output data in the Indian Ocean region.

Second order response models were built using the resulting regression coefficients. A Monte Carlo simulation of each model extended the probability distribution beyond the initial design trials to quantify variability in the modeled output data.

This dissertation is dedicated to my parents

Alfred and Barbara Visciarelli

with love and appreciation for encouraging me to achieve my dreams,

and to my beautiful children

Renee, Jennifer and Sara

ACKNOWLEDGEMENTS

There are many people who have contributed to the success of this dissertation. I would first like to acknowledge Committee Chair, Dr. Resit Unal, Old Dominion University, for expertly advising me through the research and experimental processes of this work with both kindness and patience. I am so grateful for his support and for first introducing me to Design of Experiments. His experience and enthusiasm in this area made this work both challenging and fun. His dedicated guidance and that of my committee made this dissertation possible. I would like to thank each of them individually.

Dr. Steven Cotter from Old Dominion University inspired me to appreciate statistical analysis when I took his course in engineering design. I have so much admiration for his vast knowledge in this field, and I thank him for all of the time he dedicated to ensure that my analysis was sound.

I would also like to thank Dr. Charles Daniels for reviewing several drafts of this paper and for advising me on the cohesiveness of the chapters. I also appreciate his assistance with structuring my presentation so that I would adequately convey the background, purpose and results of this work to my audience.

I extend my thanks and sincerest gratitude to Dr. Paul Stackhouse, Jr. of the National Aeronautics and Space Administration (NASA) for affording me the opportunity to use experimental design to for analysis of the Surface Radiation Budget Shortwave algorithm. I am honored to be a part of such a huge contribution to the study of earth's climate. I also thank him for reviewing the written drafts, attending many of my milestone presentations and for all of the scientific information and reference materials he provided.

This work would have not have been possible without the help of Dr. Stephen Cox of Science Systems and Applications, Inc. (SSAI). Dr. Cox spent countless hours explaining and clarifying details about earth's radiant energy system. I thank him so much for reviewing all of the drafts and providing valuable insight and recommendations. I also thank him for confirming the results of the analysis that allowed me to move forward in my research. I am so very grateful for his time, patience and expertise.

Thank you again to Dr. Unal and all of my committee members for their guidance and support of my research and analysis. I will never be able to say it enough.

I would also like to express my sincere gratitude to the Virginia Air National Guard for funding most of my Ph.D. courses. My employer, Science Systems Applications, Inc., SSAI, funded the research portion making the completion of this graduate work possible. I hold Om Bahethi, past President of SSAI, and current President, Anoop Mehta, in the highest regard for their leadership of the company. I offer my sincere gratitude for the generosity and kindness they always bestow on their employees.

Thank you to my children, Renee, Jennifer and Sara for their support and patience during my study times. I hope that through my efforts on this degree that they understand how important education is to a successful life and that by continually challenging my potential, I have set an example for them to follow.

Last, but most importantly, thank you, God, for the plans you have for me and showing me how to fulfill them.

The views expressed in this dissertation are those of the author and do not reflect the official policy or position of NASA or the U.S. Government.

NOMENCLATURE

BSRN	Baseline Surface Radiation Network
CERES	Clouds and the Earth's Radiant Energy System
ECMWF	European Center for Medium range Weather Forecasting
GCM	General Circulation Model
GEOS	Goddard Earth Observing System data
GEWEX	Global Energy and Water Cycle Experiment
GISS	Goddard Institute for Space Studies
GMAO	Global Modeling and Assimilation Office
ISCCP	International Satellite Cloud Climatology Project
LPLA	Langley Parameterized Longwave Algorithm
LPSA	Langley Parameterized Shortwave Algorithm
NASA	National Aeronautics and Space Administration
NCDC	National Climatic Data Center
NCEP	National Centers for Environmental Prediction
NCAR	National Center for Atmospheric Research
PAR	Photosynthetically Active Radiation
RSM	Response Surface Methodology
SMOBA	Stratospheric Monitoring Ozone Blended Analyses
SRB	Surface Radiation Budget
TOA	Top of Atmosphere
TOMS	Total Ozone Mapping Spectrometer

TOVS	TIROS Operational Vertical Sounder
WMO	World Meteorological Organization

METEOROLOGICAL AND STATISTICAL DEFINITIONS

Albedo	Fractional reflectance calculated at the surface or top of the atmosphere.
Anisotropy	Property of being directionally dependent.
Climatology	Weather conditions over a period of time.
Degrees of Freedom	The number of ways a system can be varied without violating constraints in the design space.
D-Optimal Design	Determinant Optimal Experimental Design.
Emissivity	A measure of thermal energy emitted by the surface of the earth as a fraction of the theoretical black-body maximum.
Nadir	Directly beneath.
Solar Zenith Angle	The angle of the sun away from vertical.
Radiative Transfer Model	Calculates transmittance, absorbance and scattering of electromagnetic radiation.

ALGORITHM PARAMETER DEFINITIONS (PREDICTOR VARIABLES)

Predictor Variables	Definition
aerosol optical depth	Measure of column aerosol concentration in dimensionless unit related to the attenuation of radiation stream through the column.
aerosol single scattering albedo	Measure of proportion of radiation attenuated by aerosol which is scattered rather than absorbed.
aerosol asymmetry parameter	Measure of directionality of radiation scattered by aerosol.
azimuth angle	Measurement of the angle formed between an observer, a reference point, and a position in the sky.
cosine solar zenith angle	Cosine of the measured angle from zenith (i.e., overhead) to the center of the sun; varies from the sun on the horizon (= 0) to sun overhead (= 1.0).
cosine satellite zenith angle	Cosine of the measured angle from zenith (i.e., overhead) to the center of the satellite that varies from satellite on the horizon (= 0) to satellite overhead (=1.0).
cloud fraction	Fraction of the grid cell covered by clouds (varies from 0 to 1).
cloud phase	Unitless reference to cloud properties where liquid is 1 and ice is 2.
cloudy radiance	Mean narrowband scaled radiance from cloudy pixels measured in reflectance units.
clear sky radiance	Narrowband scaled radiance from clear pixels measured in radiance units.
clear sky composite radiance	A statistical measure of recent clear sky radiance at a location meant to approximate a background value.
latitude	Angular distance north or south of the equator.
longitude	Angular distance east or west of the equator.
ozone	Gas consisting of three oxygen atoms; measurement of the amount integrated from the upper atmosphere to the earth's surface.
satellite id	Unit to identify a named man-made satellite.
snow/ice flag	Unitless reference to presence of snow/ice. Present = 1, not present =0.
total column precipitable water	Measurement in mm of the depth of water in a column of air.

ALGORITHM OUTPUT PARAMETER DEFINITIONS (DEPENDENT VARIABLES)

Dependent Variables	Definition
TOA shortwave downward flux (toadwn)	Total (shortwave) energy received by the earth from the sun at the top of the atmosphere.
TOA shortwave upward flux (toaup)	Shortwave (0.2 – 4 μm) energy leaving the top of the atmosphere based on the amount of energy reflected by the surface/atmosphere system.
Surface downward flux (srfdwnflx)	Shortwave energy reaching the surface.
Surface downward diffuse flux (srfdwndiff)	Shortwave energy reaching the surface outside of the direct beam.
Surface upward flux (srfupflx)	Shortwave energy reflected by the surface of the earth.
Surface downward diffuse PAR (srfdwndifpar)	Shortwave energy reaching the surface between 400nm and 700nm outside of the direct beam.
Surface downward PAR (srfdwnpar)	Shortwave energy reaching the surface between 400nm and 700nm (photosynthesis) wavelengths.
TOA shortwave upward clear sky flux (toaupclrsky)	Shortwave energy leaving the top of the atmosphere based on the amount of energy reflected by the surface/atmosphere system for clear sky (no clouds) part of the grid cell.
Surface downward clear sky flux (srfdwnclrsky)	Shortwave energy reaching the surface for only the clear sky parts of the grid cell.
Surface upward clear sky flux (srfupclrflx)	Shortwave energy reflected by the surface of the earth for the clear sky part of the grid cell.
Output aerosol optical depth (oaod)	Calculated column aerosol concentration.
Output cloud optical depth (ocod)	Calculated optical depth of cloud field.
Surface downward pristine sky flux (srfdwnprs)	Theoretical measure of what the surface downward flux would be in a pristine sky with no clouds or aerosols.
TOA upward pristine sky flux (toaupprs)	Theoretical measure of what the TOA upward flux would be in a pristine sky.

TABLE OF CONTENTS

Page

LIST OF TABLES

LIST OF FIGURES

Figure Page

Figure Page

Figure Page

CHAPTER 1. INTRODUCTION

1.1 Research Objective

The NASA/Global Energy and Water Cycle Experiment (GEWEX) Surface Radiation Budget (SRB) global surface and top-of-atmosphere (TOA) shortwave radiative flux data products are estimates of incoming radiation from the sun, as well as estimates of radiation that is absorbed and reflected back to space by the Earth and the atmosphere. The project produces and archives long-term global longwave and shortwave datasets representative of these energy exchanges. The goal of this project is to produce reliable, globally derived atmospheric products that overcome the spatial limitations posed by ground site measurements over enough years to establish a trend.

This work supports the SRB vision to provide a complete long-term global picture of solar irradiance. Ground sites are capable of obtaining direct measurements of all of the components of the SRB, but since it is not practical to cover the entire globe, including ocean, with a dense network of sites, it is desirable to use satellites to acquire this information. The challenge is that surface irradiance cannot be directly measured from the top of the atmosphere by satellites, so it must be derived or modeled from a variety of satellite and atmospheric assimilation products and acquired atmospheric data. This is done using flux retrieval algorithms and methods such as radiative transfer theory (Stackhouse et al., 2011).

Research indicates that input product uncertainty is an important source of variability of the output data; therefore the objective of this study was to identify those input parameters and parameter interactions that most significantly affect the output data of the SRB algorithm and to quantify this variability.

1.2 Surface Radiation Budget Project

The SRB data are derived from a variety of satellite and atmospheric assimilation products and acquired atmospheric data. Three major releases of the data have been published. The next release will offer a substantial refinement of the previous version with increased spatial resolution and improved input products. Spatial resolution will increase from 1 ° x 1 ° nested grid with 44016 cells to 0 .5 ° x 0.5 ° global grid comprising 165,018 equal area cells.. Each of the cells has unique solar and atmospheric characteristics that affect the solar energy exchange. A partial list of such characteristics include angle of the sun, viewing angle of the satellite, gaseous constituents such as ozone and water vapor, atmospheric particulates such as clouds and aerosols, and surface reflectance using reprocessed nnHIRS, HX and GMAO GEOS data. These characteristics serve as input parameters to the SRB algorithm. Version 4.0 of the shortwave surface radiation component of the SRB offers 14 data sets over an unprecedented continuous 30-year temporal range.

1.3 SRB Data Significance

Knowledge of atmospheric properties and their fluxes is beneficial to many areas of research, space and planetary exploration and can have sustained benefits to industries from airlines to farming. With respect to SRB products, the data set supports the validation of data assimilation and climate models (Stackhouse et. al., 2002). Additionally, the NASA/GEWEX SRB project determines surface, top-of-atmosphere (TOA), and atmospheric shortwave (SW) and longwave (LW) radiative fluxes and is used in many meteorology applications to predict climate trends (NASA GEWEX, 2014). It is used in many meteorology applications.

The Surface Solar Energy project provides parameters from the data to aid with sizing and pointing or tilting of solar panels and for thermal applications. It also is used for determining size of batteries and other energy storage systems.

1.4 Surface Radiation Budget Product Applications

Many initiatives based on solar radiation information have benefited third world countries by providing cooking and water sanitation solutions. The data have also benefited the farming and transportation industries, lighting and home appliances, heating, cooling, renewable energy initiatives, academia, transportation, space exploration and climate prediction. The Prediction of Worldwide Energy Resources (POWER)/ Surface Solar Energy (SSE) project team processes SRB parameters for renewable energy, sustainable buildings and agroclimatology projects. The refinement of the SRB algorithm will provide even more reliable surface radiation data, strengthening and improving work in the fields that rely on it.

1.5 Surface Radiation Budget History

Regional studies of atmospheric data by ground observation stations, ships and telemetry instruments installed in weather balloons called radiosondes are longstanding, but being geographically constrained, do not represent the complete global picture. Aircraft have also proven to be good platforms for data retrieval, but are spatially limited to flight paths and are bounded by flying time and the cost of aircrews and fuel. Current technology offers satellites as the only method of contiguous atmospheric data retrieval on the global scale.

The first attempts at satellite retrieval of atmospheric data began with the inflatable Echo 1 Satellite, conceived by William J. O'Sullivan and launched on August 12, 1960 for the purpose of studying air density in the upper atmosphere to support design specifications of aircraft,

missiles and space vehicles (NASA, 2014a). The mission was not successful, but it paved the way for the era of satellites and the possibility of capturing atmospheric data from every grid point on the globe (Ellis, et al., 1978). The finding by Fritz (1963) that reflected solar flux at the top of the atmosphere observed by satellites correlated well with ground site observations inspired work that led to the current SRB studies. These led to other studies assessing the relationships between the reflected visible radiance from satellite and the surface solar flux (or short wavelength radiation from the sun called shortwave) measured at the surface of the Earth (i.e. Mosher and Raschke, 1984). Development at NASA LaRC led to Darnell et al., (1992) providing one of the first shortwave (SW) and thermal infrared (LW) climatology from satellite.

The Darnel et al., (1992) research was also unique because it not only incorporated imager data but also but also top-of-atmosphere radiative flux information from the Earth Radiation Budget Experiment (ERBE). ERBE was built and flown on the Earth Radiation Budget Satellite (ERBS) NASA dedicated satellite launched in 1984 by the Space Shuttle, Challenger, and on two National Oceanic and Atmospheric Administration (NOAA) satellites (NOAA-9 and NOAA-10). "The ERBE instruments on board the NOAA-9 and NOAA-10 satellites provide global spatial coverage, while the scanner instruments on board the ERBS provides coverage between 67.5 degrees north and south latitude and the nonscanner instruments on board the ERBS provide coverage between 60 degrees north and south latitude. Because ERBS is in a precessing (57-degree) orbit, the ERBE instruments on board this satellite provide diurnal sampling" (EOSWEB, 2016a). The campaign was successful in providing top-of-atmosphere global albedo, fluxes, and solar incidence measurements, but the combined limited spatial and temporal coverage of these satellites were restrictive.

Shortwave satellite algorithms to estimate radiation at the surface of the earth were first tested in 1986 using field experiment data by the World Climate Research Program (WCRP) at NASA Langley Research Center (Whitlock, et al, 1994, 1995). The first estimation of surface shortwave radiation modeled from satellite data was completed in 1994 and yielded a globally complete data product associated with atmospheric components of the SRB. The data set used as input satellite visible data as collected, calibrated and processed by the International Satellite Cloud Climatology Project (ISCCP, Rossow and Gardner, 1993a, 1993b). At the completion of the project, a collection of 52 shortwave parameters representing a 280 x 280 km equal area grid of global coverage were computed and compared with ground truth data. The *First Global WCRP Shortwave Surface Radiation Budget Dataset***,** SRB Version 1.1, presented with minimal coverage deficiency as compared with ground site capabilities and rendered finer spatial resolution over smaller time periods (Whitlock, et al., 1994).

To diversify the approach to SRB estimation, the Pinker/Lazlo primary shortwave algorithm (Pinker & Lazlo, 1992) and another algorithm developed by W. F. Staylor at NASA Langley Research Center (Darnell, et al., 1992) were used to generate and compare data for the SRB version 1.1 (Whitlock et al., 1995) and the Pinker models have been improved and extended. This particular Surface Radiation Budget effort is now affiliated with the Global Energy and Water Cycle Exchange Program (GEWEX) of the World Climate Research Programme (WCRP). The current SW algorithm is based upon the Pinker and Lazlo model framework, but now uses the Fu-Liou radiative transfer model to compute monochromatic radiative fluxes that are integrated to the total SW spectrum (Cox et al., 2016; Fu & Liou, 1997). The model also uses scaled radiance, cloud amount, precipitable water, and ozone as input parameters with satellite calibration from the ISCCP data.

Table 1 (ASDC, 2014b) summarizes the evolution of the publically released versions of the SRB shortwave dataset since the origin of the NASA/WCRP-GEWEX/SRB project and provides a short description of product improvement for each version. A complete list of available SRB output products and versions is available at (GEWEX, 2015b).

As evidence of the importance of deriving the radiation fluxes at the TOA and surface of the atmosphere, co-incident with the advancements of surface radiation from imagers are the advancements in top-of-atmosphere radiative fluxes from the Clouds and the Earth's Radiant Energy System (CERES) extended the ERBE project with instruments launched in 1997 on the Tropical Rainfall Measuring Mission (TRMM) satellite and again on satellites EOS-TERRA and EOS-AQUA in 1999 and 2000 respectively. The newest CERES instrument orbits on board the Suomi National Polar-orbiting Satellite (Suomi NPP) that was launched in 2011. The data provided by these instruments help in understanding clouds and energy cycles from the top of the atmosphere to the surface of the earth with data compiled to show solar-reflected and earth-emitted radiation (CERES, 2016). Besides providing the most accurate TOA radiative flux information to date (Loeb et al., 2009; Wielicki et al., 1995), the CERES mission also includes a comprehensive effort to estimate the long-term variation in the surface radiation components with a suite of the data products (Kato et al., 2012; Rutan et al., 2015). These produces at the 1x1 degree resolution provide excellent validation relative to surface measurements and an important benchmark for assessment of GEWEX SRB data products. This speaks to the importance to accurately determining the TOA and surface radiative flux components.

SRB SHORTWAVE DATASET VERSION HISTORY	
VERSION	DESCRIPTION
LaRC 1.0	8 year dataset (July 1983-June 1991) on 2.5 degree equal area grid using ISCCP C1 and ERBE data for both the SW and LW (Darnell et al., 1992).
WCRP SW SRB 1.1	4 year WCRP SW only data set (March 1985 – Dec. 1988) on 280x280 km equal area grid using ISCCP C1 data and both the SW algorithm of Darnell et al., 1992 and the WCRP selected Pinker et al., 1989 (Whitlock et al., 1995).
GEWEX SRB 2.0	12 year SW and LW SRB dataset (July 1983-October 1995), on $1^{o}x1^{o}$ equal angle based nested grid using ISCCP DX pixel data. (Stackhouse et al., 2000)
GEWEX SRB 2.81	As cited from the eosweb.larc.nasa.gov webpage, (EOSWEB, 2016b), "Atmospheric transmissivity/reflectivity lookup tables extended to cosine solar zenith angles as low as 0.01. Revamping of the methodology used to fill data gaps. These changes allowed data to be computed for locations with low sun angles the entire month (polar twilight areas)." And "Improvement of the TOA insolation calculation. Previously each January 1 the Earth began in the same orbital point. Leap years were handled by making day 366 a duplicate of day 1. The new scheme was a Julian day based approach from the Astronomical Almanac." and "The effective solar constant was increased to 1367 W/m2 from 1359 W/m2, for consistency with other products. The Pinker/Laszlo algorithm computes radiation in the range from 0.2-4.0 microns. That does not cover the full range of solar output, which extends past 4 microns. The extra energy was placed in the 0.7-4.0 micron band.
GEWEX SRB 3.0	As cited from the eosweb.larc.nasa.gov webpage, (EOSWEB, 2016c), "Replacement of simple climatological aerosol optical depth based on surface type with full monthly climatology based on MATCH aerosols. Improved treatment of clear vs. cloudy skies over bright surfaces" (personal correspondence Dr. Stephen Cox). Improved gap filling. Temporal coverage of Release 3.0 is extended to December 2007.
GEWEX 4.0	Increase of spectral band numbers from 5 to 18. ISCCP HXS cloud and radiance inputs at higher resolution than DX. Full treatment of aerosol optical properties in lookup tables, with inputs coming from Max-Planck Aerosol Climatology. New water vapor from nnHIRS.

Table 1 Publicly Released Version History of Global Shortwave SRB Dataset.

1.6 Surface Radiation Budget Reprocessing

Reprocessing of the shortwave data for Version 4.0 uses the latest version of the ISCCP HXS full calibrated data set. The 10km satellite pixels for the ISCCP DX and HXS data, but only the ISCCP DX are subsampled to 30 km. Clear, cloudy radiances and cloud fraction are processed for each grid box prior to code execution from geosynchronous satellites with VIS/IR imagers and polar orbiting satellite with AVHRR from 1983 to near real time (Stackhouse, 2016). Version 4.0 will provide for a higher resolution of 0.5 ° x 0.5 ° over previous 1 ° x 1 ° in order to provide better local coverage to resolve more local features. This also improves accuracy as the uncertainty of atmospheric information is greatly dependent on box size as shown by (Jethva, et al., 2013). The data span a time record of 30 years as compared with 22 years in the 3.0 version series (Stackhouse, 2014). Upon completion, this data set will meet the climatological standard normal as defined by the World Meteorological Association (WMO) publication in recognition of long term climate flux (WMO, 2007). A valid time period refers to the most recent 30 year time record of available data. The input data for SRB Version 4.0 use a temporal resolution of three hours as for previous versions. All of the ancillary products, their sources and subsystems are shown in Table 2 modified from SRB Release 4.0 Baseline Processing System Inputs (NASA/GEWEX, 2012).

Referencing Table 2 below, the nnHIRS data product is acquired by measurements of the global distributions of temperature and relative humidity varied temporally (NOAA, 2016a). "The Goddard Earth Observing System Model, Version 5 (GEOS-5) is a system of models integrated using the Earth System Modeling Framework (ESMF). The GEOS-5 DAS integrates the GEOS-5 AGCM with the Gridpoint Statistical Interpolation (GSI) atmospheric analysis developed jointly with NOAA/NCEP/EMC. The GEOS-5 systems are being developed in the

GMAO to support NASA's earth science research in data analysis, observing system modeling and design, climate and weather prediction, and basic research" (GMAO, 2016). As previously mentioned, the ISCCP HXS is similar to ISCCP DX data using all of the pixels within each grid cell for each satellite with no sub-sampling to produce clear and cloudy radiances and cloud fraction before running the algorithm. Blended ozone is produced using data from the total ozone mapping spectrometer (TOMS), TIROS Operational Vertical Sounder (TOVS), anensemble of three instruments including a High Resolution Infrared Radiation Sounder (HIRS), a Microwave Sounding Unit (MSU) and a Statospheric Sounding Unit (SSU), (NOAA, 2016b), a 3-D daily global ozone analysis, and a Stratosphere Monitoring Ozone Blended Analysis (SMOBA) using SBUV/2 and HIRS/TOVS in the polar- night regions (NOAA, 2016c). All of the instruments are flown on earth orbiting satellites identified in their respective references. The vegetation map obtained from the International Geosphere Biosphere Programme provides satellite images of the earth for use in identifying regional climate characteristics. The CO_2 Global Marine product contains CO_2 trends as measured from air sampling sites distributed globally (NOAAd, 2016). Tropical aerosols are represented by the Max-Planck-Institute Aerosol Climatology version 1 (MAC-v1). Albedo is a measurement of the fraction of radiation that is reflected by the surface of the earth. Surface albedo for the shortwave products was estimated at five different spectral wavelengths. Column ozone is a measurement of the total ozone at each cell location. Column ozone is calculated as derived in the Langley Parameterized Shortwave Algorithm (LPSA) (Gupta, et al., 2001).

Input Data	Source	Parameters
ISCCP HXS	GISS/NCEI http://www.ncei.noaa.gov	Satellite radiances, cloud properties, surface reflectance
ISCCP nnHIRS	NOAA/CREST	Column Water vapor
MAC-v1	Max Planck Institute Aerosol Climatology	Aerosol optical properties
ISCCP Blended Ozone product	GISS http://isccp.giss.nasa.gov	Column Ozone
Surface Type Map	IGBP http://igbp.net	Code identifying land/water/ice/vegetation
Surface Elevation Map	GTOPO30 http://lta.cr.usgs.gov/GTOPO30	Mean altitude for each grid box
Spectral Surface Albedoes	Computed for each surface type	18 band albedo by surface types

Table 2 SRB GSW Rel 4 Planned ancillary inputs, sources and parameters.

2. LITERATURE REVIEW

2.1 SRB Data Collection and Integrity

There are currently two ways to obtain a value for solar irradiance over a given location. It can be measured from the ground or derived from satellite data. Ground site positioning is problematic as placement is limited and not evenly distributed. Figure 1 serves to illustrate the sparse sampling of available sites and the impracticality of use for global assessment.

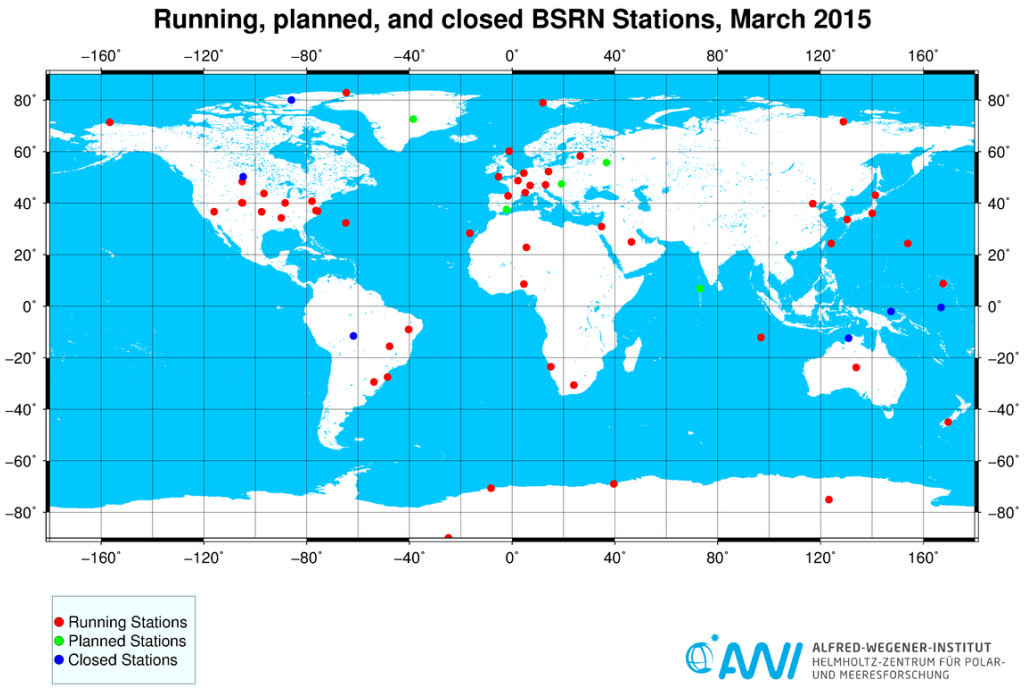

Figure 1 BSRN Site Network (BSRN, 2015)

Satellite coverage overcomes the challenges of ground site positioning, providing an opportunity for obtaining a global estimate. It should be noted that data from one ground site are assumed to be representative of the entire cell where satellite data covers every latitude and longitude point within a cell. While some variation is expected, comparison studies from 1950 to present indicate that satellite derived estimates on the global scale detect the same trends as ground station data with solar irradiance increasing and decreasing over the same time record, and provide extensive validation of the data. Table 3 and Figure 2 summarize these previous studies as culled from (Hinkelman et al., 2009) and highlight the trends.

Researchers	Finding	Year	Data Source
Russak, 1990	Decrease in downwelling solar irradiance.	1955-1986	Ground Stations Satellite
Liepert et al., 1994	Decrease in downwelling solar irradiance.	1961 -1990	Ground Stations
Dutton et al., 2006	Decrease in downwelling solar irradiance.	1977 -2004	Ground Stations
Stanhill & Moreshet 1992	Decrease in insolation.	1958,1965, 1975, 1985	Ground Stations
Gilgen et al. 1998	Decrease over large portions of the Earth. Increase restricted to a few small regions.	1950 -1990	Ground Stations (GEBA)
Stanhill and Cohen, 2001	A worldwide spatially variable reduction in [surface insolation].	1950 -1990	Ground Stations
Wild et al.,2005	Increase at many locations beginning around 1990.	1950 -1994	Ground Stations (GEBA) and (BSRN)
Ohmura, 2006	Increase at many locations beginning around 1990.	1950 -1994	Ground Stations (GEBA) and (BSRN)
Pinker et al. , 2005	Increase in global mean insolation from 1983 to 2001.	1983 -2001	Satellite surface flux records and Ground Stations.
Hinkelman et al., 2009	Decrease Global SRB SW flux.	1983 -1991	Satellite
Hinkelman et al., 2009	Increase Global SRB SW flux.	1991 -1999	Satellite
Hinkelman et al., 2009	Decrease Global SRB SW flux.	1999 -2004	Satellite
Gilgen et al., 1998; Stanhill & Cohen, 2001; Liepert,2002	Decrease in surface SW irradiance from the 1950s until about 1990.	1950 -1990	Ground Stations
Wild et al., 2005; Ohmura, 2006.	Increase at the majority of these locations.	1980 -2005	Ground Stations
Dutton et al.,2006 Hatzianastassiou et al. 2005	Decrease in solar downwelling fluxes.	1977 -2004	NOAA observations
Loeb, 2008	Increase in global mean insolation.	2000 +	CERES data

Table 3 Tabular Comparison of SW Flux Estimation Studies

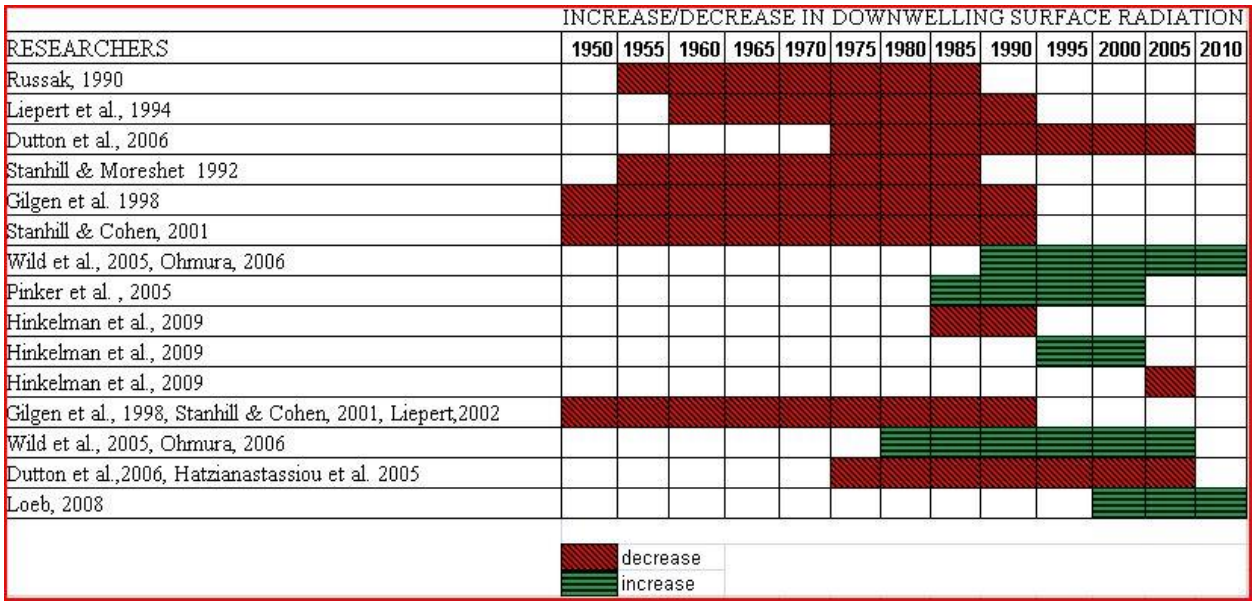

Figure 2 Graphical Representation of SW Flux Estimation Studies

2.2 Algorithm Viability

The SRB shortwave algorithm has undergone many changes and improvements since Version 1.0. Methods for improving solar energy output data sets include checking instrument calibration and geostationary satellite viewing angles (Hinkelman, et al., 2009) along with traceability of the inputs, and adherence to a more analytical framework for computations in a later work (Gupta et al., 2001). In a previous shortwave radiance study (Pinker et al., 1992) the physics of a solar irradiance model produced earlier (Pinker et al., 1985) was improved and adapted for use with global data. Several sensitivity studies on algorithm input parameters were conducted (Rossow, et al., 1995) and (Zhang, et al., 1995) and the results applied to calculations in subsequent studies. For example, the ocean albedo algorithm was reformulated and aerosol forcing was applied to a constrainment algorithm in order to reduce uncertainty in key parameters (Rose, et al., 1997). Aerosol scattering changes solar energy distribution and is

accounted for in solar radiation algorithms. The computation for aerosol attenuation was therefore addressed in (Gupta, et al., 1999) and improved over (Darnell et al., 1992) using standard aerosols in climatological data with radiative parameters tailored to regional conditions, and albedos from ERBE measurements. When newly measured data became available from the Global Energy Balance Archive (GEBA) and the Baseline Surface Radiation Network (BSRN), it was used for analysis for quantifying errors in shortwave radiation estimates. Four radiation schemes were studied to show cause for errors over temperature and humidity profile inputs used to calculate radiance in layers of the atmosphere of varying scattering and absorption incidences, commonly known as a radiative transfer models (Wild, et al., 2001). As a result, improved cloud products and ancillary data sets were used in advanced radiative transfer models in order to reduce errors in input data. This did not completely eliminate uncertainties in the output data sets and the problematic input parameters (Zhang, et al., 2004). Input data and specific cloud parameters were also identified as error sources when long-term climatological data from ISCCP, NCEP/NCAR and ECMWF were used in a radiative transfer model (Hatzianastassiou, et al., 2005). Discrepancies were found in input parameters when surface flux calculations were computed using various global data sources (Zhang et al., 2006). Data sources were also varied to test uncertainties in the input parameters (Stephens, et al., 2011). Input parameters persisted as sources of errors (Stephens, et al., 2012). In an uncertainty estimate study by (Kato, et al., 2012) it was found that cloud and aerosol properties derived by satellite products cause uncertainty in temperature and precipitable water measurements that propagate to both surface downward longwave and shortwave irradiance uncertainties. While studies identified different input parameters, there was enough evidence to suggest that all of the inputs should be evaluated. "Larger errors were found where there are larger uncertainties in the input data such as over

snow/ice covered surfaces and where the site data did not represent the entire grid box. Larger errors in downward SW flux were also found over African and South American locations where aerosols from biomass burning are not accounted for in the SW model" (Konzelman et al., 1995). While independent research persisted in evaluating clouds and aerosols as the key source of uncertainty (Kato, et al., 2011), a quantitative evaluation of data sources used to calculate surface radiative flux (Zhang et al., 2006) had previously revealed that surface downward longwave flux was most influenced by input factors such as surface air temperature and humidity causing uncertainty and notable error propagation among various global datasets. Other input factors such precipitable water presented bias in model outputs, (Hinkelman, 2009) and (Kato, et al., 2012), supporting (Zhang, et al., 2007) that input parameters and broadband emissivity should be improved as they are a leading contributor to the errors in both longwave and shortwave products. In general it was found that surface albedo, cloud optical depth, aerosol optical depth, cloud fraction, surface temperature and precipitable water were most commonly tagged for further investigation with instrument calibration, sampling space and satellite viewing angles as key sources of instability (Hinkelman, 2009).

All of these studies influenced improvements to subsequent versions of the SRB algorithm and resulting datasets. Progress has been generally good with regard to reducing errors in retrieval methods, instrument failures, data product anomalies, satellite degradation and calibration, and inspection of spectral channels, all of which can never be eliminated (McDonald, 2011). Nonetheless, improvements to the algorithm has reduced the potential for error propagation and resulted in superior performance and sustained interest by the GEWEX/SRB and the Clouds and the Earth's Radiant Energy System (CERES) projects (Gupta, 2011).

2.3 SRB Uncertainty Quantification (Historical)

The literature shows that the greatest cause of uncertainty is associated with the input data. Uncertainty is a result of variability, and variability in the SRB input data is still not well understood (Kato et al., 2012; Stephens et al., 2012). Uncertainty analysis methods have not varied significantly over time beyond a few trusted approaches discussed here. The review included irradiance estimate analyses for both longwave and shortwave products that were constrained either globally or regionally and were sourced from a variety of data products and instruments.

One of the commonly used methods used in conducting uncertainty and sensitivity analyses for satellite derived data products is the comparison of model outputs with ground site measurements. It has been shown that ground site data are reliable and useful for algorithm comparisons and for validation of the final results of satellite data analysis (Hinkelman, et. al., 2009). This uncertainty method has been used in many studies and typically involves a delta comparison of the quadratic mean, root mean squared (RMS), of the ground site (observed) and satellite (modeled) surface irradiances. Parameter perturbation is another method that uses estimated uncertainties as inputs to the algorithm (Ramanathan, 2008; Kato, 2012). In one study, two irradiance models were evaluated against each other and the combined uncertainties were evaluated against surface observations with the largest uncertainties observed in the input parameters of near-surface air temperature and precipitable water (Kato et al., 2012). Recent validation of SRB Version 3.0 shortwave and longwave flux was done by comparing quality controlled BSRN sites measurements with model output (Zhang et al., 2013, 2015). The bias/RMS for the monthly mean shortwave fluxes when compared with BSRN measurements are -5.2/23.3 W m^{-2} under all-sky conditions (Zhang et al., 2013). These values are improved over

(Whitlock et al., 1994) where bias between satellite and surface measurements was calculated between 10 – 25 W m^{-2}.

3. LITERATURE GAP ANALYSIS

3.1 Uncertainty Studies

Methods used to identify key input parameters most responsible for causing variability in satellite estimation data products were found through a literature review of several uncertainty and sensitivity analyses. A gap was identified in the analyses that could be filled to both identify key input parameters and quantify variability using multivariate input factor analysis. The past uncertainty and sensitivity analyses found in literature are summarized in the literature review summary, Table 5, to illustrate this gap. All of the referenced work focused on irradiance estimated in terms of longwave and shortwave, and constrained either globally or regionally from a variety of data products and instruments. The following keys in Table 4 reconcile with corresponding references in the literature review summary shown in Table 5.

Irradiance Uncertainty and Sensitivity Methods Key	
Key	Description
M1	Compared satellite estimation model results with the results of existing satellite estimation models.
M2	Compared satellite estimation model results with ground station measurements.
M3	Assigned nominal values to select input parameters and compare results to previous results.
M4	Changed one input parameter at a time and computed and compared the bias of the resulting output datasets.
M5	All parameters, parameter interactions and squared terms (measuring the parameter against itself) were evaluated by experimental design over a scientifically prescribed distribution range at three distinct levels. A second-order approximation model was constructed from the results of least squares regression analysis. A Monte Carlo simulation of the model output extended the probability distribution beyond the initial design trials to expose variability in the modeled data.
M6	Quantify uncertainty of different global data sets.
M7	Compare satellite estimation models with satellite observations.
M8	Compare inputs from various sources.
M9	Analyze irradiance differences
M10	Variations are represented by first-, second-, and third-degree polynomials and a sinusoidal fit.
M11	Comparison of two algorithms with each other and against site measured data.

Table 4 Uncertainty Methods Key

Researchers	Irradiance Uncertainty and Sensitivity Quantification Methods										
	M1	M2	M3	M4	M5	M6	M7	M8	M9	M10	M11
Whitlock et al., 1994	*	*									
Hinkelman et al., 2009	*	*									
Zhang et al., 2007						*					
Kandel et al., 2010	*										
Hatzianastassiou et al., 2005	*	*									
Pinker et al., 1992		*									
Rose et al., 1997	*						*				
Gupta et al., 1999		*									
Kato et al., 2012	*	*									
Zhang et al., 1995			*								
Rossow et al., 1995							*				
Stephens et al., 2011	*	*									
Wild et al., 2001		*									
Zhang et al., 2004		*					*				
Zhang et al., 2006								*			
Darnell et al., 1985		*									
Darnell et al., 1988			*								
Ellis et al., 1978		*									
Darnell et al., 1992		*									
Gupta et al., 1987			*								
Gupta et al., 1992	*										
Konzelmann et al., 1995		*									
Kato et al., 2013									*		
Dutton et al, 2005		*								*	
Cox (unpublished)				*							
Quigley, 2017					*						
Zhang, et al., 2013		*									
Zhang, et al, 2015		*									*

Table 5 Literature Review Summary Table

3.2 Research Gap Solution

Methods to quantify variability in satellite estimation data products were reviewed through literature and a gap was found that was filled by multivariate input factor analysis overcoming the limitations of one factor at a time analysis. This included linear experiments that evaluated the output data when one input parameter at a time was increased or decreased or where all of the input factors were changed by equal percentages. This could result in millions of experiments without taking parameter interactions into account.

A sensitivity analysis of the input products has not yet been conducted at the interactive and multivariate level where input parameters are systematically and simultaneously varied in succession. An augmented D-Optimal design was constructed to enable this level of experimentation. The experimental design consisted of 128 trials constructed with the 13 SRB algorithm input parameters studied at three levels of two-factor interactions and squared terms to establish non-linearity.

4. RESEARCH PROTOCOL

4.1 SRB Input Data

The input data used for the SRB Version 4.0 algorithm were obtained from various sources. Cosine solar zenith angle, cosine satellite zenith angle and azimuth angle were obtained from an angular distribution model. Cloud fraction, cloudy shortwave radiance, clear shortwave radiance and clear sky composite shortwave radiance are ISCCP products. Precipitable water, column ozone and aerosol asymmetry parameters are meteorological measurements and first guess aerosol optical depth and aerosol single scattering albedo are estimates. All of these products have been refined over the SRB versioning process. Ongoing issues include satellite

calibration shifts due to orbital drift, small discontinuities during satellite transitions and changes to the TOVS algorithm (GEWEX, 2015a).

The resulting datasets of previous SRB versions have undergone extensive testing and validation to include comparison studies among researchers and against ground site measurements obtained from the Baseline Surface Radiation Network (BSRN), the Swiss Federal Institute of Technology's Global Energy Balance Archive (GEBA) and NOAA's Climate Monitoring and Diagnostics Laboratory (CMDL) to justify that while error exists, the input values are within acceptable limits. With respect to trend analysis and integrity, literature proves that the data record of 30 years meets the climatological standard normal for establishing a trend as defined by the World Meteorological Association (WMO, 2007).

4.2 SRB Output Data

The SRB shortwave algorithm has produced reliable data since its inception in 1994 and has been successfully used in science and industry. The output data sets for this study were produced using a modified version of the same code running the Pinker/Laszlo algorithm, a modified version of an earlier physical model that derives surface solar irradiance from satellite observations (Pinker et al., 1991) and comprised of atmospheric properties calculations with radiative transfer. Where this code produces yearly global data averaged from several points within a cell, the modified software operates on a single latitude and longitude point and uses an average of one month of daily data. It produces 14 output parameters as shown in Table 6.

Output Parameter Information	
Parameter	Units
TOA downward flux	W/m^2
TOA upward flux	W/m^2
Surface downward flux	W/m^2
Surface downward diffuse flux	W/m^2
Surface upward flux	W/m^2
Surface downward diffuse photosynthetically active radiation (PAR)	W/m^2
Surface downward PAR	W/m^2
TOA upward clear sky flux	W/m^2
Surface downward clear sky flux	W/m^2
Surface upward clear sky flux	W/m^2
Output Aerosol Optical Depth	unitless
Output Cloud Optical Depth	unitless
Surface downward pristine sky flux	W/m^2
TOA upward pristine sky flux	W/m^2

Table 6 SRB Algorithm Output Parameters

4.3 Input Predictor Bounds

The ranges of predictor values used for the DOE, and subsequently to be used as input parameters to the SRB algorithm, were scientifically prescribed by geographic region. All predictors, predictor interactions and predictor squared terms (measuring the predictor against itself) were evaluated by the experimental design over the distribution range at three levels in order to construct a second-order approximation model such as done in (Unal, et al., 2015). Three levels are used to model the non-linearity of the output data, and squared terms are included to determine all possible two-factor interactions.

4.4 Experimental Design

Designed experiments have proven to be extremely useful in identifying the predictors and their interactions that are influencing the characteristics of systems and processes for the purpose of identifying variability in the dependent variables. They are also a robust means of

gaining information about these variations using the minimum number of experiments necessary to gain precision while reducing experimental cost (Unal, 2006). Experiments increase exponentially as more predictors and levels are studied requiring considerable computing power and an unreasonable amount of time.

Methods have been developed to reduce the number of experiments while maintaining the integrity and accuracy of the analysis. In 1926, Ronald A. Fisher described and proved the value of Design of Experiments (DOE) methodology for optimization of system performance with designed experiments. These formed the basis and justification for modern experimental design methodologies (Bell et al., 2013; Marengo et al., 1995). His premise was that even small effects due to changes can be revealed (Ek, 2005) and his goal was to identify variables that contribute to optimum processing proving using smaller polls and maintaining superior sampling (Ek, 2005). DOE also ensures that the design space is efficiently sampled to determine any dependencies among the predictors, and the magnitude and relative importance of the predictors and predictor interactions to the dependent variables. George E.P. Box effectively deployed experimental design techniques on process improvement (Box, et al., 1951) and his work is still the foundation of designed experimentation. Least squares regression serves to identify predictors and predictor interactions that significantly influence the dependent variables.

5. PROBLEM ANALYSIS

5.1 Hypothesis Scope

This study focused on one latitude and longitude point in each of four atmospherically distinct regions, so one hypothesis was proposed to test predictor and predictor interaction significance for each region and another to test commonality of predictor significance among the

regions. Significance among regions may be useful for assessing the global SRB algorithm. The following hypotheses describe the problem:

5.2 Significance by Region

H1o (NULL): There is no statistically significant predictor variable or predictor interaction influencing any dependent variable in a given region.

$\beta_{a\,r} = \beta_{br} = \beta_{cr} = \beta_{dr} = \beta_{er} = \beta_{fr} = \beta_{gr} = \beta_{hr} = \beta_{ir} = \beta_{jr} = \beta_{kr} = \beta_{lr} = \beta_{mr} = 0$

H1a: There is at least one statistically significant predictor variable or predictor interaction influencing any dependent variable in a given region.

$\beta_{a\,r} = \beta_{br} = \beta_{cr} = \beta_{dr} = \beta_{er} = \beta_{fr} = \beta_{gr} = \beta_{hr} = \beta_{ir} = \beta_{jr} = \beta_{kr} = \beta_{lr} = \beta_{mr} \neq 0$

5.3 Significance among Regions

H2o (NULL): There are no globally common statistically significant predictor variables among regions.

$\beta_{a\,r} = \beta_{br} = \beta_{cr} = \beta_{dr} = \beta_{er} = \beta_{fr} = \beta_{gr} = \beta_{hr} = \beta_{ir} = \beta_{jr} = \beta_{kr} = \beta_{lr} = \beta_{mr} = 0$

H2a: There is at least one globally common statistically significant predictor variables among regions.

$\beta_{a\,r} = \beta_{br} = \beta_{cr} = \beta_{dr} = \beta_{er} = \beta_{fr} = \beta_{gr} = \beta_{hr} = \beta_{ir} = \beta_{jr} = \beta_{kr} = \beta_{lr} = \beta_{mr} \neq 0$

6. EXPERIMENTAL DESIGN

6.1 Design Structure

The research approach involves a sequence of procedures in order to identify the strong predictor and predictor interactions that most significantly affect the output data of the SRB algorithm and also to quantify variability in the dependent variable output values. Minimizing the design space to four regions enabled screening of the process and offered inference about the

results that could be obtained from a global sampling. The methodology described in this section describes sample space selection, construction of a DOE, development of software tools to handle thousands of SRB algorithm transactions, regression analysis, beta testing evaluation, second order quadratic model equation construction for each dependent variable in each region and the application of a sensitivity analysis of these models to quantify variability using Monte Carlo simulation.

6.2 Methodology

Define the sample space

Four global regions were selected for study to include heavy foliage, pelagic, desert and mountainous in order to represent unique reciprocality to atmospheric conditions and to correlate some latitude and longitude points with ground site locations (BSRN sites and PMEL buoys) as shown in Table 7. Future studies could use the results from this study for comparison with measurements obtained from these locations. There is no ground site located at the highest point of Mt. Everest. This point was selected to endorse and illustrate the advantage of satellite derived data. Satellites pass over the geographic coordinates for locations where measuring equipment positioning is not possible.

REGION	LOCATION	LAT	LON	GROUND SITE
Amazon Rain Forrest	Rolim de Moura, Brazil	-11.58	298.22	BSRN 73
Sahara Desert	Gobabeb, Namib Desert, Africa	23.56	15.04	BSRN 20
Indian Ocean	Indian Ocean	-7.97	67.00	BOUY RBJ
Mt Everest	Highest Point	27.59	273.45	Not Represented

Table 7 Correlation of Regions with Ground Sites

Design the experiments

There are 13 input parameters, each having a defined range of values. The ranges were studied at three levels (low, medium and high), with the mean of the range representing the medium value. JMP® Statistical Software was used to construct an orthogonal array matrix of 105 rows using coded values -1, 0, or 1 for the three levels. The design was then augmented with an additional 23 rows to allow for regression statistic computation. Figure 3 shows a view of the coded design used for each of the four regions.

Trial	colza	catza	azi	cldfrc	cldrad	clrrad	cmprad	pwater	ozone
1	1	1	-1	-1	-1	1	1	1	1
2	-1	0	-1	-1	1	-1	1	1	1
3	1	0	-1	1	-1	0	-1	1	0
4	-1	1	-1	1	0	1	-1	-1	1
5	-1	-1	0	1	1	0	1	-1	1
6	-1	-1	1	-1	-1	-1	1	-1	1
7	-1	1	-1	-1	1	1	1	-1	0
8	1	-1	-1	-1	-1	-1	-1	1	-1
9	1	1	-1	-1	1	-1	-1	-1	1
10	1	-1	1	-1	-1	1	-1	-1	-1
*	*	*	*	*	*	*	*	*	*
*	*	*	*	*	*	*	*	*	*
*	*	*	*	*	*	*	*	*	*
121	0	1	1	0	-1	-1	1	-1	-1
122	1	-1	-1	-1	0	0	0	1	1
123	1	1	1	1	0	1	1	1	1
124	-1	-1	-1	-1	-1	1	-1	0	-1
125	1	1	-1	1	-1	1	-1	-1	-1
126	1	-1	1	1	-1	-1	-1	1	1
127	0	0	1	-1	1	-1	-1	0	-1
128	-1	-1	1	0	1	1	0	-1	-1

Figure 3 D-Optimal Design with Coded Values

The input parameters for the SRB algorithm displayed in Figure 3 are the predictors of the SRB output data and the design responses. These parameters and their short names are listed in Table 8. Table 8 also includes the full range of values for each parameter and their data sources.

Algorithm Input Variables			
Parameter Assignment	Description	Full Range	Source
colza	Cosine solar zenith angle	0.0(sun on horizon) - 1.0(sun overhead)	Angular Distribution Model
catza	Cosine satellite zenith angle	0.0 (satellite on horizon)- 1.0(satellite over cell)	Angular Distribution Model
azi	Azimuth angle	0.0 - 180.0	Angular Distribution Model
cldfrc	Cloud fraction	0.0 - 1.0	ISCCP
cldrad	Cloudy shortwave radiance	0.0 - 1.11	ISCCP
clrrad	Clear shortwave radiance	0.0 - 1.11	ISCCP
cmprad	Clear sky composite shortwave radiance	0.0 - 1.11	ISCCP
pwater	Precipitable water	1.0 - 50.0	Meteorological
ozone	Column ozone	5.0 - 50.0	Meteorological
pshcld	Phase of the cloud	1 = liquid 2 = ice	ISCCP
aertau	First guess aerosol optical depth	0.0 - 1.0	Estimate
aerssa	Aerosol single scattering albedo	0.9 - 1.0	Estimate
aerasy	Aerosol asymmetry parameter	0.5 - 1.0	Meteorological

Table 8 Predictor Names and Descriptions

The coded values (-1, 0 and 1) in each row of the D-Optimal design were then converted to actual values within the ranges for each parameter shown in Table 8. Figure 4 shows the partial design for the Amazon Region. Each of the 128 rows of the design represents a different combination of the SRB input parameters. Values labeled as VAR will be discussed in Step 3. Figures 10, 11, 12 and 13 in Appendices A through D, show the partial designs for each of the four regions.

TRIAL	colza	catza	azi	cldfrc	cldrad	clrrad	cmprad	pwater	ozone	phscld	aertau	aerssa	aerasy
	0.20	0.32	0.01	0.00	0.07	0.05	0.05	13.48	24.21	1	0.07	0.89	0.58
	0.58	0.66	89.51	0.50	VAR	VAR	VAR	36.86	26.09	n/a	0.41	0.93	0.61
	0.96	0.99	179.00	1.00	0.60	0.36	0.33	60.25	27.96	2	0.76	0.97	0.64
1	0.96	0.99	0.01	0.00	0.20	0.36	0.33	60.25	27.96	2	0.76	0.97	0.61
2	0.20	0.66	0.01	0.00	0.20	0.05	0.12	60.25	27.96	1	0.07	0.97	0.64
3	0.96	0.66	0.01	1.00	0.20	0.30	0.24	60.25	26.09	1	0.07	0.97	0.64
4	0.20	0.99	0.01	1.00	0.14	0.13	0.05	13.48	27.96	1	0.07	0.97	0.64
5	0.20	0.32	89.51	1.00	0.20	0.09	0.12	13.48	27.96	2	0.07	0.89	0.58
6	0.20	0.32	179.00	0.00	0.07	0.05	0.12	13.48	27.96	1	0.07	0.97	0.58
7	0.20	0.99	0.01	0.00	0.20	0.13	0.12	13.48	26.09	2	0.07	0.97	0.58
8	0.96	0.32	0.01	0.00	0.20	0.24	0.24	60.25	24.21	2	0.76	0.89	0.64
9	0.96	0.99	0.01	0.00	0.60	0.24	0.24	13.48	27.96	1	0.07	0.97	0.58
10	0.96	0.32	179.00	0.00	0.20	0.36	0.24	13.48	24.21	1	0.76	0.97	0.64
*	*	*	*	*	*	*	*	*	*	*	*	*	*
*	*	*	*	*	*	*	*	*	*	*	*	*	*
*	*	*	*	*	*	*	*	*	*	*	*	*	*
118	0.20	0.66	0.01	1.00	0.20	0.09	0.12	60.25	24.21	2	0.07	0.89	0.61
119	0.20	0.66	179.00	1.00	0.14	0.13	0.12	36.86	24.21	1	0.07	0.89	0.58
120	0.20	0.32	89.51	0.00	0.20	0.05	0.12	13.48	24.21	2	0.76	0.97	0.61
121	0.58	0.99	179.00	0.50	0.16	0.14	0.26	13.48	24.21	1	0.41	0.89	0.61
122	0.96	0.32	0.01	0.00	0.40	0.30	0.29	60.25	27.96	2	0.07	0.97	0.58
123	0.96	0.99	179.00	1.00	0.40	0.36	0.33	60.25	27.96	2	0.07	0.89	0.64
124	0.20	0.32	10.00	0.00	0.07	0.13	0.10	36.86	24.21	2	0.41	0.97	0.58
125	0.96	0.99	0.01	1.00	0.20	0.36	0.24	13.48	24.21	1	0.76	0.93	0.58
126	0.96	0.32	179.00	1.00	0.20	0.24	0.24	60.25	27.96	2	0.07	0.97	0.61
127	0.58	0.66	179.00	0.00	0.60	0.14	0.14	36.86	24.21	1	0.76	0.89	0.64
128	0.20	0.32	159.00	0.50	0.20	0.13	0.10	13.48	24.21	2	0.76	0.93	0.58

Figure 4 D-Optimal Design for Amazon Rainforest with Actual Values

The SRB algorithm also takes as input 6 additional static parameters. Spatial inputs such as latitude and longitude are set for each region. One month of a year was chosen for the temporal values for all regions to establish a fixed distance from the earth to the sun. The satellite position ID was set to 1 for all regions and was predefined based on orbital paths. For this study, atmospheric and space weather observations were obtained from the NOAA-9 sun-synchronous satellite, launched on December 12, 1984 (OSCAR, 2015). The snow/ice unit was set to 0 for all of the regions except for the Mt. Everest Region. The snow/ice value is determined by region. The values for the static parameters are shown in Table 9.

Algorithm Static Input Variables						
REGION	MONTH	YEAR	LATITUDE	LONGITUDE	SATELLITE POSITION ID	SNOW/ ICE
Amazon Rainforest	JUL	2007	-11.58	298.23	1	0
Indian Ocean	JUL	2007	-7.97	67.00	1	0
Mt. Everest	JUL	2007	27.59	273.45	1	1
Sahara Desert	JUL	2007	23.56	15.04	1	0

Table 9 Static Input Values for the SRB Algorithm

Execute the SRB algorithm to conduct the experiments

For each region, the DOE was programmatically parsed to extract and pass one row of inputs to the SRB algorithm software. This process is represented in Figure 5. Executing and compiling the results was automated for efficiency, speed, scalability and reuse. A utility script created 128 NAMELIST files that contained a value for each of the 13 varied input parameters and the 6 static input parameters. After the SRB algorithm processed all of the 128 NAMELIST files, the utility script created a table of all of the output parameters to be used as dependent variables for the regression analysis. This was done for each of the four regions equating to 4 x 14 x 128 = 7,168 experiments.

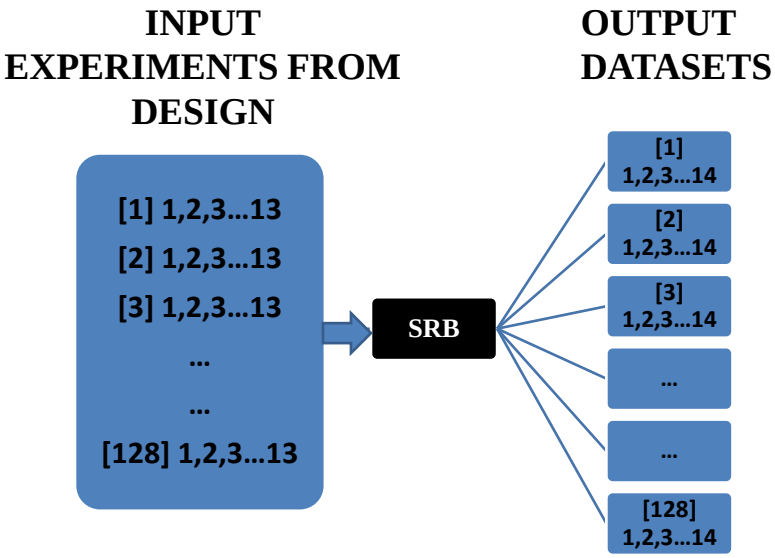

Figure 5 Surface Radiation Budget Algorithm Processing

Evaluate the results of the output data

The Amazon Rainforest region was selected for beta testing. Analysis of the output data sets indicated that input parameter ranges should be more finely tuned as some produced infeasible solutions. This was due to codependency among cosine of the solar zenith angle with clear sky radiance (clrrad), cloudy sky radiance (cldrad) and clear sky composite shortwave radiance (cmprad). These predictor values cannot extend to the limits of range during conditions of low sun and low satellite angles. The values were then set depending on the value of the cosine of the solar zenith angle (colza) and correlated well with the atmospheric profile of each region. Table 10 shows the adjustment of the predictors in the Amazon region as the cosine of the solar zenith angle varied from 0.2 to 0.58 to 0.96. Infeasible solutions were managed for the other three regions as well.

colza	0.2			0.58			0.96		
	clrrad	cldrad	cmprad	clrrad	cldrad	cmprad	clrrad	cldrad	cmprad
low	0.05	0.07	0.05	0.14	0.16	0.14	0.24	0.20	0.24
med	0.09	0.135	0.085	0.205	0.38	0.20	0.30	0.40	0.285
high	0.13	0.20	0.12	0.27	0.60	0.26	0.36	0.60	0.33

Table 10 Adjusted Predictor Value Bounds for Amazon Region

Perform a regression analysis for each dependent variable

To measure the goodness of the model, a least squares regression analysis was performed for each dependent variable in each region to obtain a minimum generalized variance of the estimates of the model coefficients and to show the correlation among predictors. JMP® Statistical Software was prescribed for this effort and was commercially available. The response surface Fit Model regression included all of the predictors, predictor interactions and squared terms. A separate regression was done for every dependent variable in all four regions.

The model specification results of the regression analysis included P value statistics and regression coefficients that were used to determine the significant predictors and predictor interactions. P value analyses serve as a standard for identifying influential predictors and predictor interactions that were significantly impacting the dependent variables, and provided evidence for rejecting or not rejecting the null hypothesis. For this study, the predictors with P values that were approximately within the $90^{\%}$ confidence range were considered significant in order to include more predictors in the model. Specifically, this was where $P \leq$ to .11. The P value statistic for 56 (14 dependent variable sets of 128 x 4 regions) individual analyses was examined. Figure 6 shows the P value statistics for TOAUP in the Amazon Rainforest region.

AMAZON TOAUP	
Predictor	***P-Value***
colza	0
cldfrc*cldrad	0
cldrad	0
cldfrc	0
colza*cldrad	0
colza*cldfrc	0.00003
azi*azi	0.00018
colza*catza	0.00036
pwater*pshcld	0.00188
colza*colza	0.00384
azi*pwater	0.00644
catza	0.00979
pwater	0.02555
cmprad*aerasy	0.03931
catza*aertau	0.04264
aertau*aerssa	0.04434
clrrad*clrrad	0.06447
azi*pshcld	0.06861
clrrad	0.07346
cmprad	0.0842
colza*clrrad	0.08601
cldfrc*aerasy	0.08618
colza*aertau	0.09291
cldfrc*aertau	0.10158
colza*azi	0.10652

Figure 6 P Value Statistics for TOAUP in Amazon Region

Construct model equations

A second order math model, approximating the relationship between the dependent variables and each of the predictor variables (Unal, 2015) in each of the four regions, was built for each dependent variable using the significant predictors and predictor interactions as determined by the P value analysis. The equation was generated using the coefficients of each dependent variable where predictors and predictor interactions satisfied the P value criteria of P

≤ to .11. The purpose of this model was to create an equation that could be used in a Monte Carlo simulation to extend the capabilities of the design and show variability of the output data as the inputs changed. The model equation is in the form $Y = b_0 + \sum b_i x_i + \sum\sum b_{ij} x_{ij} + \sum b_{ii} x_i^2$ where b_0 is the Y intercept, Y is the dependent variable value, lower case b_i represents the coefficients from the regression analysis and x's represent one of the three possible levels of the predictors. Lower case i and j represent the experiment numbers where i=1-n and j=1-n. Software was developed in order to rapidly build the 56 model equations for each of the 14 dependent variable values in each of the four regions.

The model equation for the dependent variable TOAUP in the Amazon Rainforest region is shown on the far right in Figure 7. It was built using the coefficients from the regression analysis as shown in the table in the center of Figure 7 where significant predictors and predictor interactions are listed with their corresponding coefficient value. For this equation, Y is the dependent variable. The alpha character 'A' followed by a number is a cell in a spreadsheet that represents the high, medium or low value for each predictor as illustrated by the table on the left in Figure 7. These were varied using appropriate probability distributions for the sensitivity analysis. Two predictor interactions and squared terms are multiplied as denoted by the asterisks.

A3	colza	H,M,L
A4	catza	H,M,L
A5	azi	H,M,L
A6	cldfrc	H,M,L
A7	cldrad	H,M,L
A8	clrrad	H,M,L
A9	cmprad	H,M,L
A10	pwater	H,M,L
A11	ozone	H,M,L
A12	pshcld	H,M,L
A13	aertau	H,M,L
A14	aerssa	H,M,L
A15	aerasy	H,M,L

TOAP	
Predictor	*coeff*
Intercept	316.505385
colza	154.111742
cldfrc*cldrad	54.064277
cldrad	65.568597
cldfrc	60.5750548
colza*cldrad	43.0150125
colza*cldfrc	24.2120005
azi*azi	-65.674031
colza*catza	-19.861128
pwater*pshcld	-31.34222
colza*colza	-54.421118
azi*pwater	-15.360723
catza	17.5129775
pwater	15.0105291
cmprad*aerasy	-9.7826131
catza*aertau	-10.073629
aertau*aerssa	10.3136588
clrrad*clrrad	29.6186082
azi*pshcld	-17.40929
clrrad	12.0928359
cmprad	11.6893114
colza*clrrad	8.94938664
cldfrc*aerasy	-8.7228263
colza*aertau	-8.0108616
cldfrc*aertau	-8.3427717
colza*azi	8.14932366

MODEL EQUATION
Amazon Region

Y=316.505385+154.1117419*A3+54.064
27701*A6*A7+65.56859697*A7+60.575
05477*A6+43.0150125*A3*A7+24.2120
0051*A3*A6+-65.6740312*A5*A5+-
19.86112823*A3*A4+-
31.34222036*A10*A12+-
54.42111832*A3*A3+-
15.3607226*A5*A10+17.51297749*A4+
15.01052909*A10+-
9.782613058*A9*A15+-
10.07362949*A4*A13+10.31365884*A13
*A14+29.61860823*A8*A8+-
17.40928998*A5*A12+12.09283592*A8
+11.68931142*A9+8.94938664*A3*A8+-
8.72282627*A6*A15+-
8.010861627*A3*A13+-
8.342771651*A6*A13+8.149323664*A3*
A5

35

Figure 7 P Values and Coefficients Summary

Sensitivity Analysis

To determine the variability in the output data for each dependent variable, a Monte Carlo simulation using @Risk® commercial software. This enabled more variations of predictor levels beyond the designed experiment to be evaluated. Setup entailed using the dependent variable as the risk output and the predictor values varied by three levels as the input. Triangular distributions that can model skewness were used. The parameters of these distributions were determined by using expert judgment. To avoid correlation of the predictor values in the equation, the high, medium and low actual values for each predictor were normalized by coding the actual values back to 1, 0 and -1 respectively. The simulation varied all of the input parameters in the model equation about their normalized distribution ranges 10,000 times for each dependent variable and for each region.

6.3 Tool Development

Software tools were created to assist with the following tasks for customization and automation of the SRB algorithm execution, construction of tables for the regression analysis and the model equations:

1. Histogram files containing the ranges for each of the predictors were provided by the scientist. A program was written to extract the high and low values for the parameters and compute the medium values from the histogram text files. These values were then used to convert the coded predictor values of the computer generated D-Optimal DOE to actual predictor values in a spreadsheet with a simple Excel function.

2. After porting the DOE to the directory where the SRB algorithm is stored, it was parsed with a script to create 128 NAMELIST files for each region. The NAMELIST files are used as input to the SRB algorithm.

3. A utility script successively passed each NAMELIST file to the SRB algorithm for processing. The algorithm created 128 output datasets for each of the 14 output data sets. These were then programmatically combined into a matrix of 128 rows and 14 columns. The values in the 14 columns became the dependent variables.

4. JMP® Statistical Software was used to do a regression analysis for each output parameter. The summary effects and P-value results for each regression were ported into tables. A script extracted P-values and coefficients from the regressions that were used to determine the strong predictors and predictor interactions and test H1o and H1a.

5. Second order quadratic equations were programmatically constructed using the coefficients from the regression for use in the Monte Carlo simulation.

6. A script was used to compare and report the significant predictors and predictor interactions among all of the regions to test H2o and H2a.

A report file was written containing detailed instructions for accomplishing all of the tasks. A README file containing instructions for executing code for sequential SRB processing is also available.

7. DATA ANALYSIS

7.1 Predictor Analysis Results

It was found by identifying predictors and predictor interactions having the lowest P value in each region that there were predictors and predictor interactions that very strongly influenced the dependent variables. These are shown in Table 11.

REGION	PREDICTOR	PREDICTOR INTERACTIONS
Amazon Rainforest	colza	colza*cldfrc
Sahara Desert	colza	colza*cldfrc,cldfrc*cldrad
Mt. Everest	colza	colza*cldfrc
Indian Ocean	colza	cldfrc*cldrad

Table 11 Strongest Predictor and Predictor Interactions by Region

Statistics were also analyzed to identify the dependent variables that had the most predictors and predictor interactions with P-values less than 0.11. These are shown in Table 12.

REGION	DEPENDENT VARIABLE (P-value < 0.11)
Amazon Rainforest	SRFDWNFLX
Sahara Desert	SRFDWNPRS
Mt Everest	SRFDWNFLX
Indian Ocean	SRFDWNPAR

Table 12 Dependent Variables with Highest Number of Influential Predictors and Predictor Interactions by Region

An analysis was performed to determine if there were significant predictors and predictor interactions that were common among the regions. A comparison of all of the strong predictor and predictor interactions tables sorted by dependent variable was conducted. The results are shown in Table 13. For each dependent variable in the first column of Table 13, a predictor or predictor interactions that were found in all four regions are listed in the second column.

Dependent Variable	Predictors and Predictor Interactions
OAOD	clrrad
OCOD	colza, catza*cldrad
SRFDWNCLRSKY	colza, clrrad
SRFDWNDIFF	colza, cldfrc*cldrad
SRFDWNDIFPAR	colza
SRFDWNFLX	cldfrc*cldrad, cldfrc, colza, cldrad, cldfrc*pshcld, colza*cldfrc
SRFDWNPAR	cldrad, colza, cldfrc*cldrad, cldfrc*pshcld, colza*cldfrc
SRFDWNPRS	pshcld*aerasy, cldfrc*ozone, catza, pwater*pwater, colza, colza*catza, ozone*aertau, cmprad, aerasy, cldfrc*pshcld, colza*colza, pwater, cmprad*aerssa, ozone, colza*pwater
SRFUPCLRFLX	colza
SRFUPFLX	colza*catza, cldrad, cldfrc
TOAUP	pwater*pshcld, azi*pwater, cldfrc*cldrad, cldfrc, cldrad, colza, colza*cldrad, catza*aertau, azi*pshcld, azi*azi, clrrad*clrrad, colza*cldfrc, clrrad
TOAUPCLRSKY	cmprad, colza, colza*catza, catza*azi
TOAUPPRS	cmprad, colza, colza*catza, colza*cmprad

Table 13 Common Significant Predictors for Dependent Variables among Regions

7.2 Sensitivity Analysis Results

The second objective was to quantify variability of the output data sets as the input values changed. The Monte Carlo simulation varied the normalized values of all of the input parameters in the model about their normalized distribution ranges 10,000 times for each dependent variable and for each region. The resulting distribution curve of three standard deviations for each simulation along with statistical output quantified the variability. Figure 8 shows the approximated variability for each dependent variable by region.

	VARIABILITY			
Dependent Variable	**Amazon**	**Sahara**	**Mt Everest**	**Indian Ocean**
TOAUP	254	202.5	319	306
SRFDWNFLX	548	447	720	492
SRFDWNDIFF	221.5	277	116.2	317
SRFUPFLX	190.3	125.3	43.4	74.1
SRFDWNDIFPAR	55.8	155.1	60.5	158.1
SRFDWNPAR	258	211.5	272	242
TOAUPCLRSKY	174.3	114.8	43.9	87
SRFDWNCLRSKY	586	586	630	525
SRFUPCLRFLX	205.7	142.6	49.3	61.4
OAOD	0.488	0.977	0.057	0.613
OCOD	146.7	146.3	130.2	140.2
SRFDWNPRS	604	655	628	599
TOAUPPRS	199.5	139.7	52.1	160.3

Figure 8 Results of Sensitivity Analysis (W m^{-2})

Figure 8 shows the graphical representation of the analysis statistics for the dependent variable TOAUP in the Amazon Rainforest region to include the coefficient table, a graph of the coefficient table and the variability histogram produced by @Risk® software. A complete collection of the graphical representations for each dependent variable in each region is shown in Figures 14 through 65.

TOAP	
Factor	*coeff*
colza	154.1117419
cldfrc*cldrad	54.06427701
cldrad	65.56859697
cldfrc	60.57505477
colza*cldrad	43.0150125
colza*cldfrc	24.21200051
azi*azi	-65.6740312
colza*catza	-19.86112823
pwater*pshcld	-31.34222036
colza*colza	-54.42111832
azi*pwater	-15.3607226
catza	17.51297749
pwater	15.01052909
cmprad*aerasy	-9.782613058
catza*aertau	-10.07362949
aertau*aerssa	10.31365884
clrrad*clrrad	29.61860823
azi*pshcld	-17.40928998
clrrad	12.09283592
cmprad	11.68931142
colza*clrrad	8.94938664
cldfrc*aerasy	-8.72282627
colza*aertau	-8.010861627
cldfrc*aertau	-8.342771651
colza*azi	8.149323664

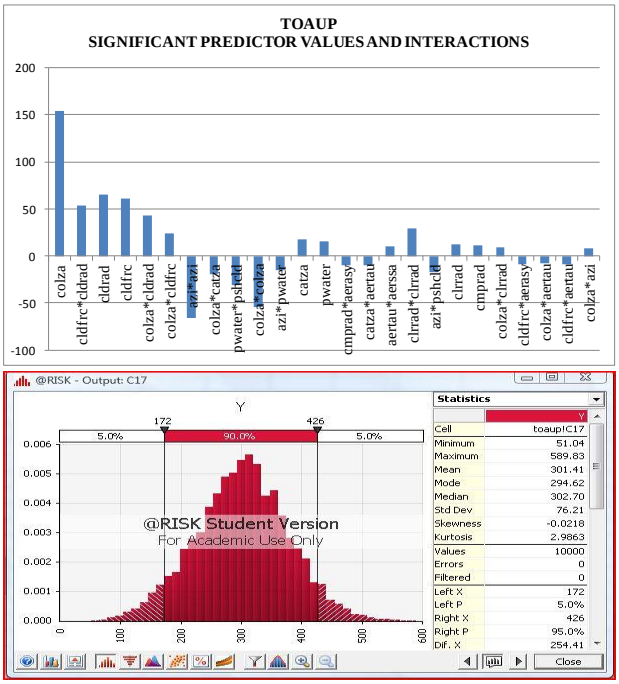

Figure 9 Amazon Region Sensitivity Analysis - TOAUP

Model equations were not constructed for TOADWN for any of the regions. This variable represents the sunlight coming into the earth's atmosphere and is not affected by surface or atmospheric properties; therefore the only significant input was cosine of the solar zenith angle (colza).

7.3 Resolution of Research Objectives

The first objective was to identify significant input parameters and parameter interactions that significantly affected the output data sets of the SRB algorithm. This was accomplished by analysis of the regression statistics.

H1a: There is at least one statistically significant predictor variable or predictor interaction influencing any dependent variable in a given region.

$$\beta_{a\,r} = \beta_{br} = \beta_{cr} = \beta_{dr} = \beta_{er} = \beta_{fr} = \beta_{gr} = \beta_{hr} = \beta_{ir} = \beta_{jr} = \beta_{kr} = \beta_{lr} = \beta_{mr} \neq 0$$

P value analysis showed that the NULL hypothesis H1o should be rejected because each dependent variable in all four regions was significantly influenced by at least one predictor and/or predictor interaction.

The results showed that the null hypothesis H2o can be rejected. There is at least one globally common statistically significant predictor variable among regions.

H2a: There is at least one globally common statistically significant predictor variables among regions.

$$\beta_{a\,r} = \beta_{br} = \beta_{cr} = \beta_{dr} = \beta_{er} = \beta_{fr} = \beta_{gr} = \beta_{hr} = \beta_{ir} = \beta_{jr} = \beta_{kr} = \beta_{lr} = \beta_{mr} \neq 0$$

8. SUMMARY

8.1 Statistical Approach to Predictor Analysis

An analytical and statistical framework was developed to determine significant predictors and predictor interactions that influenced the output products of the SRB algorithm and quantified the variation in the resulting output data sets. This was accomplished using DOE, regression analysis and Monte Carlo simulation. Predictor variables and second order interactions that strongly influenced the dependent variables were determined. The influence of predictors and predictor interactions varied among the dependent variables and among regions, but that there was some commonality with the cosine of the solar zenith angle having the strongest influence on the output data in all four regions. The interaction of Cosine Solar Zenith Angle and Cloud Fraction had the strongest influence on output data in the Amazon Rainforest, Sahara Desert and Mt. Everest Regions, and the interaction of Cloud Fraction and Cloudy Shortwave Radiance most significantly affected output data in the Indian Ocean region. Tools

were developed to simplify and automate the processes and to make the analyses much more efficient.

8.2 Summary of Results

Methods to identify influential input parameters and quantify variability in satellite estimation data products were reviewed through literature. A gap in analytic methods was identified and filled by multivariate input factor analysis. A D-Optimal design of 128 experiments was constructed to enable many combinations of the input data to be evaluated simultaneously. Key predictor and predictor interactions were identified and the variability of the output data was quantified. Tools were built to automate and streamline processes.

The SRB algorithm requires 13 input parameters and 6 static parameters to complete execution and delivers 14 output parameters each time it runs. Changing the values of the input parameters changes the values of the output parameters. The research problem was to identify those input parameters that caused the most significant influence on the output parameters and to quantify the impact. In the past, these were tested by changing one input parameter at a time. In order to address this problem more efficiently, both input parameters and input parameter interactions were studied as two factor interactions and squared terms. This was accomplished using a D-Optimal experimental design. The design provided 128 variations of the inputs that were then processed by the SRB algorithm. The result was 128 different responses for each output parameter. This was done for each of the four atmospherically distinct regions using a modified configuration of the SRB algorithm.

A regression analysis was conducted using the design matrix of 128 rows and 13 columns as the predictor variables and each output parameter set of 128 experiments as the dependent variables. The regression included all of the predictor values and all possible interactions of the

predictor values. Square terms of each predictor value were also included. Summary statistics were provided after each regression to include P-values. This enabled the significance of each predictor variable and the relationships among the predictor variables to be measured. Predictor and predicator interactions with P-values < 0.11 were flagged as significant and presented as tables and graphs. There were several significant predictors and predictor interactions influencing the dependent variables, so the null hypothesis H10 was rejected.

In addition, it was found by identifying predictors and predictor interactions having the lowest P-value in each region that there were predictors and predictor interactions that very strongly influenced the dependent variables. These were shown in Table 11. Statistics were also analyzed to identify the dependent variables that had the most predictors and predictor interactions with P-values less than 0.11. These were shown in Table 12.

Commonality of strong predictors and predictor interactions was the basis of hypotheses H20 and H2a. Tables containing the strong predictors and predictor interactions for each dependent variable for all four regions were programmatically parsed and compared. H20 was rejected as the results of the comparison showed that there was at least one significant predictor and/or predictor interaction common to all of the regions. These were shown in Table 13.

The dependent variable SRFDWNPRS was most strongly affected in every region by colza, colza*colza, colza*pwater, colza, pwater and pwater*pwater. The only difference was that SRFDWNPRS in the Mt. Everest region was also strongly affected by ozone. It was found that Cosine solar zenith angle was the strongest influence on the output data in all four regions. The interaction of Cosine Solar Zenith Angle and Cloud Fraction had the strongest influence on the output data in the Amazon, Sahara Desert and Mt. Everest Regions, while the interaction of

Cloud Fraction and Cloudy Shortwave Radiance most significantly affected output data in the Indian Ocean region.

In order to quantify the impact that the significant predictors and predictor interactions had on the dependent variables, a second order quadratic equation was constructed for each dependent variable using the coefficients for each of its significant predictor and predictor interactions from the regression analysis. Monte Carlo simulation extended the capability of the DOE by varying the predictor values for each dependent variable 10,000 times. The results showed the range for the possible outcomes and quantified the variability of the output data. These are shown for each dependent variable in each region in figures 14 - 65.

9. RESEARCH CONTRIBUTIONS

9.1 Contribution to Atmospheric Science Analysis Method

A D-Optimal design was constructed to enable many combinations of the input data to be evaluated simultaneously, overcoming the limitations of one value at a time analysis (OVAT) by evaluating the interactions of the inputs as well as the main effects. The design consists of 128 trials constructed to handle the large number of input parameters and dependent variables needed to run the experiments. This is a software-generated, minimum point design with additional experiments added for greater degrees of freedom. Codependency of the cosine of the solar zenith angle with cloudy radiance, clear radiance and clear sky composite shortwave radiance due to incidences of low sun and satellite angles at certain zenith angles was quickly managed using software to add scientifically prescribed values as the bounds when infeasible outputs occurred.

9.2 Contribution to Atmospheric Science Computing Process

The research approach enabled input values to be programmatically extracted from the design, formatted as required by the algorithm and then passed into the algorithm as arguments allowing for automatic rapid and repeated execution of the design trials. This also served to eliminate the task of manually entering input values into the NAMELIST files. A software tool for building quadratic math models from regression analysis output was developed to reduce the level of effort in building second order quadratic models with multiple parameter inputs and parameter interactions.

10. LIMITATIONS AND ADVANTAGES

10.1 Limitations

It is not yet known if the variability at the regional level applies to the global signal, but it was found that there is at least one globally common statistically significant predictor variables among regions (cosine of the solar zenith angle) and the interaction of cosine of the solar zenith angle and cloud fraction was significant in the Amazon, Mt. Everest and Sahara regions. The results in this analysis are based on a point in one cell out of 44016 possible cells with many points and should be extended to other regions in order to get a global picture. The SRB algorithm produces an approximation to the value of the dependent variable so the regression results may not be an accurate representation of the actual site measured values. The relative significance of the predictors and their interactions would not be expected to change. Similarly, the Monte Carlo simulation provided a good indication of relative variability, but results may not be accurate as the model equation is an approximation of an algorithm that is also an approximation.

10.2 Advantages

Input parameters used by the SRB algorithm are notably a key source of variability in the resulting output data sets. The relative significance of these parameters and their interactions would not be expected to change. Previous studies included linear techniques such as varying one input parameter at a time while keeping all others constant or by increasing all input parameters by equal random percentages. This research used D-Optimal DOE and reduced the number of trials required by full factorial designs or by linear analyses from millions to 128. Second order quadratic model equations constructed from the results of least squares multiple regressions were used in Monte Carlo simulations. This provided further indication of relative uncertainty. Another advantage over one variable at a time (OVAT) analyses is that parameter interactions were determined. These can be stronger than main effects as seen in the results of this study. The result of this framework enabled an efficient and structured analysis approach to identify those parameters and parameter interactions that most significantly affected the SRB output products.

11. CONCLUSIONS AND FUTURE RESEARCH

There is much potential for further study of SRB output data at the regional level. This work provided a very small sampling of the globe where there are a total of 44016 candidate cells that could also be studied. Studying more cells may further identify commonality of strong predictor and predictor interactions on the global scale. Ground site comparison studies showed good correlation of the modeled SRB data to measured values so studies should be done using to model optimization techniques where the dependent variable values are constrained to site measurements. Strong predictors and predictor interactions were common among certain

dependent variables. Scientific analysis of this finding is suggested and may result in testing input parameters outside of the ranges used in this study.

A power analysis using information from the current design and scientific reasoning can be used to optimize future designs. This is done by computing the signal to noise ratio where the signal is equal to the desired delta in the response (not predicted in this study), and the noise is the standard deviation computed for the dependent variables that were calculated in this study.

This sensitivity analysis modeled a triangular distribution of the input ranges. Future studies could use a skewed distribution with orthogonal polynomials. Model and validate prior covariance distributions and then using a Bayesian hierarchical approach to regression modeling in addition to the current model.

Finally, taking known uncertainties of the input parameters into consideration, establish an error profile for each of the output parameters so that uncertainty can be established on a global scale.

REFERENCES

Atmospheric Science Data Center (ASDC, 2014a). *SRB Data and Information*. Retrieved September 13, 2014 from https://eosweb.larc.nasa.gov/project/srb/srb_table

Atmospheric Science Data Center (ASDC, 2014b). *SRB_REL3.0_SHORTWAVE_MONTHLY (binary)- GEWEX Shortwave Monthly README file*. Retrieved September 14, 2014 from https://eosweb.larc.nasa.gov/project/srb/srb_rel3.0_sw_monthly_table

Atmospheric Science Data Center (ASDC, 2014c). *SRB_REL3.1_LONGWAVE_MONTHLY - GEWEX Longwave Monthly-Average Data Set README File.* Retrieved September 14, 2014 from https://eosweb.larc.nasa.gov/project/srb/srb_rel3.1_lw_monthly_table/

Baseline Surface Radiation Network (BSRN (2015). Retrieved June 30, 2015 from http://bsrn.awi.de/stations/maps.html

Bell, A.E. & Unal, R. (April 2013). Application of Taguchi methods to nextgen integrated safety risk management. E7-1.

Box G E P & Wilson K B. (1951). On the experimental attainment of optimum conditions. *Journal of the Royal Statistical Society, B13*(1), 1-45.

Clouds and the Earth's Radiant Energy System (CERES, 2016). *CERES ERBE-like subsystem overview*. Retrieved August 25, 2016 from http://ceres-erbelike.larc.nasa.gov/cgi-bin/erbelike.pl

Clemson, B. (1984). *Cybernetics: A new management tool*, Philadelphia: Gordon and Breach.

Collins, W. D., Rasch, P. J., Eaton, B. E., Khattatov, B. V., Lamarque, J. F. & Zender, C. S. (April 16, 2001). Simulating aerosols using a chemical transport model with assimilation of satellite aerosol retrievals: Methodology for INDOEX. *Journal of Geophysical Research, 106*(D7), 7313-7336.

Cox, S. J. (May, 2016). Email personal communication.

Cox, S. J., Stackhouse, Jr., P. W., Gupta, S. K., Mikovitz, C. J., Zhang, T., Hinkelman, L. M., Wild, M., & Ohmura, A. (July, 2006). The nasa/gewex surface radiation budget project: Overview and analysis. Presented at the *12th Conference on Atmospheric Radiation, Hampton, VA.* Retrieved April 22, 2016 from https://ams.confex.com/ams/Madison2006/techprogram/paper_112990.htm

Darnell, W. L., Gupta, S. K. & Staylor, W. F. (1986). Downward longwavesurface radiation from sun-synchronous satellite data: Validation of methodology. *Journal of Climatology and Meteorology, 25,* 1012-1021.

Darnell, W. L., Staylor, W. F., Gupta, S. K. & Denn, F. M. (1988). Estimation of surface insolation using Sun-synchronous satellite data. *Journal of Climate, 1*, 820-835.

Darnell, W. L., Staylor, W. F., Gupta, S. K., Ritchey, N. A. & Wilber, A. C. (1992) Seasonal variation of surface radiation budget derived from ISCCP-C1 data. *Journal of Geophysical Research*, 97(D14), 15741-15760.

Earth Observing System (EOSWEB, 2016a). *ERBE Data and information*. Retrieved August 10, 2016 from https://eosweb.larc.nasa.gov/project/erbe/erbe_table

Earth Observing System (EOSWEB, 2016b). *SRB Previously released data and information.* Retrieved April 2016 from https://eosweb.larc.nasa.gov/project/srb/srb_previous_table

Earth Observing System (EOSWEB, 2016c). *SRB Data and information*. Retrieved June 16, 2016 from https://eosweb.larc.nasa.gov/project/srb/srb_table

Ek, L.T. (2005). *Quality improvement using factorial design.* Pakistan's 9th International Convention on Quality Improvement, 14-15.

Fritz, S., Krishna, R. & Weinstein, M. (August, 1964). Satellite measurements of reflected solar energy and the energy received at the ground. *Journal of the Atmosphere, 74*(4). Retrieved September 21, 2015 from http://journals.ametsoc.org/doi/pdf/10.1175/1520-0469%281964%29021%3C0141%3ASMORSE%3E2.0.CO%3B2

Global Energy and Water Exchange Project (GEWEX, 2015a). *Known Data Irregularities.* Retrieved June 10, 2015 from http://gewex-srb.larc.nasa.gov/common/php/SRB_known_issues.php

Global Energy and Water Exchange Project (GEWEX, 2015b). *Surface Radiation Budget. SRB data products*. Retrieved June 10, 2015 from http://gewex-srb.larc.nasa.gov/common/php/SRB_data_products.php

Global Modeling and Assimilation Office (GMAO, 2016). The GOE-5 System. Retrieved June 22, 2016 from http://gmao.gsfc.nasa.gov/GEOS/

Gupta, S. K., Kratz, D. P., Stackhouse, Jr., P. W., Wilber, A.C. (December, 2001). The Langley Parameterized Shortwave Algorithm (LPSA) for Surface Radiation Budget Studies Version 1.0. NASA/TP-2001-21127. Retrieved June 22, 2016 from http://ntrs.nasa.gov/archive/nasa/casi.ntrs.nasa.gov/20020022720.pdf

Hinkelman, L. M., Stackhouse, Jr., P.W., Wielicki, B. A., Zhang, T., & Wilson, S. R. (August, 2009). Surface insolation trends from satellite and ground measurements: Comparisons and challenges. *Journal of Geophysical Research, 114*(D00D20), 1- 18. doi:10.1029/2008JD011004.

Jackson, M. (2003). *Systems thinking: Creative holism for managers*. Chichester: John Wiley & Sons, Inc..

Jethva, H., Torres, O., Waquet, F., Chand, D., & Hu, Y. (October 2013). How do A-train sensors intercompare in the retrieval of above-cloud aerosol optical depth? A case study-based assessment. *Geophysical Research Letters*, *41*, 186-192, doi: 10.1002/2013GL058405.

Kato, S., Loeb, N. G., Rutan, D. A., Rose, F. G., Sun-Mack, S., Miller, W. F., & Chen, Y. (January, 2012). Uncertainty estimate of surface irradiances computed with MODIS-, CALIPSO-, and CloudSat-derived cloud and aerosol properties. *Surveys in Geophysics, 33*(3), 395-412. doi:10.1007/s10712-012-9179-x.

Katz, D., & Kahn, R. L. (1978). The *social psychology of organizations*. New York, NY: John Wiley & Sons, Inc.

Keating, C. B, Peterson, W., & Rabadi, G. (2003). *Framing of complex system of systems engineering problems*", Proceedings of the American Society for Engineering Management, St. Louis, MO, 15-18 October 2003, pp. 8-15.

Keating, C.B. (2010). Balancing structural tensions in complex systems. *Proceedings of the American Society for Engineering Management*. Huntsville: ASEM Press.

Kratz, D. P., Stackhouse, Jr., P. W., Gupta, S. K., Wilber, A. C., Sawaengphokhai, P., & McGarragh, G. R. (September, 2013). The fast longwave and shortwave flux (FLASHFlux) data product: Single-scanner footprint fluxes. *Journal of Applied Meteorology and Climatology, 54*(4), 1059-1079.

Leighton, H. C. (1980). Application of the delta-Eddington method to the absorption of solar radiation in the atmosphere. *Atmosphere-Ocean, 18*(1), 43-52. Retrieved August 14, 2015 from http://www.tandfonline.com/doi/pdf/10.1080/07055900.1980.9649076

Marengo, E., Gennaro, M.C., & Abrigo, C. (1995). Investigation by experimental design and regression models of the effect of five experimental factors on ion-interaction high-performance liquid chromatographic retention. *Analytica Chimica Acta, 321*(2), 225-236.

Medvigy, D., & Beaulieu, C. (September, 2011). Trends in daily solar radiation and precipitation coefficients of variation since 1984. *Journal of Climate, 25,* 1330-1339.

National Aeronautics and Space Administration. (NASA, 2014a). *Project ECHO*. Retrieved September 13, 2014 from http://www.nasa.gov/centers/langley/about/project-echo_prt.htm

National Aeronautics and Space Administration and Global Energy and Water Exchange Project (NASA/GEWEX, 2012). SRB Rel 4.0 Baseline Production Plan_120927

National Oceanic and Atmospheric Administration (NOAA, 2014). What is measured? Retrieved September 13, 2014 from http://www.ncdc.noaa.gov/crn/elements.html#sr

National Oceanic and Atmospheric Administration (NOAA, 2016a). GEWEX Global Energy and Water Cycle Products. *NNhirs Dataset.* Retrieved June 22, 2016 from http://noaacrest.org/rscg/Products/GGEWC/NNHIRS.html

National Oceanic and Atmospheric Administration (NOAA, 2016b). Statospheric ozone monitoring and research in NOAA. TIROS Operational Vertical Sounder (TOVS). Retrieved June 22, 2016 from http://www.ozonelayer.noaa.gov/action/tovs.htm

National Oceanic and Atmospheric Administration (NOAA, 2016c). National Weather Service Climate Prediction Center. SMOBA: A 3-dimensional daily ozone analysis using SBUV/2 and TOVS measurements. Retrieved June 22, 2016 from http://www.cpc.ncep.noaa.gov/products/stratosphere/SMOBA/smoba_doc.shtml

National Oceanic and Atmospheric Administration (NOAA, 2016d). Earth System Research Laboratory Global Monitoring Division. Trends in atmospheric carbon dioxide. Retrieved June 22, 2016 from http://www.esrl.noaa.gov/gmd/ccgg/trends/global.html

NASA/GEWEX. (2014). *NASA GEWEX SRB Release 4.0 Baseline Processing Plan.*

Observing Systems Capability Analysis and Review Tool (OSCAR, 2015). Satellite: NOAA-9. Retrieved July 12, 2015 from http://www.wmo-sat.info/oscar/satellites/view/331

Pinker, R., & Ewing, J. A. (1985). Modeling of surface solar radiation: Model formulation and validation. *Journal of Climate and Applied Meteorology, 24*(5), 389-401.

Pinker, R., & Laszlo, I. (1992). Modeling of surface solar irradiance for satellite applications on a global scale. *Journal of Applied Meteorology, 31*(2), 194-211. Retrieved June 22, 2016 from http://journals.ametsoc.org/doi/pdf/10.1175/1520-0450%281992%29031%3C0194%3AMSSIFS%3E2.0.CO%3B2

Skyttner, L. (1996). *General Systems Theory: An Introduction*. Philadelphia: Trans-Atlantic.

Stackhouse, Jr. P. W. (June 20, 2016). Email personal communication.

Stackhouse, Jr., P. W., Gupta, S. K., Cox, S. J., Mikovitz, J. C. & Chiaachio, M. (2002). New results from the NASA/GEWEX Surface Radiation Budget Project: Evaluating El Nino effects at different scales. 11th Conference on Atmospheric Radiation, American Meteorological Society, Ogden, UT, June 3-7.

Stackhouse, Jr., P. W. (2014) NASA GEWEX SRB Release 4.0

Stephens, G. L, Li, J., Wild, M., Clayson, C. A., Loeb, N., Kato, S., L'Ecuyer, T., Stackhouse, Jr. P.W. & Andrews, T. A. (2012). An update on Earth's energy balance in light of the latest global observations. *Nature Geoscience, 5*, 691–696 doi:10.1038/ngeo1580 Retrieved July 12, 2015 from http://www.nature.com/ngeo/journal/v5/n10/abs/ngeo1580.html

Unal, R. (March 2003). *Reducing design risk using robust design methods: a dual response surface approach.* (Doctoral dissertation). University of Missouri, Rolla, Rolla, Missouri.

Unal, R. (April 11, 2006). *Optimization on cost basis and robust design approaches for reducing risk.* Slide presentation for Engineering Management and Systems Engineering, Old Dominion University, Norfolk, VA.

Unal, R., Lepsch, R. A., Lockwood, Mary K., & McMillin, M. L. (2015). *Model building for rapid multidisciplinary integration and optimization using experimental designs.* Old Dominion University & NASA Langley Research Center.

Whitlock, C. H., Charlock, T. P., Staylor, W. F., Pinker, R. T., Laszlo, I., Ohmura, A., Gilgen, H. Konzelman, T., DiPasquale, R. C., Moats, C. D., LeCroy, S. R., & Ritchey, N. A. (1994). First global WCRP shortwave surface radiation budget dataset. *Bulletin of the American Meteorological Society, 76*(6), 905-922.

Zhang, Y., Rossow, W. B., & Stackhouse, Jr. P.W. (July, 2006). Comparison of different global information sources used in surface radiative flux calculation: Radiative properties of the near-surface atmosphere. *Journal of Geophysical Research: Atmospheres, 112*(D1), , 1-13. doi:10.1029/2005JD006873.

Zhang, Y., Rossow, W. B. & Stackhouse, Jr., P. W. (January, 2007). Comparison of different global information sources used in surface radiative flux calculation: Radiative properties of the surface. *Journal of Geophysical Research, 112*(D1), 1-20. doi: 10.1029/2005JD007008.

Zhang, T., Stackhouse, Jr., P. W., Gupta, S. K., Cox, S. J., Mikovitz, J. C., & Hinkelman, L. M. (June 2013). The validation of the GEWEX SRB surface shortwave flux data products using BSRN measurements: A systematic quality control, production and application approach. *Journal of Quantitative Spectroscopy and Radiative Transfer, 122*, 127-140. Retrieved July 31 from http://www.sciencedirect.com/science/article/pii/S0022407312004335

Zhang, T., Stackhouse, Jr., P. W., Gupta, S. K., Cox, S. J., Mikovitz, J. C., & Hinkelman, L. M. (January 2015). The validation of the GEWEX SRB surface longwave flux data products using BSRN measurements. *Journal of Quantitative Spectroscopy and Radiative Transfer, 150*, 134-147. Retrieved July 31 from http://www.sciencedirect.com/science/article/pii/S0022407312004335

APPENDICES

A. Design Matrix for Amazon Rainforest

TRIAL	colza	catza	azi	cldfrc	cldrad	clrrad	cmprad	pwater	ozone	phscld	aertau	aerssa	aerasy
	0.20	0.32	0.01	0.00	0.07	0.05	0.05	13.48	24.21	1	0.07	0.89	0.58
	0.58	0.66	89.51	0.50	VAR	VAR	VAR	36.86	26.09	n/a	0.41	0.93	0.61
	0.96	0.99	179.00	1.00	0.60	0.36	0.33	60.25	27.96	2	0.76	0.97	0.64
1	0.96	0.99	0.01	0.00	0.20	0.36	0.33	60.25	27.96	2	0.76	0.97	0.61
2	0.20	0.66	0.01	0.00	0.20	0.05	0.12	60.25	27.96	1	0.07	0.97	0.64
3	0.96	0.66	0.01	1.00	0.20	0.30	0.24	60.25	26.09	1	0.07	0.97	0.64
4	0.20	0.99	0.01	1.00	0.14	0.13	0.05	13.48	27.96	1	0.07	0.97	0.64
5	0.20	0.32	89.51	1.00	0.20	0.09	0.12	13.48	27.96	2	0.07	0.89	0.58
6	0.20	0.32	179.00	0.00	0.07	0.05	0.12	13.48	27.96	1	0.07	0.97	0.58
7	0.20	0.99	0.01	0.00	0.20	0.13	0.12	13.48	26.09	2	0.07	0.97	0.58
8	0.96	0.32	0.01	0.00	0.20	0.24	0.24	60.25	24.21	2	0.76	0.89	0.64
9	0.96	0.99	0.01	0.00	0.60	0.24	0.24	13.48	27.96	1	0.07	0.97	0.58
10	0.96	0.32	179.00	0.00	0.20	0.36	0.24	13.48	24.21	1	0.76	0.97	0.64
*	*	*	*	*	*	*	*	*	*	*	*	*	*
*	*	*	*	*	*	*	*	*	*	*	*	*	*
*	*	*	*	*	*	*	*	*	*	*	*	*	*
118	0.20	0.66	0.01	1.00	0.20	0.09	0.12	60.25	24.21	2	0.07	0.89	0.61
119	0.20	0.66	179.00	1.00	0.14	0.13	0.12	36.86	24.21	1	0.07	0.89	0.58
120	0.20	0.32	89.51	0.00	0.20	0.05	0.12	13.48	24.21	2	0.76	0.97	0.61
121	0.58	0.99	179.00	0.50	0.16	0.14	0.26	13.48	24.21	1	0.41	0.89	0.61
122	0.96	0.32	0.01	0.00	0.40	0.30	0.29	60.25	27.96	2	0.07	0.97	0.58
123	0.96	0.99	179.00	1.00	0.40	0.36	0.33	60.25	27.96	2	0.07	0.89	0.64
124	0.20	0.32	10.00	0.00	0.07	0.13	0.10	36.86	24.21	2	0.41	0.97	0.58
125	0.96	0.99	0.01	1.00	0.20	0.36	0.24	13.48	24.21	1	0.76	0.93	0.58
126	0.96	0.32	179.00	1.00	0.20	0.24	0.24	60.25	27.96	2	0.07	0.97	0.61
127	0.58	0.66	179.00	0.00	0.60	0.14	0.14	36.86	24.21	1	0.76	0.89	0.64
128	0.20	0.32	159.00	0.50	0.20	0.13	0.10	13.48	24.21	2	0.76	0.93	0.58

Figure 10. Design Matrix for Amazon Rainforest

B. Design Matrix for Sahara Desert

TRIAL	colza	catza	azi	cldfrc	cldrad	clrrad	cmprad	pwater	ozone	phscld	aertau	aerssa	aerasy
	0.20	0.44	0.00	0.00	0.07	0.05	0.07	2.02	24.01	1	0.12	0.93	0.66
	0.60	0.71	89.50	0.50	0.31	0.20	0.22	19.32	27.41	n/a	0.37	0.94	0.69
	0.99	0.99	179.00	1.00	0.55	0.35	0.33	36.62	30.81	2	0.61	0.95	0.72
1	0.99	0.99	0.00	0.00	0.07	0.35	0.33	36.62	30.81	2	0.61	0.95	0.69
2	0.20	0.71	0.00	0.00	0.55	0.05	0.33	36.62	30.81	1	0.12	0.95	0.72
3	0.99	0.71	0.00	1.00	0.07	0.20	0.07	36.62	27.41	1	0.12	0.95	0.72
4	0.20	0.99	0.00	1.00	0.31	0.35	0.07	2.02	30.81	1	0.12	0.95	0.72
5	0.20	0.44	89.50	1.00	0.55	0.20	0.33	2.02	30.81	2	0.12	0.93	0.66
6	0.20	0.44	179.00	0.00	0.07	0.05	0.33	2.02	30.81	1	0.12	0.95	0.66
7	0.20	0.99	0.00	0.00	0.55	0.35	0.33	2.02	27.41	2	0.12	0.95	0.66
8	0.99	0.44	0.00	0.00	0.07	0.05	0.07	36.62	24.01	2	0.61	0.93	0.72
9	0.99	0.99	0.00	0.00	0.55	0.05	0.07	2.02	30.81	1	0.12	0.95	0.66
10	0.99	0.44	179.00	0.00	0.07	0.35	0.07	2.02	24.01	1	0.61	0.95	0.72
*	*	*	*	*	*	*	*	*	*	*	*	*	*
*	*	*	*	*	*	*	*	*	*	*	*	*	*
*	*	*	*	*	*	*	*	*	*	*	*	*	*
118	0.20	0.71	0.00	1.00	0.55	0.20	0.33	36.62	24.01	2	0.12	0.93	0.69
119	0.20	0.71	179.00	1.00	0.31	0.35	0.33	19.32	24.01	1	0.12	0.93	0.66
120	0.20	0.44	89.50	0.00	0.55	0.05	0.33	2.02	24.01	2	0.61	0.95	0.69
121	0.60	0.99	179.00	0.50	0.07	0.05	0.33	2.02	24.01	1	0.37	0.93	0.69
122	0.99	0.44	0.00	0.00	0.31	0.20	0.22	36.62	30.81	2	0.12	0.95	0.66
123	0.99	0.99	179.00	1.00	0.31	0.35	0.33	36.62	30.81	2	0.12	0.93	0.72
124	0.20	0.44	0.00	0.00	0.07	0.35	0.07	19.32	24.01	2	0.37	0.95	0.66
125	0.99	0.99	0.00	1.00	0.07	0.35	0.07	2.02	24.01	1	0.61	0.94	0.66
126	0.99	0.44	179.00	1.00	0.07	0.05	0.07	36.62	30.81	2	0.12	0.95	0.69
127	0.60	0.71	179.00	0.00	0.55	0.05	0.07	19.32	24.01	1	0.61	0.93	0.72
128	0.20	0.44	179.00	0.50	0.55	0.35	0.22	2.02	24.01	2	0.61	0.94	0.66

Figure 11. Design Matrix for Sahara Desert

C. Design Matrix for Indian Ocean

TRIAL	colza	catza	azi	cldfrc	cldrad	clrrad	cmprad	pwater	ozone	phscld	aertau	aerssa	aerasy
	0.20	0.40	0.00	0.00	0.01	0.00	0.18	25.98	23.83	1	0.05	0.96	0.64
	0.58	0.69	84.50	0.50	0.47	0.05	0.21	44.93	25.56	n/a	0.08	0.98	0.67
	0.96	0.99	169.00	1.00	0.93	0.11	0.26	63.88	27.29	2	0.11	0.99	0.71
1	0.96	0.99	0.00	0.00	0.01	0.11	0.26	63.88	27.29	2	0.11	0.99	0.67
2	0.20	0.69	0.00	0.00	0.93	0.00	0.26	63.88	27.29	1	0.05	0.99	0.71
3	0.96	0.69	0.00	1.00	0.01	0.05	0.18	63.88	25.56	1	0.05	0.99	0.71
4	0.20	0.99	0.00	1.00	0.47	0.11	0.18	25.98	27.29	1	0.05	0.99	0.71
5	0.20	0.40	84.50	1.00	0.93	0.05	0.26	25.98	27.29	2	0.05	0.96	0.64
6	0.20	0.40	169.00	0.00	0.01	0.00	0.26	25.98	27.29	1	0.05	0.99	0.64
7	0.20	0.99	0.00	0.00	0.93	0.11	0.26	25.98	25.56	2	0.05	0.99	0.64
8	0.96	0.40	0.00	0.00	0.01	0.00	0.18	63.88	23.83	2	0.11	0.96	0.71
9	0.96	0.99	0.00	0.00	0.93	0.00	0.18	25.98	27.29	1	0.05	0.99	0.64
10	0.96	0.40	169.00	0.00	0.01	0.11	0.18	25.98	23.83	1	0.11	0.99	0.71
*	*	*	*	*	*	*	*	*	*	*	*	*	*
*	*	*	*	*	*	*	*	*	*	*	*	*	*
*	*	*	*	*	*	*	*	*	*	*	*	*	*
118	0.20	0.69	0.00	1.00	0.93	0.05	0.26	63.88	23.83	2	0.05	0.96	0.67
119	0.20	0.69	169.00	1.00	0.47	0.11	0.26	44.93	23.83	1	0.05	0.96	0.64
120	0.20	0.40	84.50	0.00	0.93	0.00	0.26	25.98	23.83	2	0.11	0.99	0.67
121	0.58	0.99	169.00	0.50	0.01	0.00	0.26	25.98	23.83	1	0.08	0.96	0.67
122	0.96	0.40	0.00	0.00	0.47	0.05	0.21	63.88	27.29	2	0.05	0.99	0.64
123	0.96	0.99	169.00	1.00	0.47	0.11	0.26	63.88	27.29	2	0.05	0.96	0.71
124	0.20	0.40	0.00	0.00	0.01	0.11	0.18	44.93	23.83	2	0.08	0.99	0.64
125	0.96	0.99	0.00	1.00	0.01	0.11	0.18	25.98	23.83	1	0.11	0.98	0.64
126	0.96	0.40	169.00	1.00	0.01	0.00	0.18	63.88	27.29	2	0.05	0.99	0.67
127	0.58	0.69	169.00	0.00	0.93	0.00	0.18	44.93	23.83	1	0.11	0.96	0.71
128	0.20	0.40	169.00	0.50	0.93	0.11	0.21	25.98	23.83	2	0.11	0.98	0.64

Figure 12. Design Matrix for Indian Ocean

D. Design Matrix for Mt Everest

TRIAL	colza	catza	azi	cldfrc	cldrad	clrrad	cmprad	pwater	ozone	phscld	aertau	aerssa	aerasy
	0.20	0.45	3.99	0.00	0.00	0.00	0.07	12.76	23.21	1	0.09	0.95	0.62
	0.60	0.72	80.07	0.50	0.45	0.05	0.09	35.80	28.69	n/a	0.14	0.96	0.65
	0.99	0.99	156.14	1.00	0.89	0.10	0.13	58.85	34.17	2	0.18	0.98	0.67
1	0.99	0.99	3.99	0.00	0.00	0.10	0.13	58.85	34.17	2	0.18	0.98	0.65
2	0.20	0.72	3.99	0.00	0.89	0.00	0.13	58.85	34.17	1	0.09	0.98	0.67
3	0.99	0.72	3.99	1.00	0.00	0.05	0.07	58.85	28.69	1	0.09	0.98	0.67
4	0.20	0.99	3.99	1.00	0.45	0.10	0.07	12.76	34.17	1	0.09	0.98	0.67
5	0.20	0.45	80.07	1.00	0.89	0.05	0.13	12.76	34.17	2	0.09	0.95	0.62
6	0.20	0.45	156.14	0.00	0.00	0.00	0.13	12.76	34.17	1	0.09	0.98	0.62
7	0.20	0.99	3.99	0.00	0.89	0.10	0.13	12.76	28.69	2	0.09	0.98	0.62
8	0.99	0.45	3.99	0.00	0.00	0.00	0.07	58.85	23.21	2	0.18	0.95	0.67
9	0.99	0.99	3.99	0.00	0.89	0.00	0.07	12.76	34.17	1	0.09	0.98	0.62
10	0.99	0.45	156.14	0.00	0.00	0.10	0.07	12.76	23.21	1	0.18	0.98	0.67
*	*	*	*	*	*	*	*	*	*	*	*	*	*
*	*	*	*	*	*	*	*	*	*	*	*	*	*
*	*	*	*	*	*	*	*	*	*	*	*	*	*
118	0.20	0.72	3.99	1.00	0.89	0.05	0.13	58.85	23.21	2	0.09	0.95	0.65
119	0.20	0.72	156.14	1.00	0.45	0.10	0.13	35.80	23.21	1	0.09	0.95	0.62
120	0.20	0.45	80.07	0.00	0.89	0.00	0.13	12.76	23.21	2	0.18	0.98	0.65
121	0.60	0.99	156.14	0.50	0.00	0.00	0.13	12.76	23.21	1	0.14	0.95	0.65
122	0.99	0.45	3.99	0.00	0.45	0.05	0.09	58.85	34.17	2	0.09	0.98	0.62
123	0.99	0.99	156.14	1.00	0.45	0.10	0.13	58.85	34.17	2	0.09	0.95	0.67
124	0.20	0.45	3.99	0.00	0.00	0.10	0.07	35.80	23.21	2	0.14	0.98	0.62
125	0.99	0.99	3.99	1.00	0.00	0.10	0.07	12.76	23.21	1	0.18	0.96	0.62
126	0.99	0.45	156.14	1.00	0.00	0.00	0.07	58.85	34.17	2	0.09	0.98	0.65
127	0.60	0.72	156.14	0.00	0.89	0.00	0.07	35.80	23.21	1	0.18	0.95	0.67
128	0.20	0.45	156.14	0.50	0.89	0.10	0.09	12.76	23.21	2	0.18	0.96	0.62

Figure 13. Design Matrix for Mt Everest

Amazon Region Uncertainty Analysis - TOAUP

TOAP	
Factor	***coeff***
colza	154.1117419
cldfrc*cldrad	54.06427701
cldrad	65.56859697
cldfrc	60.57505477
colza*cldrad	43.0150125
colza*cldfrc	24.21200051
azi*azi	-65.6740312
colza*catza	-19.86112823
pwater*pshcld	-31.34222036
colza*colza	-54.42111832
azi*pwater	-15.3607226
catza	17.51297749
pwater	15.01052909
cmprad*aerasy	-9.782613058
catza*aertau	-10.07362949
aertau*aerssa	10.31365884
clrrad*clrrad	29.61860823
azi*pshcld	-17.40928998
clrrad	12.09283592
cmprad	11.68931142
colza*clrrad	8.94938664
cldfrc*aerasy	-8.72282627
colza*aertau	-8.010861627
cldfrc*aertau	-8.342771651
colza*azi	8.149323664

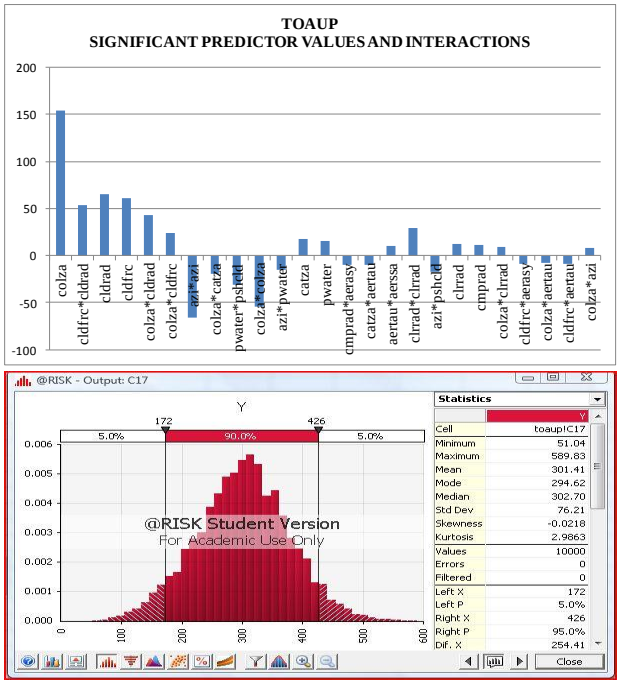

Figure 14. Amazon Region Uncertainty Analysis - TOAUP

Amazon Region Uncertainty Analysis – SRFDWNFLX

SRFDWNFLX	
Factor	***Coeff***
colza	382.9461164
colza*cldfrc	-90.63405531
pwater*pshcld	108.9176169
cldfrc*pshcld	-104.0961336
colza*pshcld	-96.54917188
cldfrc*cldrad	-53.24440353
cmprad*ozone	46.54944911
cldrad	-54.02676806
azi*aerasy	41.60918266
cmprad*aertau	38.89942004
clrrad*aerssa	-36.44564153
cldfrc*cmprad	-37.02796033
pwater	-44.26567483
colza*aerssa	-33.65453932
cldfrc	-45.10353722
catza*aerssa	-32.19221218
cldfrc*pwater	30.68786027
ozone*pshcld	52.66211027
cldrad*aerasy	24.6052091
colza*colza	93.0791078
aertau*aerasy	-23.0985605
colza*cmprad	-23.61064069
colza*pwater	23.57226813
pshcld*aertau	45.2910791
cldfrc*clrrad	-24.08195858
clrrad*ozone	21.51405464
ozone*aertau	-21.73255895
cmprad*pwater	22.39020449
aertau	-30.59768048
azi*cldrad	20.81361175
cmprad	-29.35991234

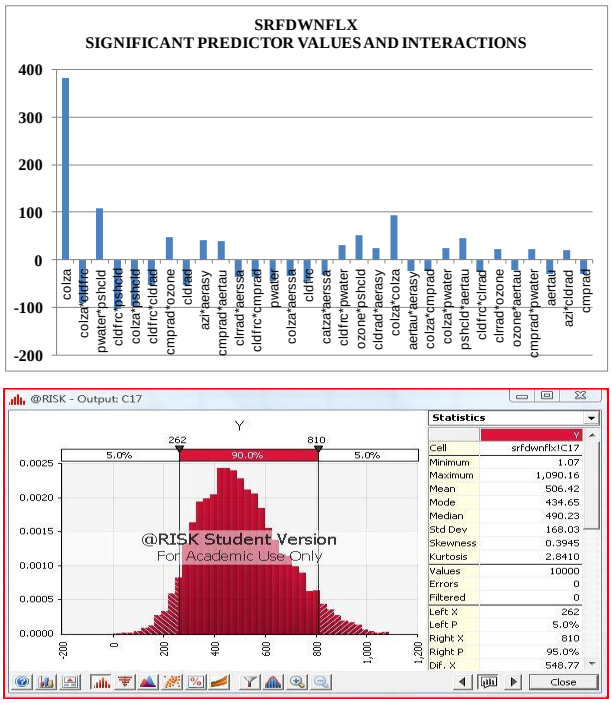

Figure 15. Amazon Region Uncertainty Analysis – SRFDWNFLX

Amazon Region Uncertainty Analysis – SRFDWNDIFF

SRFDWNDIFF	
Factor	***Coeff***
colza	140.6291315
cldfrc*clrrad	52.85939655
clrrad*aertau	-43.16895246
cmprad*aerasy	37.95462644
cldfrc*cldrad	40.40664113
colza*cldrad	40.45512973
cldrad*pwater	-36.4055498
azi*cldrad	-33.00641562
cldfrc*aerssa	-30.44506
aertau	45.61121845
colza*clrrad	-33.35983669
cmprad	43.04506968
clrrad*cmprad	-30.6144951
colza*cmprad	30.90827792
colza*catza	28.79746925
catza*aerssa	27.82603932

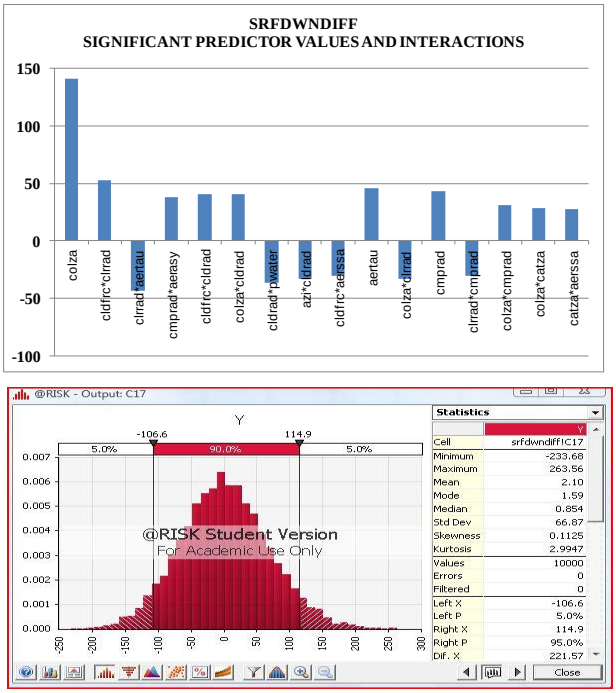

Figure 16. Amazon Region Uncertainty Analysis - SRFDWNDIFF

Amazon Region Uncertainty Analysis - SRFUPFLX

SRFUPFLX	
Factor	***Coeff***
colza	132.304397
colza*cldfrc	-31.36328236
colza*catza	-21.13445332
colza*pwater	19.71625229
cmprad*ozone	19.09001726
cldfrc*cmprad	-18.36853157
cldfrc*pshcld	-32.44337933
azi*aerasy	17.73329134
cldfrc*cldrad	-17.67275699
pwater*pshcld	31.87459228
colza*pshcld	-29.89265634
cldfrc	-21.6984442
colza*aerssa	-15.55891502
clrrad*aerssa	-14.56922056
catza*aerssa	-14.56429006
cmprad*aertau	14.63020705
catza*catza	-45.87126499
clrrad	15.78025572
cldrad	-14.87876133
cmprad	15.20509837
ozone*aertau	-10.48787161
cldfrc*pwater	10.98236064
pwater*aerasy	10.51209738

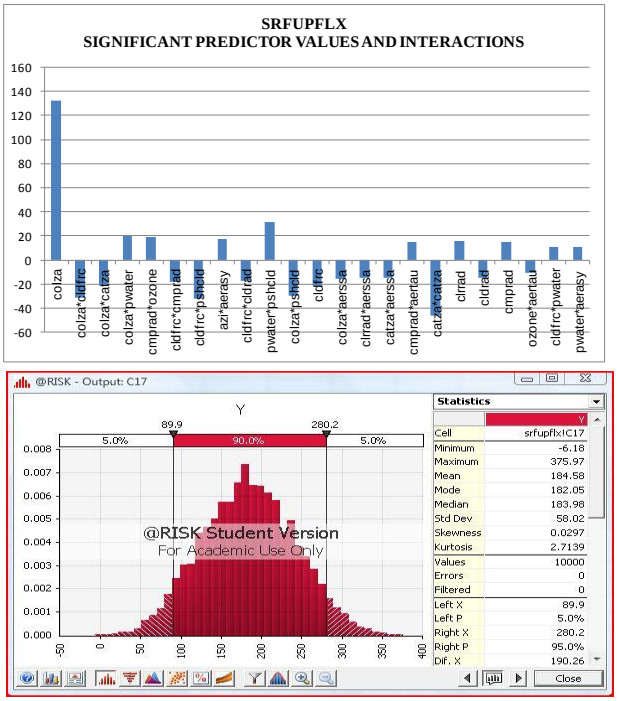

Figure 17. Amazon Region Uncertainty Analysis - SRFUPFLX

Amazon Region Uncertainty Analysis - SRFDWNDIFPAR

SRFDWNDIFPAR	
Factor	***Coeff***
colza	68.50564991
cldfrc*clrrad	24.22765232
clrrad*aertau	-20.06901209
colza*cldrad	20.06921577
cmprad*aerasy	17.42519503
cldfrc*cldrad	18.23056897
cldrad*pwater	-16.69790855
azi*cldrad	-15.82664449
cldfrc*aerssa	-14.02151098
aertau	20.61476343
colza*clrrad	-15.24468961
clrrad*cmprad	-13.89058232
cmprad	19.22129042
colza*catza	13.73947227
colza*cmprad	13.61147964

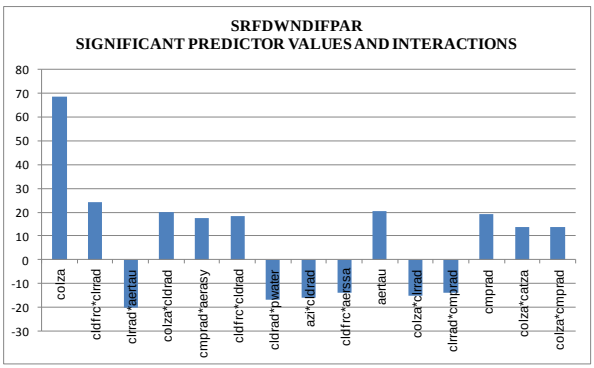

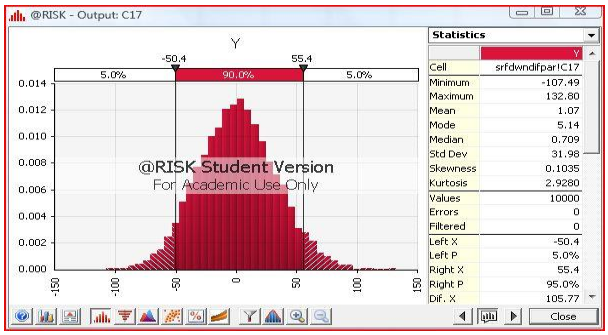

Figure 18. Amazon Region Uncertainty Analysis - SRFDWNDIFPAR

Amazon Region Uncertainty Analysis - SRFDWNPAR

SRFDWNPAR	
Factor	***Coeff***
colza	183.7465452
colza*cldfrc	-42.8286404
cldfrc*pshcld	-48.14789523
pwater*pshcld	49.25604162
cldfrc*cldrad	-25.77094842
colza*pshcld	-44.703991
cmprad*ozone	21.99729735
cldrad	-25.94422743
azi*aerasy	19.2173146
cldfrc*cmprad	-18.49930881
cmprad*aertau	17.66500732

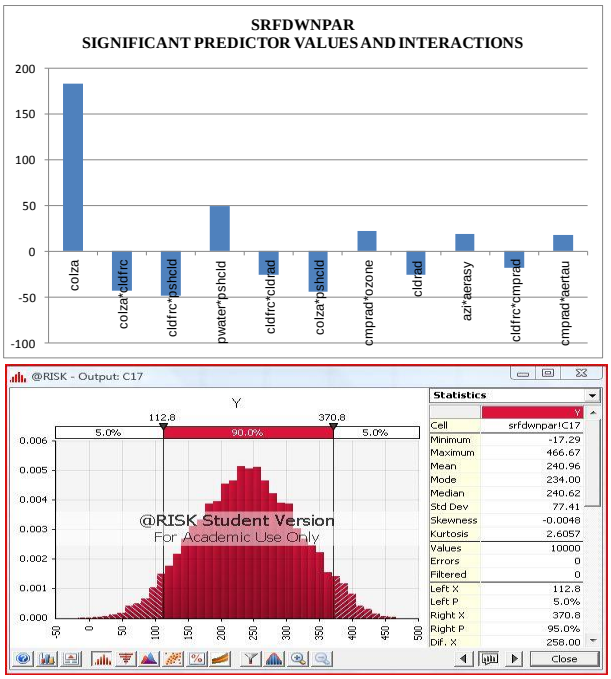

Figure 19. Amazon Region Uncertainty Analysis - SRFDWNPAR

Amazon Region Uncertainty Analysis – TOAUPCLRSKY

TOAUPCLRSKY	
Factor	***Coeff***
colza	122.5807966
colza*catza	-22.53847349
clrrad	19.43870509
catza	14.8353809
cmprad	15.30914142
colza*cmprad	10.82964395
clrrad*cmprad	9.507684515
clrrad*aerssa	-8.146602301
azi*azi	-23.24834659
colza*azi	7.359634583
colza*colza	-25.25152678
clrrad*aertau	6.096362083
cldrad	8.223917305
cldrad*ozone	5.583431609
azi*cldfrc	5.925828331
cldrad*pshcld	-9.814651575
cmprad*cmprad	-16.31044703
catza*azi	-4.391636058

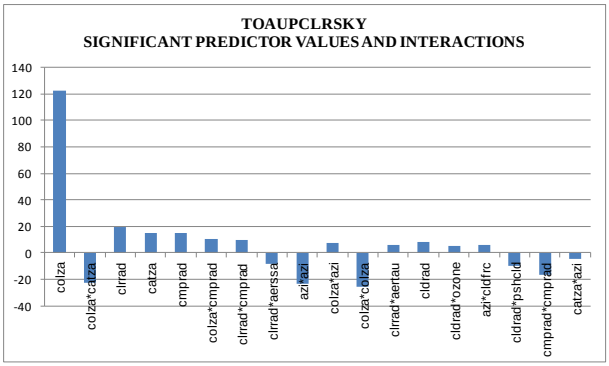

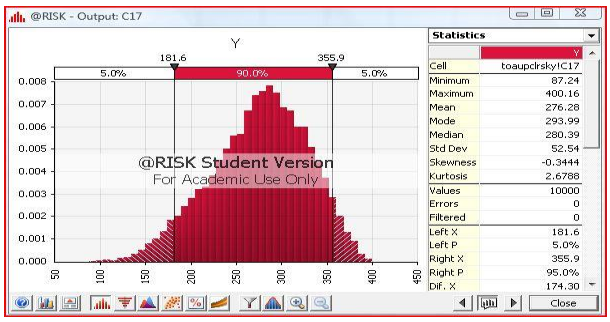

Figure 20. Amazon Region Uncertainty Analysis – TOAUPCLRSKY

Amazon Region Uncertainty Analysis – SRFDWNCLRSKY

SRFDWNCLRSKY	
Factor	***Coeff***
colza	424.8663371
clrrad*cmprad	41.46528915
clrrad	33.64663523
colza*colza	88.08843202
colza*clrrad	24.26664451
colza*cmprad	-22.93573408
catza*aerssa	-22.50504789
cmprad*aerasy	-15.79117927
cmprad*aerssa	15.39591456
pwater	-21.12603227
clrrad*aertau	15.13241847
azi*cldfrc	14.21234683
cldfrc*cmprad	-14.03179136
azi*cldrad	12.74367668
azi*aertau	-12.86929384
cldrad*pwater	12.43188218
clrrad*aerssa	-11.61363723
cldrad	15.44375107
aertau	-15.37448259
catza*azi	10.51780448
ozone	-14.46667822

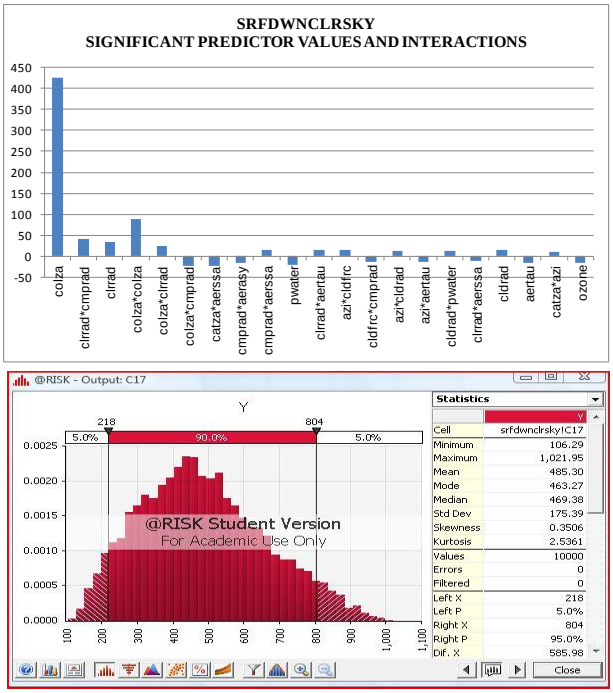

Figure 21. Amazon Region Uncertainty Analysis – SRFDWNCLRSKY

Amazon Region Uncertainty Analysis – SRFUPCLRFLX

SRFDWNCLRSKY	
Factor	***Coeff***
colza	424.8663371
clrrad*cmprad	41.46528915
clrrad	33.64663523
colza*colza	88.08843202
colza*clrrad	24.26664451
colza*cmprad	-22.93573408
catza*aerssa	-22.50504789
cmprad*aerasy	-15.79117927
cmprad*aerssa	15.39591456
pwater	-21.12603227
clrrad*aertau	15.13241847
azi*cldfrc	14.21234683
cldfrc*cmprad	-14.03179136
azi*cldrad	12.74367668
azi*aertau	-12.86929384
cldrad*pwater	12.43188218
clrrad*aerssa	-11.61363723
cldrad	15.44375107
aertau	-15.37448259
catza*azi	10.51780448
ozone	-14.46667822

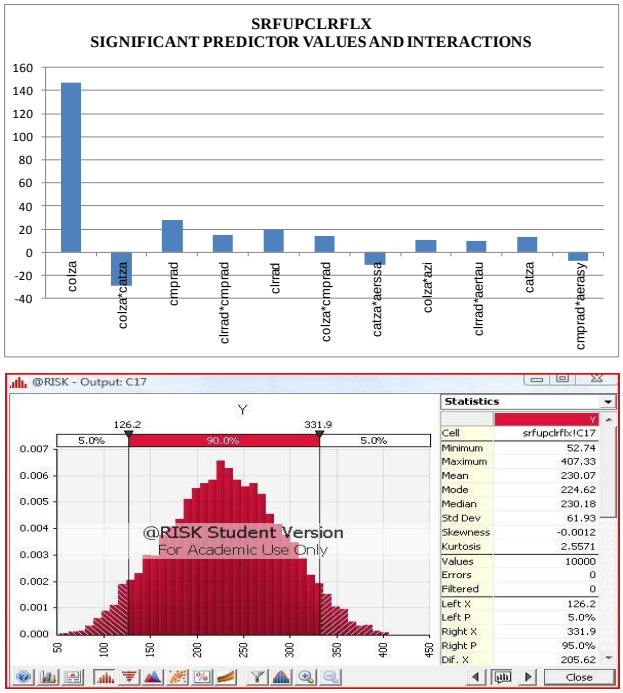

Figure 22. Amazon Region Uncertainty Analysis – SRFUPCLRFLX

Amazon Region Uncertainty Analysis – OAOD

OAOD	
Factor	***Coeff***
clrrad*cmprad	-0.305030181
catza*aerssa	0.198716425
colza*clrrad	-0.172915144
clrrad	-0.194464409
cldfrc*cmprad	0.144621442
colza*cmprad	0.136406778
catza*clrrad	-0.135760712
cmprad*aerssa	-0.119452444
cmprad*aerasy	0.112028769
catza*azi	-0.110786284
colza*colza	-0.382630735
cldfrc*cldrad	0.108306347
clrrad*aertau	-0.093842639
cldrad*pwater	-0.092198229
azi*cldrad	-0.079189527
cmprad*pwater	-0.082763043
catza	0.103241551

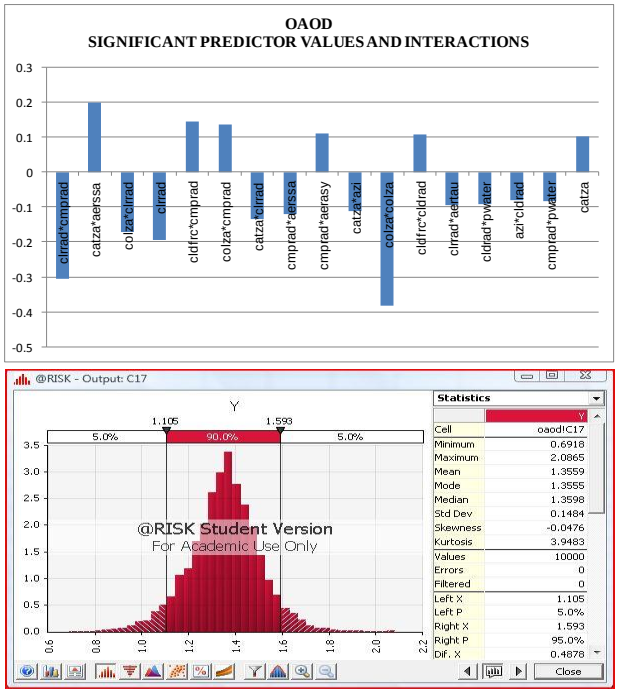

Figure 23. Amazon Region Uncertainty Analysis – OAOD

Amazon Region Uncertainty Analysis - OCOD

OCOD	
Factor	***Coeff***
colza	-44.09184205
catza*cmprad	-30.89194974
catza*cldrad	27.85814198
cldrad*cmprad	-27.47669094
colza*azi	-27.37766995
azi*aerasy	-27.62372129
cldrad*pshcld	-48.0548167
azi*cldfrc	-25.00961139
cldrad*cldrad	-87.94982735
catza*aertau	-22.89407703
colza*aerasy	22.71542643
azi*cldrad	-21.62052934
catza*azi	-21.92844007
aerasy*aerasy	-75.96754576
cmprad*aerasy	-20.95035241
catza*aerasy	21.38873158
cldrad	29.01153562
cldfrc*cldfrc	75.18018945
cmprad	29.05942361
pwater*pshcld	-40.02540502
cldrad*pwater	21.3868386
ozone	-28.29655595
cldfrc*cldrad	19.25879742
pshcld*aerasy	32.79984534
ozone*pshcld	33.43112073
pwater	23.32468689

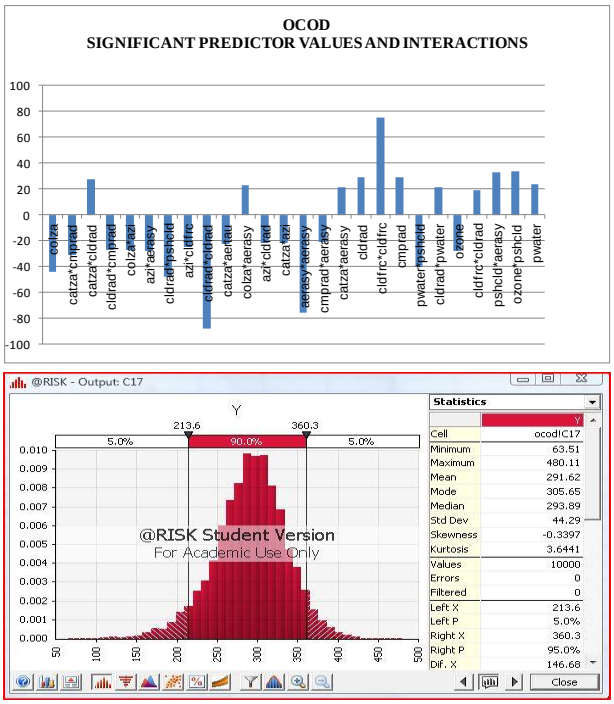

Figure 24. Amazon Region Uncertainty Analysis - OCOD

Amazon Region Uncertainty Analysis - SRFDWNPRS

SRFDWNPRS	
Factor	***Coeff***
colza	440.8498283
pwater	-24.08450211
colza*pwater	-13.96461257
colza*colza	10.31727326
pwater*pwater	8.118681791
ozone	-0.874041655
colza*catza	-0.634928098
cmprad*aerssa	-0.52841465
pshcld*aerasy	0.897757427
catza	0.578377273
cldfrc*ozone	-0.440033686
aerasy	-0.539018721
cmprad	0.542859122
colza*ozone	-0.417078256
cldfrc*pshcld	0.682143866
aerssa*aerasy	-0.332886479
ozone*aertau	0.329869542
cldrad*cldrad	-1.224983961
catza*aerssa	-0.308654634
aertau	0.429883819
azi*aerssa	-0.307208366
cldfrc*cldfrc	1.057682143
cldfrc*cldrad	0.298881948
cldfrc*aerssa	-0.25557451
cldfrc*clrrad	-0.2887614
cldrad	-0.361975341

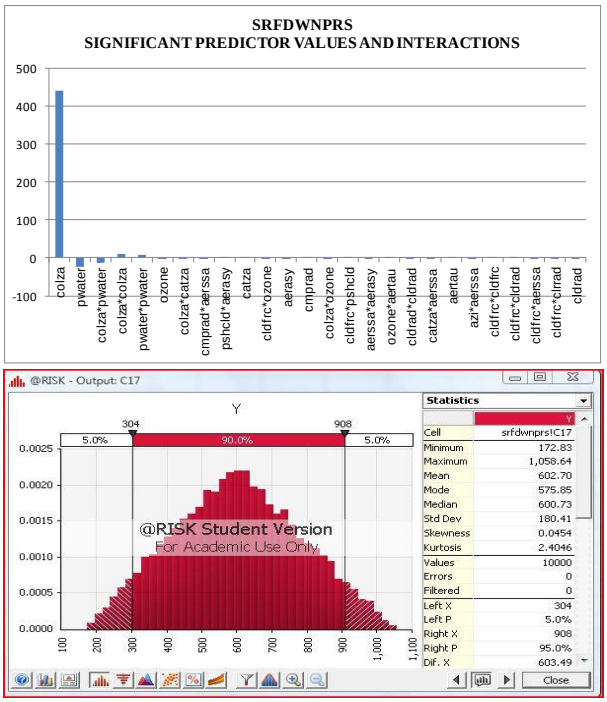

Figure 25. Amazon Region Uncertainty Analysis - SRFDWNPRS

Amazon Region Uncertainty Analysis - TOAUPPRS

TOAUPPRS	
Factor	***Coeff***
colza	139.7801037
colza*catza	-30.25740496
cmprad	34.38421492
colza*cmprad	17.27268999
catza	21.09741306
colza*colza	-38.05039006
azi*cmprad	7.360079807
azi*azi	-22.31343411
colza*azi	7.271951164
cldrad*ozone	6.487533145
cmprad*aerssa	-6.142099262

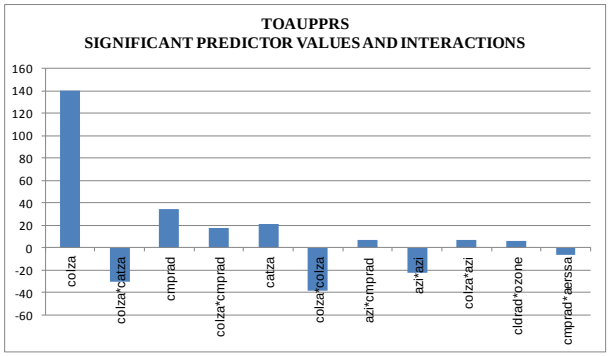

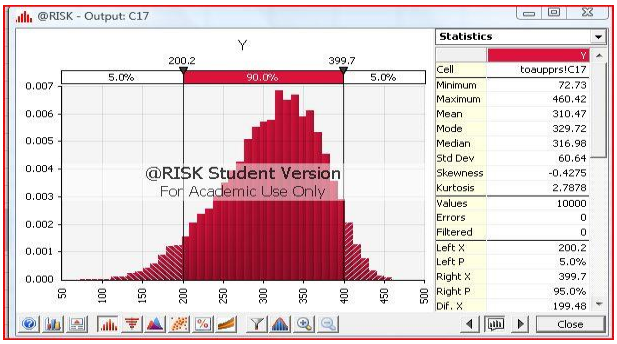

Figure 26. Amazon Region Uncertainty Analysis - TOAUPPRS

Indian Ocean Uncertainty Analysis – TOAUP

TOAP	
Factor	***coeff***
colza	136.8010444
cldfrc*cldrad	104.0002547
cldrad	116.5962273
colza*cldrad	86.67079813
cldfrc	110.5761926
colza*cldfrc	71.10861874
azi*azi	-72.74400195
pwater*pshcld	-42.82584785
azi*pwater	-23.49847519
clrrad	26.41172474
pshcld*aerasy	-34.65641767
clrrad*clrrad	58.28573306
catza*pshcld	34.21874438
aerasy	22.30614197
azi*pshcld	-30.80916273
azi*cldfrc	15.55271443
pwater	20.58112627
catza*cmprad	-15.87217278
catza*aertau	-14.1143738

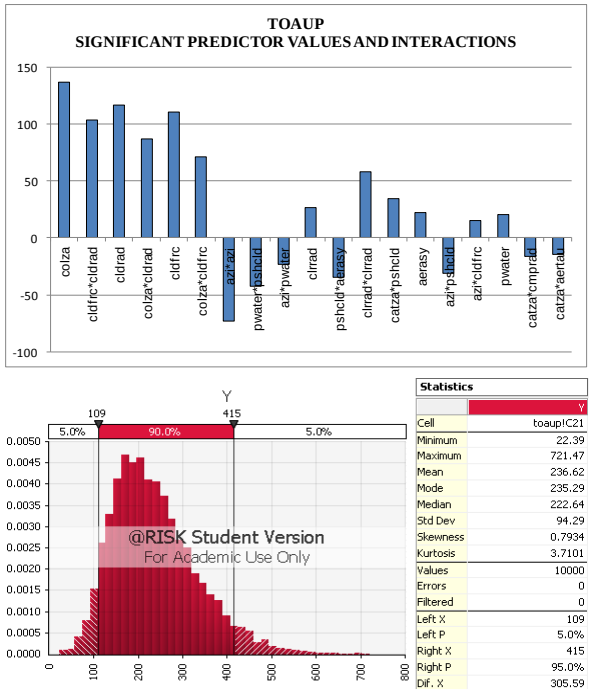

Figure 27. Indian Ocean Uncertainty Analysis – TOAUP

Indian Ocean Uncertainty Analysis – SRFDWNFLX

SRFDWNFLX	
Factor	*Coeff*
colza	302.285188
cldfrc*cldrad	-101.6666469
cldrad	-119.3190072
colza*cldrad	-93.14457016
cldfrc	-116.6031614
colza*cldfrc	-80.36859665
aerasy	-36.88045573
azi*cldfrc	-28.28445273
clrrad*clrrad	-88.02318041
colza*colza	95.16322783
colza*ozone	-28.43461819
clrrad*pshcld	50.92365042
cmprad*pshcld	50.53093944
pshcld*aerasy	44.12332711
colza*azi	-24.20124505
cmprad	-31.55044717
clrrad	-30.86844942
azi*pwater	24.56767643
ozone*aerasy	-21.24195338
colza*pwater	-20.35744395
catza*aerasy	-19.20616032
cmprad*cmprad	-64.61146675
cldfrc*pshcld	-34.48805844
colza*pshcld	-34.61188226
cldrad*aerasy	17.13321456
azi*azi	56.31494111
pshcld*aertau	-34.96479976
cldfrc*cldfrc	62.2950832
cldfrc*aerssa	16.07377331
catza*cldrad	16.9223221
catza*pwater	16.41142705

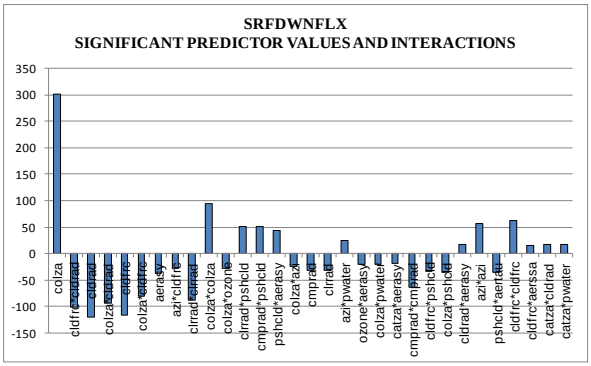

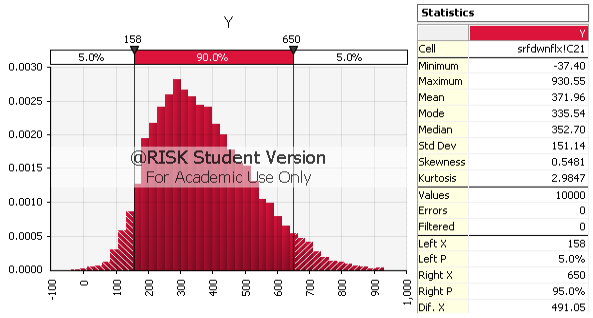

Figure 28. Indian Ocean Uncertainty Analysis – SRFDWNFLX

Indian Ocean Uncertainty Analysis – SRFDWNDIFF

SRFDWNDIFF	
Factor	*Coeff*
colza	197.6527599
cldrad	-79.90631736
colza*cldfrc	-47.27573169
cldfrc*cldrad	-48.89206639
colza*pshcld	-64.15122246
colza*cldrad	-35.62309658
cldfrc*cmprad	-30.38869746
azi	-40.90316228
cldfrc*pshcld	-52.76933685
cldfrc	-38.48473557
azi*cldrad	25.8346537
cldrad*pshcld	50.79175872
pshcld*aerasy	39.25167982
azi*pshcld	38.78534124
cmprad*cmprad	-62.08583001
aertau*aerssa	18.50481267
catza*aerasy	-17.25072563
colza*colza	61.44030884
cldfrc*aertau	-17.26400668
cldrad*cldrad	-62.03472154
catza*cmprad	17.35405751
clrrad*pwater	17.13386905
catza*pwater	16.8521054
catza*aerssa	-16.34788011
ozone*aerssa	-15.64990799
azi*ozone	15.82204443
catza*cldfrc	15.10052392
cldfrc*aerasy	-15.38867285
pwater*aerasy	14.96309904
cldrad*aerasy	14.05345666

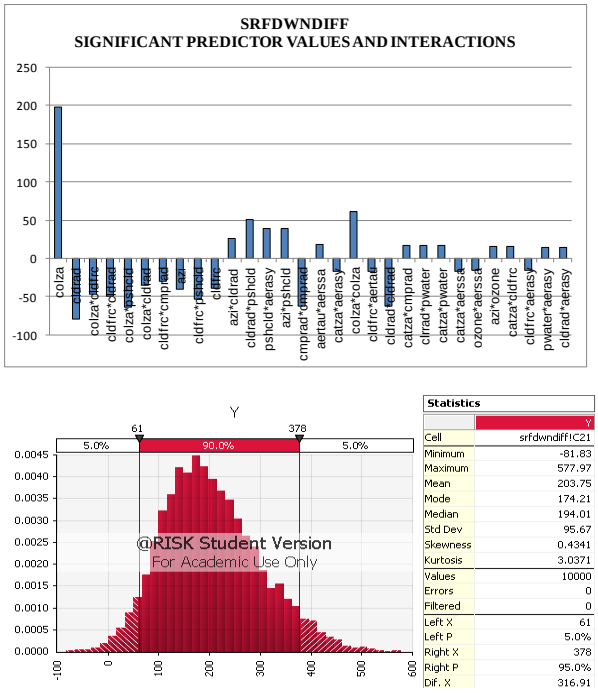

Figure 29. Indian Ocean Uncertainty Analysis – SRFDWNDIFF

Indian Ocean Uncertainty Analysis - SRFUPFLX

SRFUPFLX	
Factor	***Coeff***
cldfrc	-35.48213199
colza	27.49480954
cldfrc*cldrad	-17.58364513
colza*cldrad	-17.77339543
colza*clrrad	-10.71945244
cldrad	-12.77095662
cldfrc*clrrad	-10.00634308
catza*clrrad	9.632513299
pwater*ozone	8.856021539
cldrad*cmprad	-8.291538634
pwater*aertau	8.73064827
colza*catza	-7.999176819
catza*cldfrc	-7.670966348
cmprad*cmprad	-24.00095078
aerasy	-8.842818578
colza*ozone	-7.357600133
cldfrc*cmprad	6.886247618
pwater*aerasy	-6.650113462
catza*azi	6.495442323
colza*cmprad	6.693554502
clrrad*aertau	6.308792779
pwater*pshcld	-11.93404116
pshcld*aertau	-12.26834616
ozone*ozone	-20.80386002
colza*colza	22.13151739
cmprad*pshcld	11.95571781
clrrad	8.110109011
colza*aerssa	5.880480979
cmprad*pwater	-5.67009006
ozone*pshcld	-10.38368268

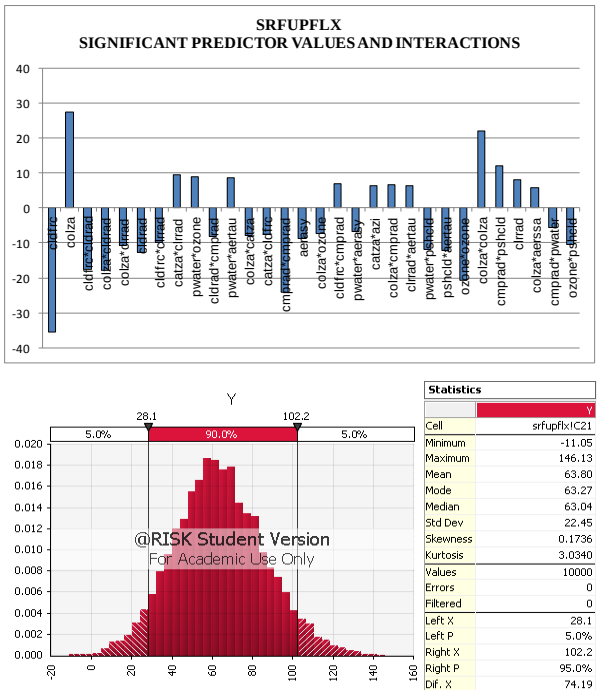

Figure 30. Indian Ocean Uncertainty Analysis - SRFUPFLX

Indian Ocean Uncertainty Analysis - SRFDWNDIFPAR

SRFDWNDIFPAR	
Factor	***Coeff***
colza	99.68472914
cldrad	-38.20346895
cldfrc*cldrad	-23.76095529
colza*cldfrc	-21.13627166
colza*pshcld	-31.3788446
colza*cldrad	-16.60581513
cldfrc*pshcld	-26.32468271
cldfrc*cmprad	-14.31476828
azi	-18.99697744
cldfrc	-18.3386321
cldrad*pshcld	23.72107986
azi*cldrad	11.89072436
pshcld*aerasy	18.6169568
azi*pshcld	18.07641417
colza*colza	31.07159078
aertau*aerssa	8.83489887
cmprad*cmprad	-29.0438892
catza*aerasy	-8.231086639
cldrad*cldrad	-31.57466677
catza*pwater	8.499458038
cldfrc*aertau	-8.373750572
catza*aerssa	-8.083806179
catza*cmprad	8.382038344
clrrad*pwater	7.978029545
azi*ozone	7.796013585
ozone*aerssa	-7.390819699
cldrad*aerasy	6.73135477
catza*cldfrc	7.028984183

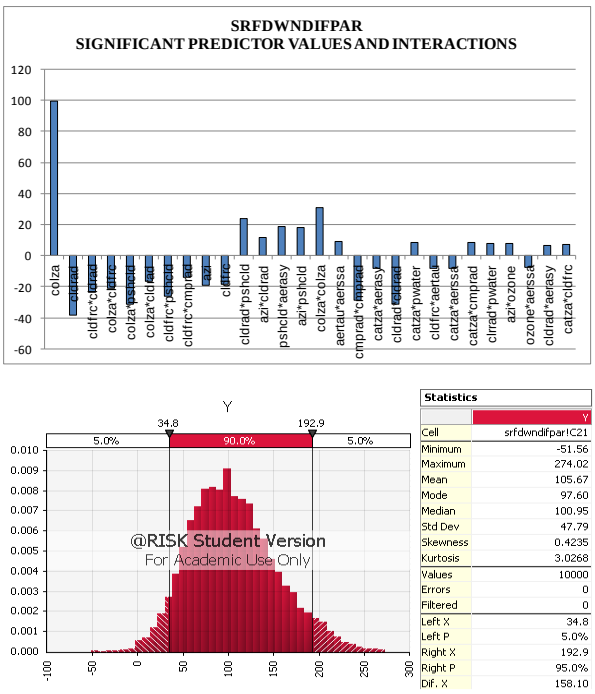

Figure 31. Indian Ocean Uncertainty Analysis - SRFDWNDIFPAR

Indian Ocean Uncertainty Analysis – SRFDWNPAR

SRFDWNPAR	
Factor	*Coeff*
colza	151.0524943
cldfrc*cldrad	-48.98385433
cldrad	-57.37255095
colza*cldrad	-43.97619625
cldfrc	-54.70286742
colza*cldfrc	-37.63316418
aerasy	-17.38388405
azi*cldfrc	-13.42976524
clrrad*clrrad	-42.94853811
clrrad*pshcld	24.72091504
colza*ozone	-13.6519993
cmprad*pshcld	24.67279354
colza*colza	44.41336576
pshcld*aerasy	20.93844783
cmprad	-15.27020893
colza*azi	-11.41071687
clrrad	-14.74576505
ozone*aerasy	-10.1301848
azi*pwater	11.35797788
cldfrc*pshcld	-17.66946753
catza*aerasy	-9.28736525
colza*pshcld	-17.72316881
cldrad*aerasy	8.47904859
cmprad*cmprad	-30.35673906
pshcld*aertau	-17.23913739
cldfrc*cldfrc	30.15757579
azi*azi	26.1995602
catza*cldrad	8.116255888
cldfrc*aerssa	7.448936096
catza*pwater	8.2464186
cmprad*aerasy	7.390423291
ozone*aertau	-7.498459322
catza*cmprad	7.937794854

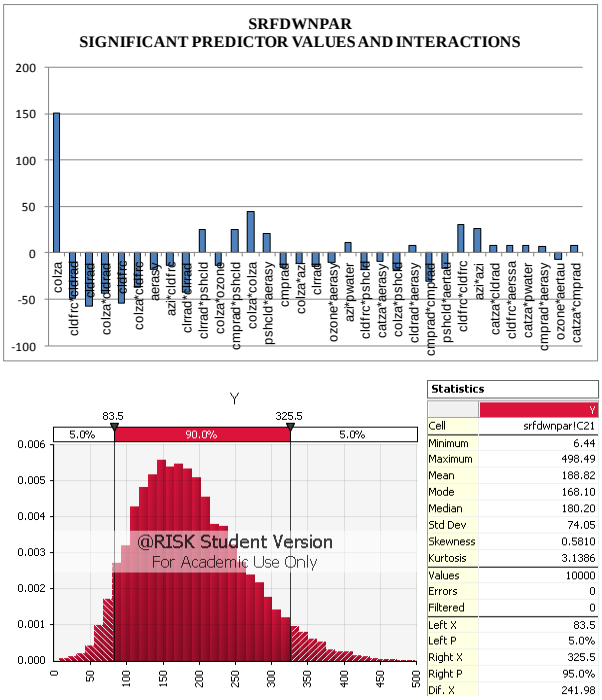

Statistics	
	Y
Cell	srfdwnpar!C21
Minimum	6.44
Maximum	498.49
Mean	188.82
Mode	168.10
Median	180.20
Std Dev	74.05
Skewness	0.5810
Kurtosis	3.1386
Values	10000
Errors	0
Filtered	0
Left X	83.5
Left P	5.0%
Right X	325.5
Right P	95.0%
Dif. X	241.98

Figure 32. Indian Ocean Uncertainty Analysis – SRFDWNPAR

Indian Ocean Uncertainty Analysis – TOAUPCLRSKY

TOAUPCLRSKY	
Factor	***Coeff***
colza	53.27486186
colza*clrrad	-14.96979348
colza*catza	-13.43416141
clrrad	16.05845461
catza*clrrad	11.15252232
cmprad	14.54675437
catza	13.0195057
colza*cmprad	9.519858727
colza*azi	8.999606874
clrrad*aertau	7.435882938
catza*azi	7.48114482
colza*colza	-25.35525729
pwater*aertau	7.271420936
clrrad*aerasy	6.650708501
cldrad*ozone	5.725442011
azi*azi	-18.65606349
azi	-8.143748579
clrrad*clrrad	18.43403917
cldfrc*aertau	-5.861520883
ozone*ozone	-18.42099755
aerssa	8.408137133
colza*aerssa	5.405921497
azi*cmprad	5.08569274
cmprad*ozone	-4.747191162
clrrad*pshcld	-8.639997435
pwater*pwater	14.40260771

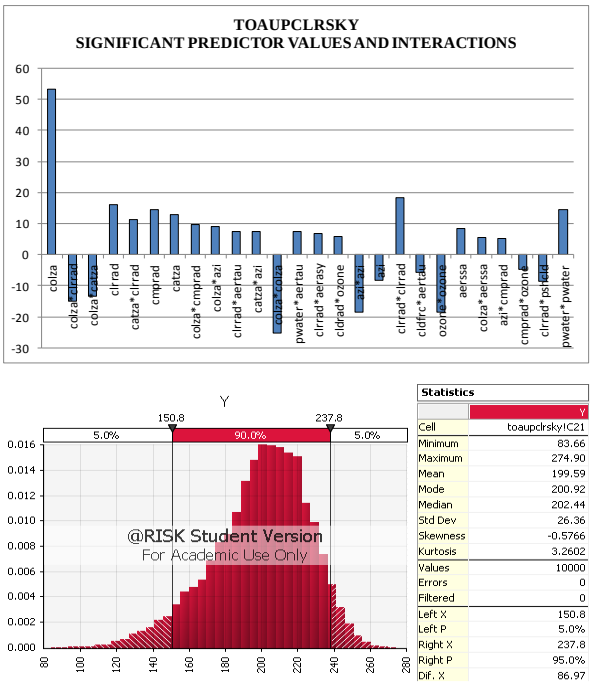

Figure 33. Indian Ocean Uncertainty Analysis – TOAUPCLRSKY

Indian Ocean Uncertainty Analysis – SRFDWNCLRSKY

SRFDWNCLRSKY	
Factor	***Coeff***
colza	381.709889
cmprad	-26.378844
colza*cmprad	-16.753786
colza*colza	47.2747457
cmprad*aerssa	10.1851715
pwater	-12.827438
colza*aerasy	-9.6088951
colza*azi	-9.6416104
colza*clrrad	-8.0418498
azi	10.4130804
clrrad*aertau	-7.1093995
cldfrc*cldfrc	23.7728968
azi*pshcld	-12.852417
clrrad	8.79498871
azi*cmprad	-6.4398671
aerssa*aerssa	-21.562312
azi*cldrad	-6.0036885
clrrad*aerasy	-6.2900644
colza*pwater	-5.9839559
aertau*aerssa	-5.832602

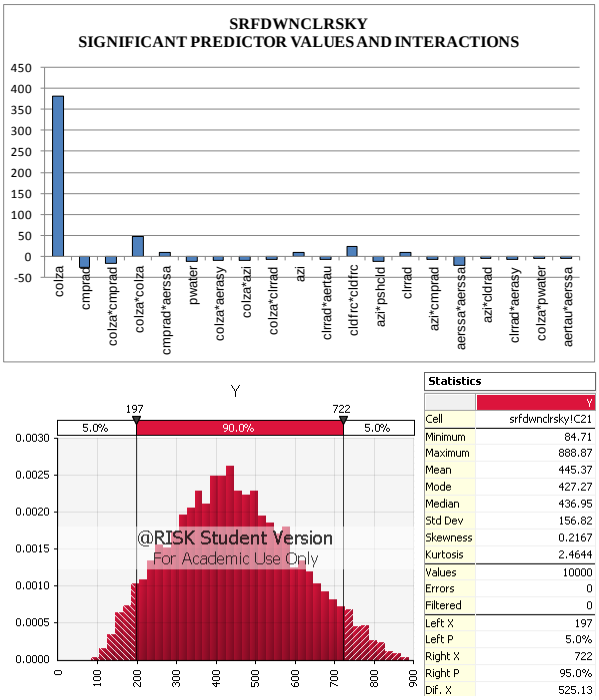

Figure 34. Indian Ocean Uncertainty Analysis – SRFDWNCLRSKY

Indian Ocean Uncertainty Analysis – SRFUPCLRFLX

SRFUPCLRFLX	
Factor	***Coeff***
colza	34.20881565
colza*clrrad	-23.13757651
clrrad	25.07496302
colza*catza	-14.39362969
catza*clrrad	14.39088894
catza	12.35718983
cmprad*aerasy	-5.926178751
clrrad*ozone	5.904533788

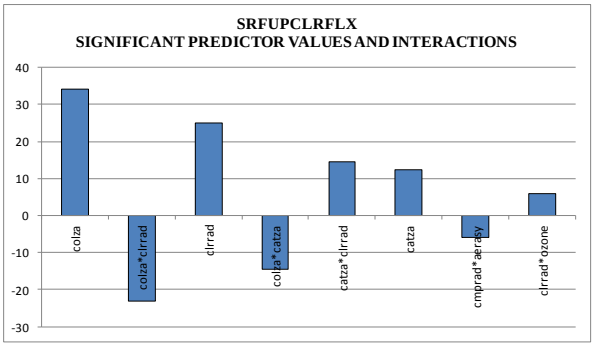

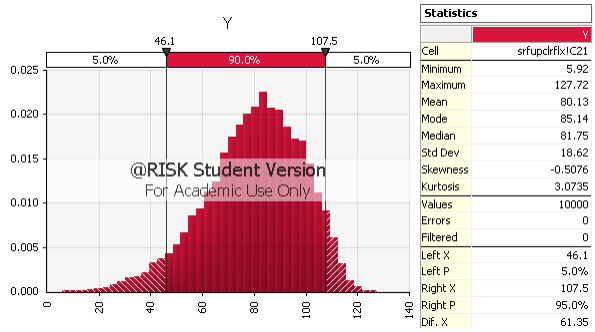

Figure 35. Indian Ocean Uncertainty Analysis – SRFUPCLRFLX

Indian Ocean Uncertainty Analysis – OAOD

OAOD	
Factor	***Coeff***
colza	0.3383956
cmprad	0.17790742
colza*cmprad	0.09984941
colza*aerasy	0.09585278
colza*azi	0.08194952
colza*clrrad	0.07635142
colza*colza	-0.259449
azi	-0.091098
cmprad*aerssa	-0.0611575
clrrad	-0.0769373
azi*cmprad	0.05438405
clrrad*aertau	0.05034663
aertau*aerssa	0.0470889
aerssa*aerssa	0.15632282
azi*pshcld	0.08758804
cldfrc*cldfrc	-0.1606022
aerasy	0.05734049
azi*cldrad	0.04327788
cmprad*aerasy	0.03789615

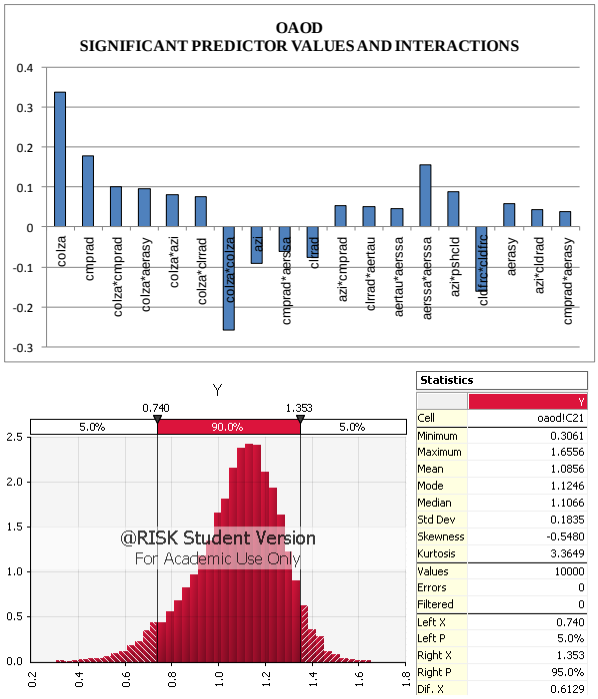

Figure 36. Indian Ocean Uncertainty Analysis – OAOD

Indian Ocean Uncertainty Analysis – OCOD

OCOD	
Factor	***Coeff***
cldrad	72.90091985
colza	-53.50029294
colza*azi	-34.00441008
catza*azi	-29.32616855
catza*cldrad	27.44828612
cmprad*aerasy	-25.82119693
cmprad*ozone	26.68555545
cldrad*pshcld	-43.64346463
azi*cldrad	-21.85713668
cldrad*aerasy	20.30323881
catza*aerssa	-20.59960078
cldfrc*cmprad	-19.99231591
cldrad*cldrad	-73.27095791
aertau*aerasy	-18.64273644
colza*catza	17.98104335

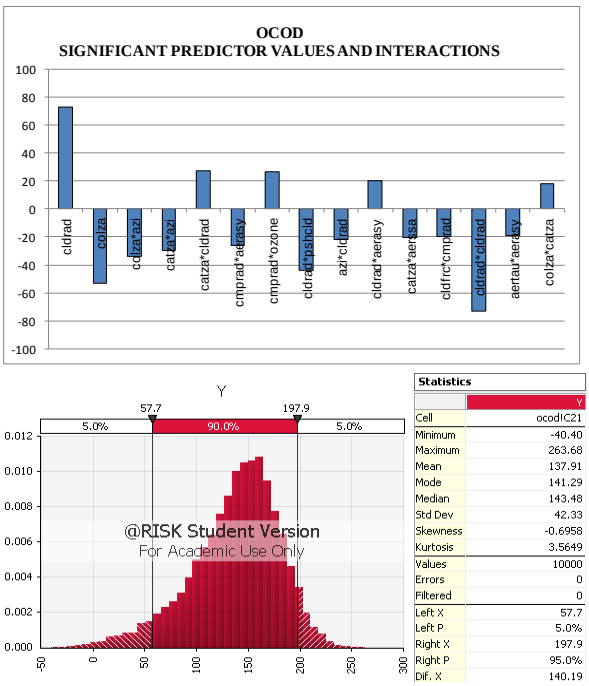

Figure 37. Indian Ocean Uncertainty Analysis – OCOD

Indian Ocean Uncertainty Analysis - SRFDWNPRS

SRFDWNPRS	
Factor	***Coeff***
colza	438.8815077
pwater	-14.16375035
colza*pwater	-8.284500806
pwater*pwater	8.976069467
colza*colza	6.108648484
cmprad	1.417858848
cmprad*aerssa	-0.980900575
colza*cmprad	0.77663444
catza	0.985820457
pshcld*aerasy	1.213982505
cldfrc*ozone	-0.647826788
colza*azi	0.644991958
clrrad*clrrad	1.983058583
cldrad*ozone	0.568015181
catza*aerssa	-0.58337155
ozone	-0.801743604
aerasy	-0.732407095
clrrad*aertau	0.553713411
ozone*aerssa	-0.540600705
azi*cmprad	0.504973275
cldfrc*pshcld	0.927331864
azi	-0.699672948
ozone*ozone	-1.661182693
pwater*aerssa	0.469325203
ozone*aertau	0.438008361
azi*cldrad	0.429066579
catza*ozone	0.412627903
colza*catza	-0.42972842
catza*azi	0.40766183

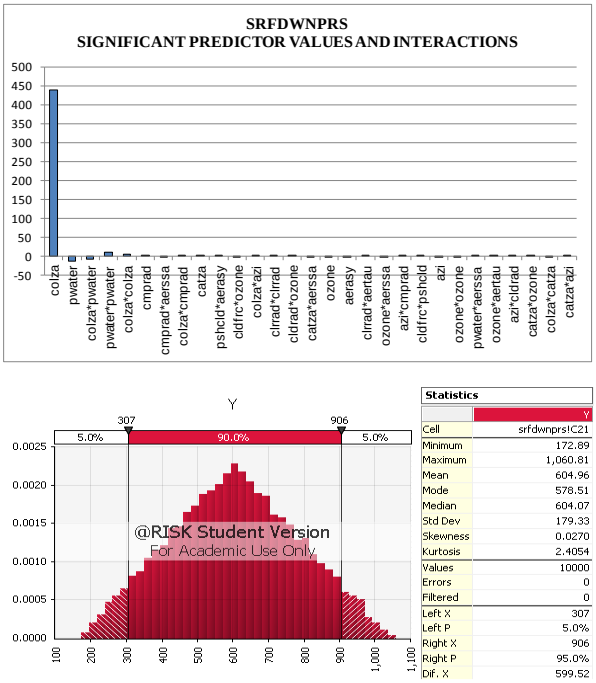

Figure 38. Indian Ocean Uncertainty Analysis - SRFDWNPRS

Indian Ocean Uncertainty Analysis – TOAUPPRS

TOAUPPRS	
Factor	***Coeff***
colza	57.8239753
colza*colza	-156.7713221
cmprad	39.44176545
colza*cmprad	22.69109428
colza*azi	21.27966364
clrrad*aertau	19.03390455
catza	24.08496039
cmprad*aerssa	-16.95676391
azi*cmprad	17.61450268
cldrad*ozone	14.83392761
azi	-21.07423632
colza*catza	-14.08941446
ozone*ozone	-42.73224904
clrrad*clrrad	39.98296437
pwater*pwater	40.50629825
cldfrc*cldfrc	-42.87752274
colza*aerssa	12.31044165
ozone*aerssa	-11.68380681
catza*azi	11.50094512
aerssa*aerssa	39.57502171
catza*aerssa	-10.35429893
azi*aerssa	10.00738144

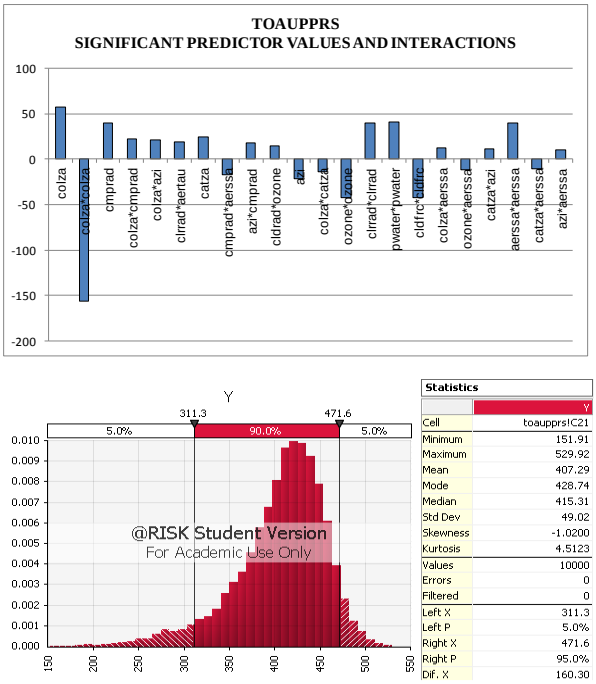

Figure 39. Indian Ocean Uncertainty Analysis – TOAUPPRS

Mt Everest Region Uncertainty Analysis – TOAUP

TOAP	
Factor	***coeff***
cldfrc*cldrad	115.2212428
cldfrc	140.2430722
colza*cldrad	107.7495571
cldrad	130.5245471
colza*cldfrc	87.93354856
colza	98.42277257
azi*azi	-93.9618548
azi*pwater	-29.5821811
aerasy	33.52102692
pshcld*aerasy	-48.76786558
azi*cldfrc	20.8863524
cmprad*cmprad	70.68902025
cmprad	27.62602964
colza*ozone	21.32667562
clrrad*clrrad	62.49226464
ozone*aerssa	19.12020808
catza*aertau	-18.22343993
clrrad	23.7189156
catza*cmprad	-18.45030038
catza*pshcld	31.41133532
pwater*pshcld	-31.09852347
azi*pshcld	-30.60353962

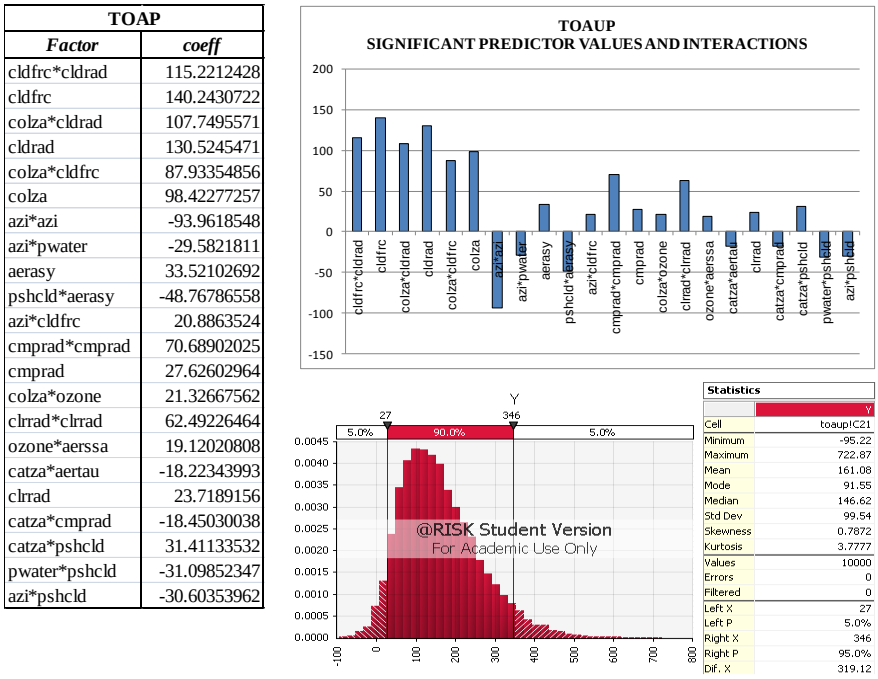

Figure 40. Mt Everest Region Uncertainty Analysis – TOAUP

Mt Everest Region Uncertainty Analysis - SRFDWNFLX

SRFDWNFLX	
Factor	***Coeff***
colza	344.8860811
colza*cldfrc	-151.5897099
cldfrc	-173.0218529
cldfrc*cldrad	-83.05843004
cldrad	-85.95620817
cldfrc*cmprad	-50.83706681
colza*pshcld	-89.89451301
colza*cldrad	-49.74735537
cmprad	-60.76467344
aertau*aerasy	-41.47535795
colza*cmprad	-43.14650501
cldrad*cmprad	39.24104553
clrrad*clrrad	-120.8463259
pwater*aertau	-39.48141655
catza*cmprad	39.61599595
cmprad*ozone	37.67947117
clrrad*aerssa	-36.53837093
azi*pshcld	68.6776565
pwater*pshcld	66.74464483
aerasy	-43.70927804
ozone*pshcld	63.33205619
cmprad*aertau	33.42633475
cldfrc*pshcld	-59.32248102
catza*aerssa	-31.4560949
cldfrc*pwater	27.72894644
ozone	-36.22776056
catza*cldrad	24.15171079

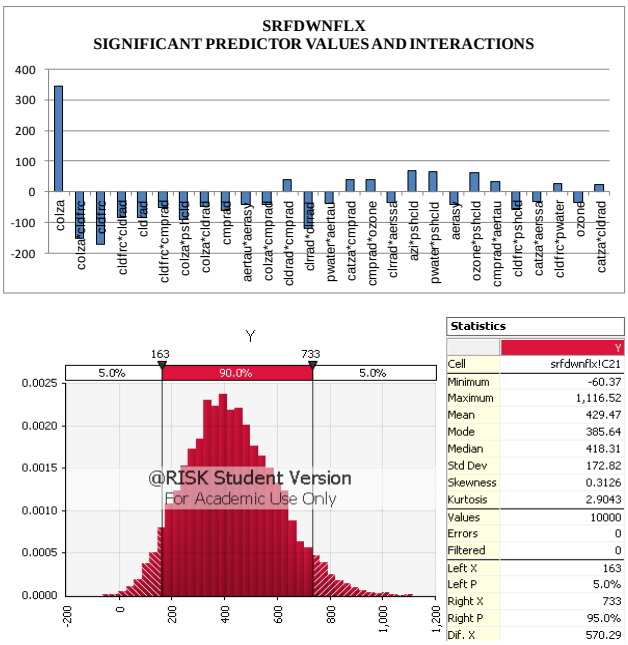

Figure 41. Mt Everest Region Uncertainty Analysis - SRFDWNFLX

Mt Everest Region Uncertainty Analysis – SRFDWNDIFF

SRFDWNDIFF	
Factor	***Coeff***
colza	48.6263565
colza*cldfrc	29.1605612
cldrad	-28.917509
cldfrc	27.2496631
cmprad*ozone	19.5594086
aertau	26.9456335
cldrad*cldrad	-65.236849
clrrad*aertau	-16.552705
cldrad*pshcld	31.565315
pwater*aertau	-17.229072
azi*ozone	16.7157453
pshcld*aertau	-31.661779
cldfrc*pshcld	-28.144761
colza*pshcld	-26.270815
cldfrc*cldrad	-13.717458
cldfrc*ozone	-13.293412
cmprad*cmprad	44.0281975
aertau*aerasy	-12.28914
azi*aerasy	12.5356271
catza*aertau	11.9471347
aerasy*aerasy	40.1197313
clrrad*ozone	10.9388214
azi*cmprad	11.4519199

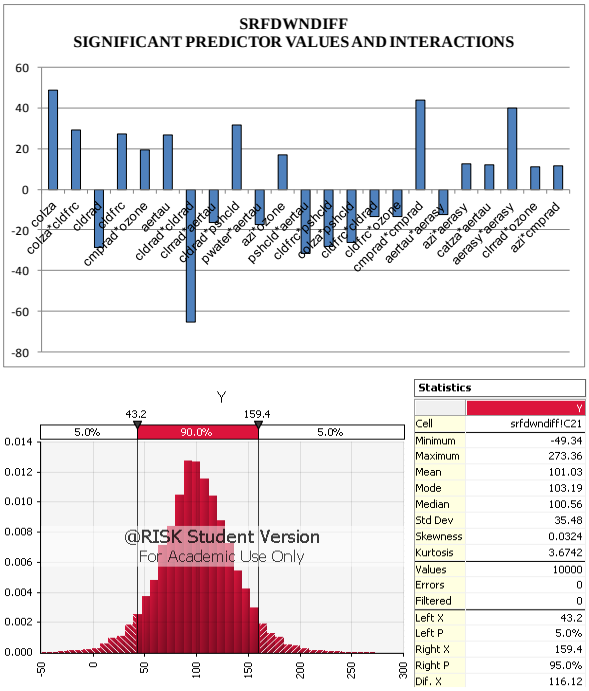

Figure 42. Mt Everest Region Uncertainty Analysis – SRFDWNDIFF

Mt Everest Uncertainty Analysis - SRFUPFLX

SRFUPFLX	
Factor	***Coeff***
cldfrc	-21.6070721
cldfrc*cmprad	-15.5029048
cmprad	17.69790063
cldfrc*cldrad	-8.46447637
azi*azi	-20.9371003
azi*cldfrc	6.019967374
colza*catza	-5.30577716
cldrad	-6.35604331
colza*pshcld	-8.8530402
colza*azi	4.604209765
colza*cldrad	4.572046291
cmprad*ozone	4.292603585
aertau*aerasy	-4.0327533
pwater*ozone	3.882777449
cldfrc*aerasy	-3.7087818
pwater	4.657257864
aertau*aerssa	3.391866386

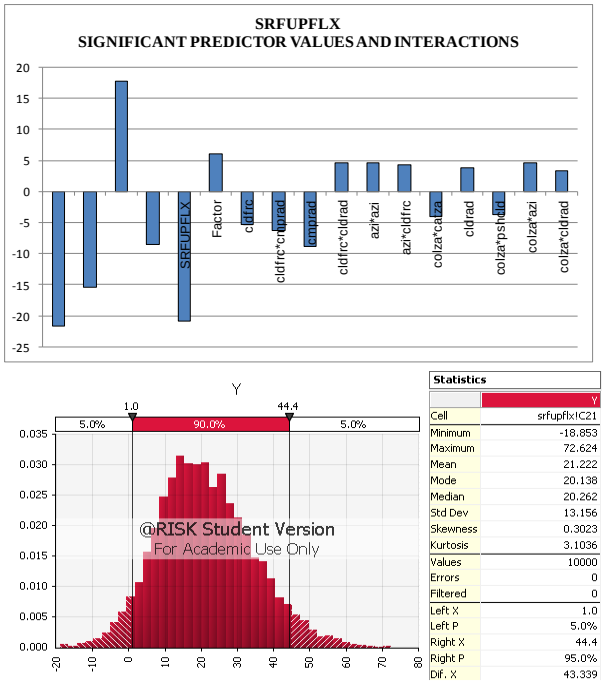

Figure 43. Mt Everest Uncertainty Analysis - SRFUPFLX

Mt Everest Uncertainty Analysis - SRFDWNDIFPAR

SRFDWNDIFPAR	
Factor	***Coeff***
colza	27.55662245
colza*cldfrc	15.21912833
cmprad*ozone	10.02241586
cldrad	-12.59457205
aertau	13.24330783
cldfrc	12.73262943
cldrad*cldrad	-33.09635656
clrrad*aertau	-8.474545476
pshcld*aertau	-16.02567791
azi*ozone	8.260736708
pwater*aertau	-8.468195067
cldfrc*pshcld	-14.6501522
colza*pshcld	-14.31561941
cldrad*pshcld	13.86675881
aertau*aerasy	-6.805166144
cmprad*cmprad	22.76637908
azi*aerasy	6.636510928
cldfrc*ozone	-6.208352845
aerasy*aerasy	20.43526445

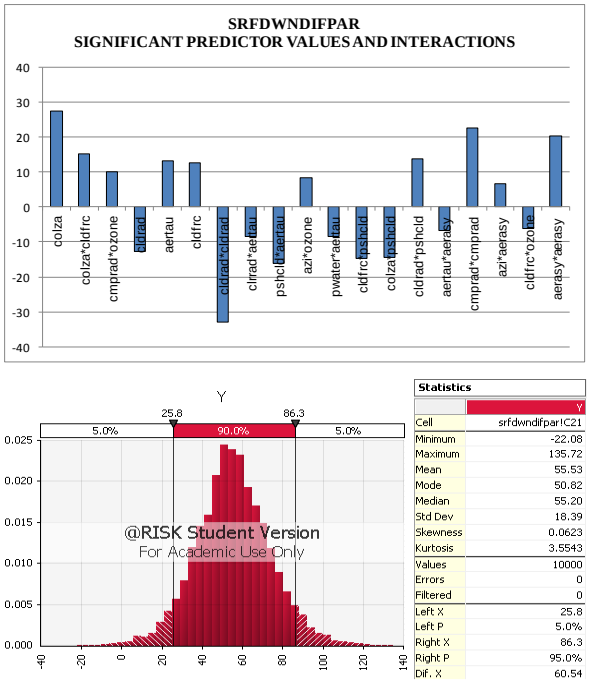

Figure 44. Mt Everest Uncertainty Analysis - SRFDWNDIFPAR

Mt Everest Uncertainty Analysis - SRFDWNPAR

SRFDWNPAR	
Factor	***Coeff***
colza	168.2567983
colza*cldfrc	-70.6303174
cldfrc	-80.28365813
cldfrc*cldrad	-38.84459673
cldrad	-40.2989868
cldfrc*cmprad	-24.46953308
colza*pshcld	-42.90398893
cmprad	-28.37812168
aertau*aerasy	-20.06630501
colza*cldrad	-21.91641512
colza*cmprad	-20.6462971
cldrad*cmprad	18.60545347
pwater*aertau	-19.36941791
catza*cmprad	19.36995387
cmprad*ozone	18.18268416
clrrad*clrrad	-56.68302705
clrrad*aerssa	-16.55920075
azi*pshcld	31.62537898
catza*aerssa	-16.15327367
ozone*pshcld	30.11253716
pwater*pshcld	29.72763399
aerasy	-19.81274577
cldfrc*pshcld	-28.69268379
cmprad*aertau	15.75480463
ozone	-17.24227806

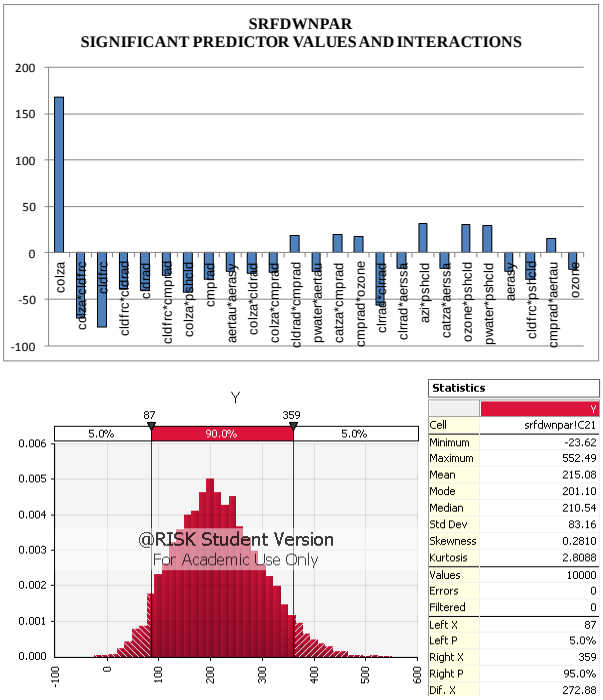

Figure 45. Mt Everest Uncertainty Analysis - SRFDWNPAR

Mt Everest Uncertainty Analysis – TOAUPCLRSKY

TOAUPCLRSKY	
Factor	***Coeff***
cmprad	28.08594375
colza*catza	-12.48455411
catza	8.542688042
azi*azi	-18.19181946
colza	-7.359728147
colza*azi	4.181818923
clrrad*cmprad	-3.579170005
azi*cldfrc	3.237370537
cldrad*aerasy	-2.991458407
colza*aertau	-2.834459597
azi	-3.717278773
cldfrc*aerasy	-2.31513047
catza*azi	2.194297311
aerasy	2.790570979
pwater*pwater	-7.23034489
cldfrc*aerssa	-1.836246912
colza*aerasy	-1.967619323
pwater*pshcld	-3.426030704
colza*colza	6.443851787
colza*clrrad	1.846923003
catza*aerssa	1.615533467
colza*ozone	1.7015175

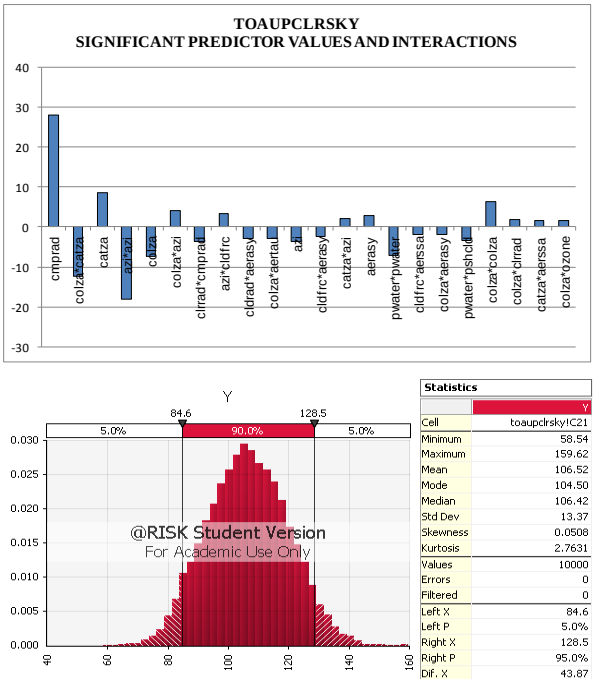

Figure 46. Mt Everest Uncertainty Analysis – TOAUPCLRSKY

Mt Everest Uncertainty Analysis – SRFDWNCLRSKY

SRFDWNCLRSKY	
Factor	***Coeff***
colza	460.366976
pwater	-23.3020002
colza*pwater	-14.9595004
colza*colza	8.62582081
colza*cmprad	2.29443524
ozone	-3.10150979
cldfrc*cldfrc	6.19800771
clrrad	-2.35605445
cldrad*aerssa	-1.60355184
azi*aertau	-1.50291742
colza*aerasy	-1.39950016
cldrad*cmprad	-1.35897829
pwater*aertau	1.33302459
catza*azi	1.17236344
colza*aertau	1.1166829
pwater*aerasy	-1.14421463
ozone*aertau	-1.11103815
cldrad*ozone	0.9820843
cmprad	1.43009056
colza*ozone	-1.11970294
azi	-1.45515446
pwater*pshcld	-1.95444577
aerasy	1.29114401

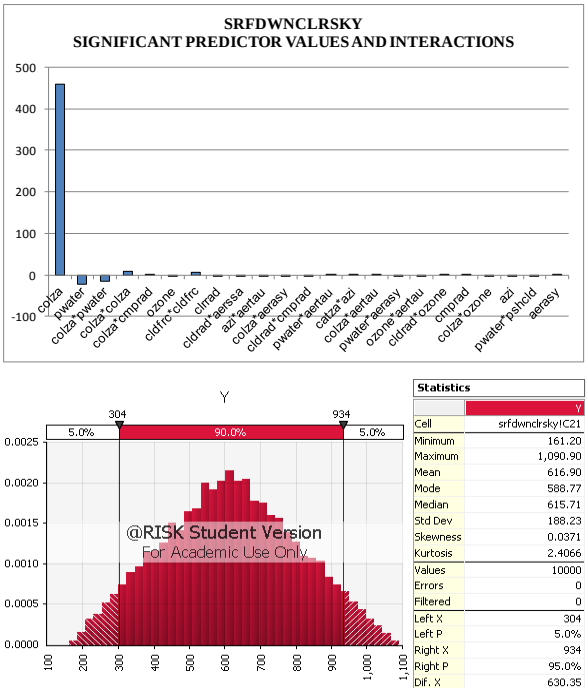

Figure 47. Mt Everest Uncertainty Analysis – SRFDWNCLRSKY

Mt Everest Uncertainty Analysis - SRFUPCLRFLX

SRFUPCLRFLX	
Factor	***Coeff***
cmprad	31.38517891
colza*catza	-13.3563205
colza	-10.98266247
catza	8.778601395
azi*azi	-19.97781363
colza*azi	4.591127184
azi*cldfrc	3.828836924
clrrad*cmprad	-3.733832879
aerasy	4.507624966

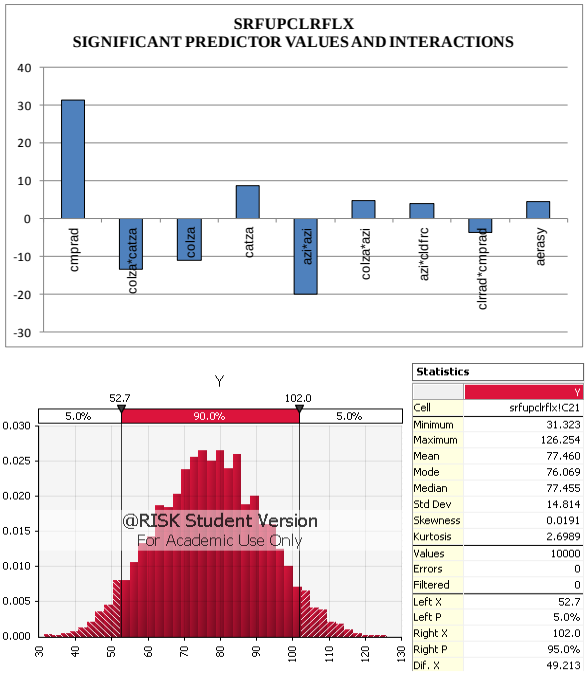

Figure 48. Mt Everest Uncertainty Analysis - SRFUPCLRFLX

Mt Everest Region Uncertainty Analysis – OAOD

OAOD	
Factor	***Coeff***
colza	-0.0223361
colza*cmprad	-0.0169499
clrrad	0.01719964
cldrad*aerssa	0.01103449
ozone*aertau	0.00951393
cldfrc*cldfrc	-0.0343328
pwater*aerasy	0.00953877
pwater*pwater	0.0308236
azi*aertau	0.00939853
colza*aerasy	0.00854435
pwater	-0.0112192
colza*aertau	-0.0080458
aerasy	-0.0105223
cldrad*cmprad	0.00810724
pwater*aertau	-0.0086045
catza*cmprad	0.00791291
pwater*pshcld	0.01395011
aerasy*aerasy	0.0231104

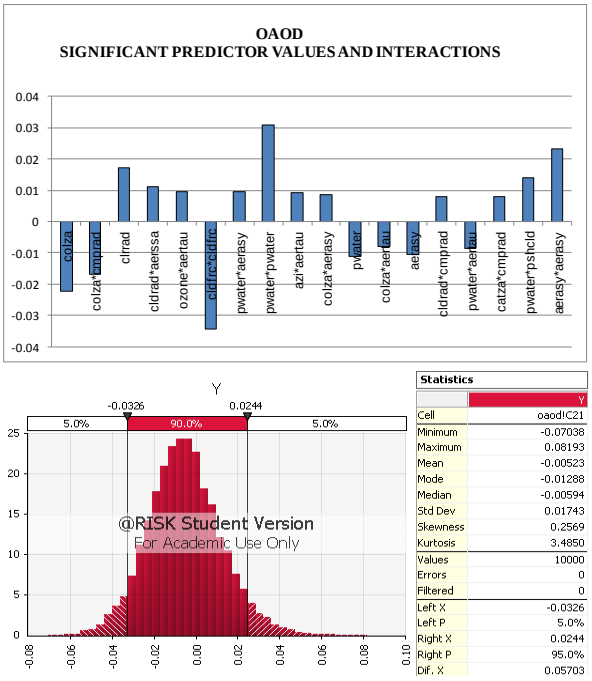

Figure 49. Mt Everest Region Uncertainty Analysis – OAOD

Mt Everest Region Uncertainty Analysis – OCOD

OCOD	
Factor	***Coeff***
catza*cldrad	40.83936264
colza	-52.3517345
colza*cmprad	40.26863886
aerasy*aerasy	-104.59517
aertau	-37.4995004
colza*catza	26.17542681
clrrad*clrrad	70.70473175
aerasy	-26.5136479

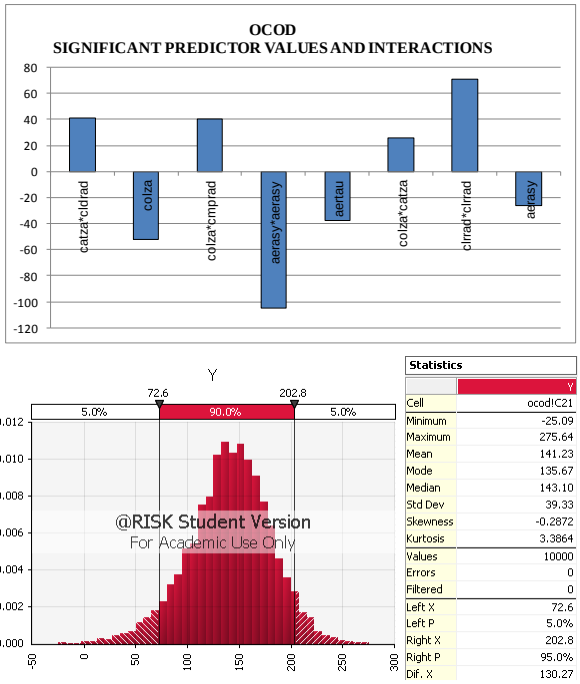

Figure 50. Mt Everest Region Uncertainty Analysis – OCOD

Mt Everest Region Uncertainty Analysis – SRFDWNPRS

SRFDWNPRS	
Factor	***Coeff***
colza	457.2931075
pwater	-25.2171887
colza*pwater	-14.7933341
colza*colza	11.36265914
pwater*pwater	7.466378164
ozone	-2.08537879
cmprad	1.182175269
colza*ozone	-0.68853019
colza*catza	-0.56383585
cmprad*aerssa	-0.39686625
pshcld*aerasy	0.744475985
cldfrc*aerssa	-0.34873931
cldfrc*ozone	-0.37666703
catza	0.461447587
cldrad	-0.44150971
ozone*aertau	0.313008611
cldfrc*cldfrc	1.128556605
aerasy	-0.38908206
cldfrc*pshcld	0.550846292
catza*azi	0.284825179
cldrad*cldrad	-1.06288006
catza*aerasy	0.272245273
aerssa*aerasy	-0.26319915
azi*aerssa	-0.27689366

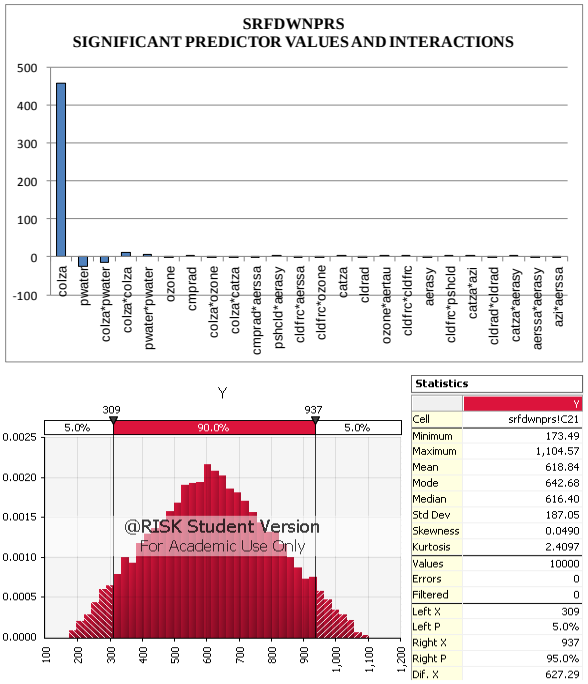

Figure 51. Mt Everest Region Uncertainty Analysis – SRFDWNPRS

Mt Everest Region Uncertainty Analysis – TOAUPPRS

TOAUPPRS	
Factor	***Coeff***
cmprad	32.97138338
colza*catza	-14.24964078
colza	-11.64593458
catza	10.96398607
azi*azi	-17.58611668
colza*azi	5.225927946
colza*cmprad	-4.063167432
catza*azi	3.660590008
cmprad*cmpra	12.20594659
azi	-4.577703504
colza*colza	11.33746548
azi*cldfrc	2.966800119
cldrad*aerasy	-2.723635533
colza*aertau	-2.715823582
cldfrc*aerssa	-2.224218589
pshcld*aertau	-4.552308406
catza*aerssa	2.214148146
colza*aerasy	-2.128742642
aerasy	2.652347719
pwater*aerssa	-2.077787043
catza*pwater	-2.129633011
cldfrc*clrrad	2.027819308
cldfrc*aerasy	-1.926544966
cldfrc*aertau	-1.921405425
clrrad*cmprad	-1.770605799

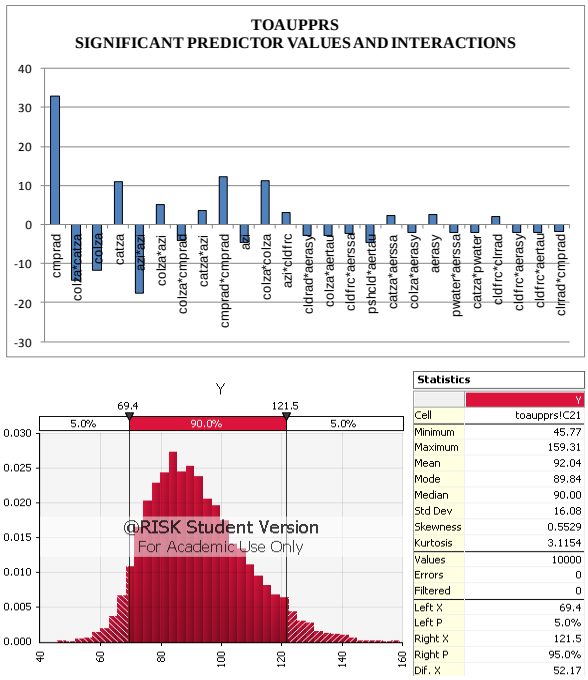

Figure 52. Mt Everest Region Uncertainty Analysis – TOAUPPRS

Sahara Region Uncertainty Analysis – TOAUP

TOAP	
Factor	***coeff***
colza*cldrad	68.39062124
cldrad	77.92255889
colza	76.23575322
cldfrc*cldrad	59.5209662
cldfrc	58.19977046
azi*azi	-81.98043011
azi*pwater	-23.79097109
clrrad	29.45267493
colza*colza	-75.21213035
cldfrc*clrrad	-19.0421274
cmprad	24.32985347
colza*ozone	17.89145481
clrrad*clrrad	53.72519768
ozone*aerssa	14.05165743
cldfrc*cmprad	-14.09628605
catza*aertau	-12.82158492
aertau*aerssa	13.23852622
catza*ozone	-12.32247855
pwater	16.95760771
aertau*aerasy	-11.87402141
cldrad*cmprad	-12.03113421
colza*cldfrc	11.65230212
pwater*pshcld	-22.05942324
azi*aerasy	11.90322809
azi*pshcld	-20.40872883
clrrad*pwater	-10.97462113
cmprad*aerasy	-9.906158987
pshcld*aerasy	-19.18440678

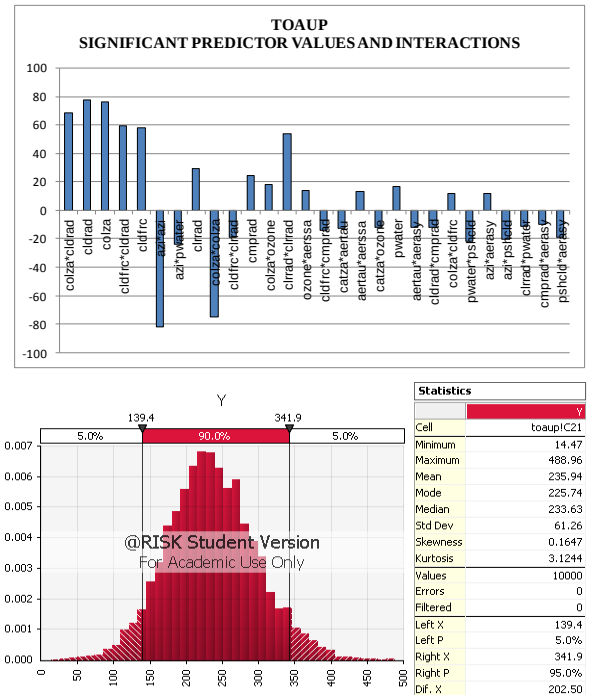

Figure 53. Sahara Region Uncertainty Analysis – TOAUP

Sahara Region Uncertainty Analysis - SRFDWNFLX

SRFDWNFLX	
Factor	***Coeff***
colza	262.934418
colza*cldfrc	-169.05225
cldfrc	-134.14734
colza*cldrad	83.2386138
clrrad	91.9743138
cldrad	70.9238804
cldfrc*cldrad	47.661131
cldfrc*aerssa	-39.725888
clrrad*cmprad	35.8124693
aerasy	43.804609
catza*cmprad	-35.680645
cldfrc*clrrad	-34.263547
azi*cldfrc	32.5972216
cldfrc*cmprad	33.2111438
cldfrc*pshcld	-59.040097
catza*pshcld	60.1106455
clrrad*pshcld	-60.256494
colza*azi	31.4107726
pshcld*aerasy	-52.594103
cldrad*ozone	25.6195362
aerssa*aerssa	87.576564

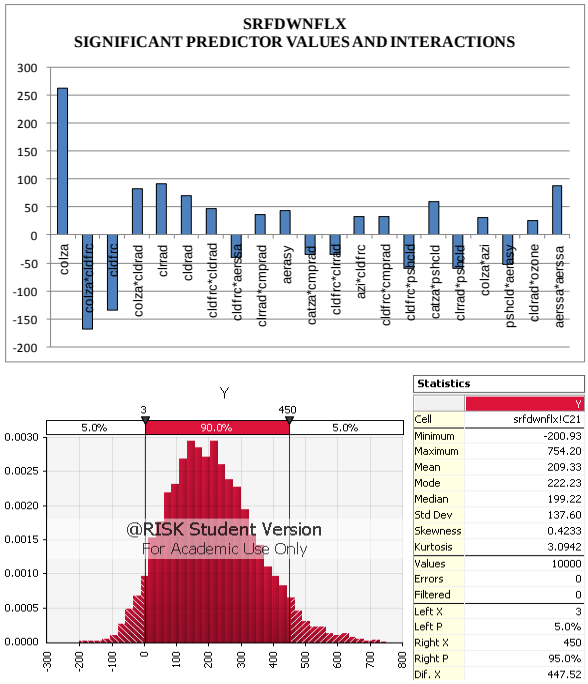

Figure 54. Sahara Region Uncertainty Analysis - SRFDWNFLX

Sahara Region Uncertainty Analysis – SRFDWNDIFF

SRFDWNDIFF	
Factor	***Coeff***
colza	158.995813
cldfrc*cldrad	73.4002988
cldrad	87.4961675
colza*cldrad	65.8438235
aerasy	57.2552866
cldfrc*clrrad	45.9843309
pwater*aerssa	41.9663957
clrrad*aerasy	-39.347206
catza*cldrad	-37.126781
pshcld*aerasy	-67.08284
cmprad	48.2678926
catza*clrrad	34.4947859
cldfrc*pshcld	-57.310566

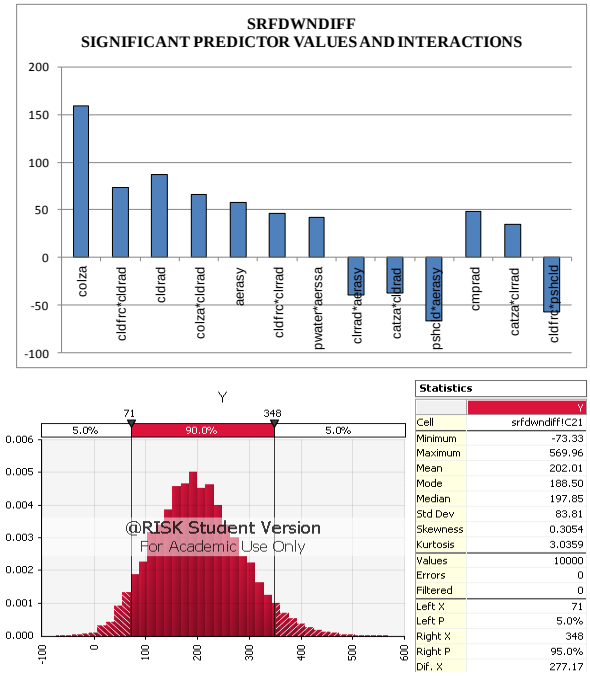

Figure 55. Sahara Region Uncertainty Analysis – SRFDWNDIFF

Sahara Region Uncertainty Analysis – SRFUPFLX

SRFUPFLX	
Factor	***Coeff***
colza*cldfrc	-39.109631
colza*cmprad	37.6194556
cmprad	42.3674919
clrrad	40.4612058
colza	36.271801
cldfrc	-38.127272
colza*cldrad	28.6975464
clrrad*cmprad	16.5567837
cmprad*ozone	17.0680577
catza*cmprad	-17.596431
azi*aerasy	16.927317
cldfrc*clrrad	-16.891187
colza*pwater	16.461125
aertau*aerasy	-15.278109
catza*azi	-15.171536
cldrad	20.09292
aerasy	18.557046
catza*pshcld	27.446019
colza*catza	-14.275139
cldrad*pwater	-13.650386
cldfrc*pshcld	-22.869758
cldrad*cldrad	45.8384275
cldfrc*aerssa	-10.926154
ozone*aertau	-11.339642
pshcld*aerasy	-21.541378

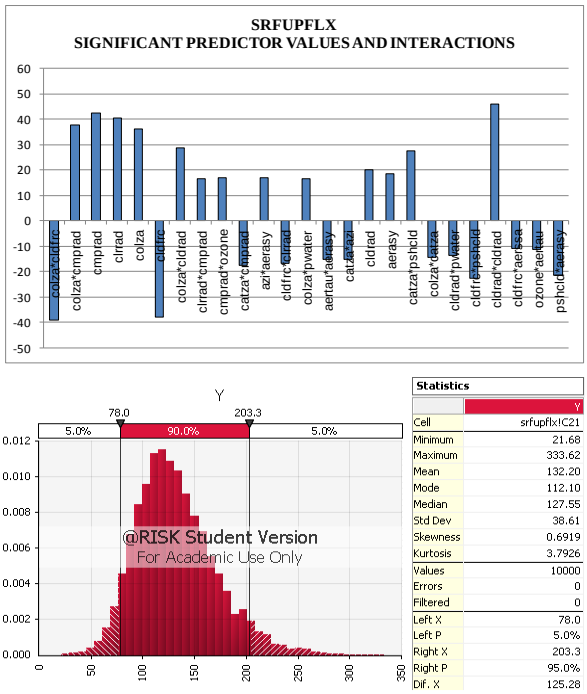

Figure 56. Sahara Region Uncertainty Analysis – SRFUPFLX

Sahara Region Uncertainty Analysis – SRFDWNDIFPAR

SRFDWNDIFPAR	
Factor	***Coeff***
colza	76.17138808
cldfrc*cldrad	35.41014362
cldrad	42.82782516
colza*cldrad	33.69493885
aerasy	28.0135521
cldfrc*clrrad	20.12885292
pwater*aerssa	18.28620359
pshcld*aerasy	-33.1264021
clrrad*aerasy	-17.7726819
catza*cldrad	-16.8915069
cmprad	22.10866832
cldfrc*pshcld	-28.1324244

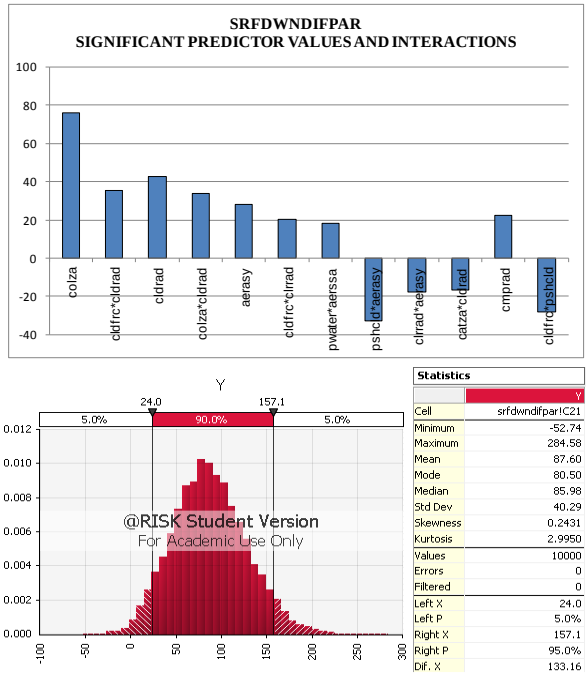

Figure 57. Sahara Region Uncertainty Analysis – SRFDWNDIFPAR

Sahara Region Uncertainty Analysis – SRFDWNPAR

SRFDWNPAR	
Factor	***Coeff***
colza	123.94878
colza*cldfrc	-74.61908
cldfrc	-58.44368
colza*cldrad	41.532625
clrrad	42.926397
cldrad	34.58565
cldfrc*cldrad	23.568943
cldfrc*aerssa	-18.22793
aerasy	22.790737
clrrad*cmprad	17.326195
catza*cmprad	-17.09944
catza*pshcld	29.671894
cldfrc*pshcld	-28.43139
azi*cldfrc	15.225023
cldfrc*cmprad	15.060658
pshcld*aerasy	-27.02957
cldfrc*clrrad	-15.13978
clrrad*pshcld	-27.75018
colza*pwater	14.138402
colza*azi	13.703002

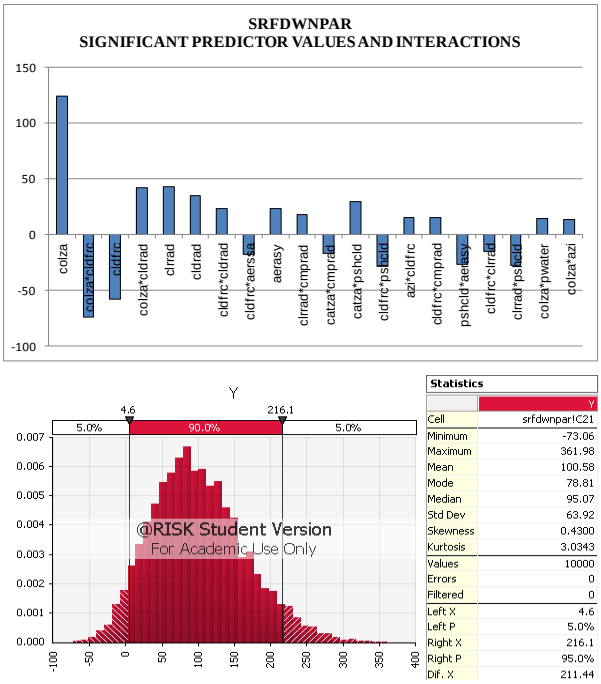

Figure 58. Sahara Region Uncertainty Analysis – SRFDWNPAR

Sahara Region Uncertainty Analysis – TOAUPCLRSKY

TOAUPCLRSKY	
Factor	***Coeff***
colza	52.0662509
colza*cmprad	31.6031883
cmprad	41.82472616
clrrad	37.87289069
clrrad*cmprad	17.02927593
colza*colza	-54.0331051
colza*catza	-12.8580388
catza*azi	-7.15745649
pwater*pshcld	-12.2930922
catza*cmprad	-6.52282036
colza*pwater	6.222012799
cldrad*ozone	5.542442481
cldfrc*aertau	-6.08537905
ozone*ozone	-18.9576108

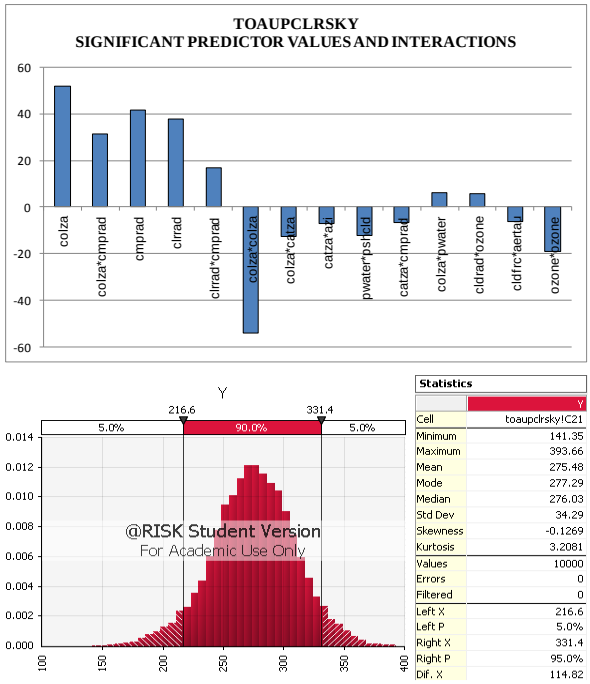

Figure 59. Sahara Region Uncertainty Analysis – TOAUPCLRSKY

Sahara Region Uncertainty Analysis – SRFDWNCLRSKY

SRFDWNCLRSKY	
Factor	***Coeff***
colza	411.541155
clrrad	106.3595251
catza*clrrad	-36.30101584
clrrad*cmprad	23.91685801
clrrad*aerasy	23.79899311
pwater*aerssa	-23.06573262
pwater	-28.76275957
cldfrc*aerssa	-18.73160873
catza*ozone	-17.93359175
colza*clrrad	19.05508947
catza*cldrad	17.34402443
aerssa*aerssa	59.98843646
pshcld*aertau	34.45971052
pwater*pwater	55.14423974

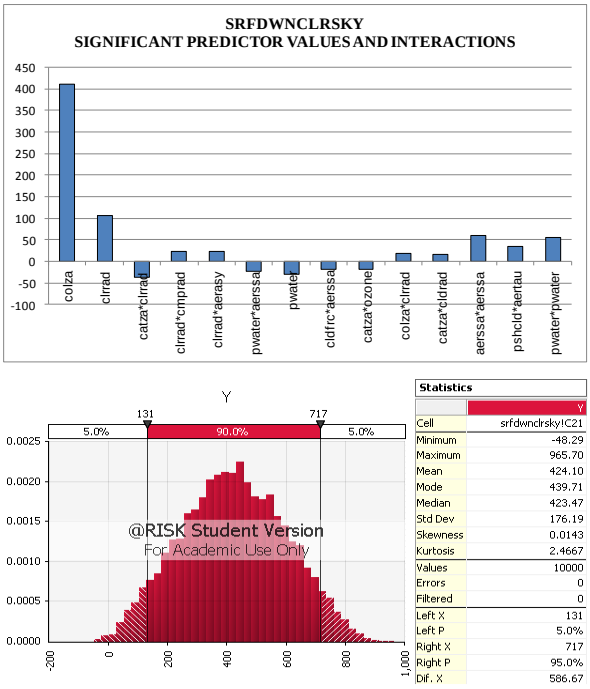

Figure 60. Sahara Region Uncertainty Analysis – SRFDWNCLRSKY

Sahara Region Uncertainty Analysis – SRFUPCLRFLX

SRFUPCLRFLX	
Factor	***Coeff***
colza	62.1431711
colza*cmprad	46.8815612
cmprad	60.0330833
clrrad	48.8075758
colza*colza	-58.927408
colza*catza	-16.253341
clrrad*cmpra	13.819982
colza*pwater	11.0304883
colza*clrrad	-11.179131
catza*azi	-9.3333395
cldrad*ozone	7.04082853
cldfrc*aertau	-7.6872693

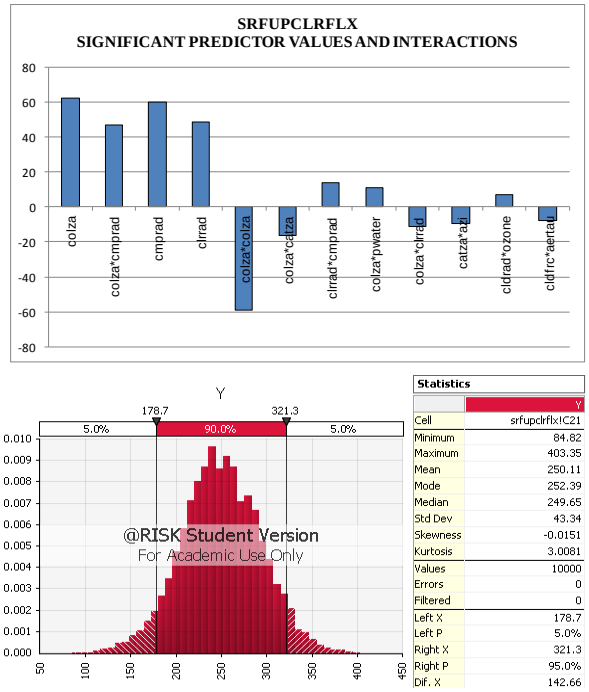

Figure 61. Sahara Region Uncertainty Analysis – SRFUPCLRFLX

Sahara Region Uncertainty Analysis – OAOD

OAOD	
Factor	***Coeff***
clrrad	-0.698158
catza*clrrad	0.15598779
colza*clrrad	0.13353706
clrrad*aerasy	-0.1230666
clrrad*cmprad	-0.1048407
pwater*aerssa	0.10221233
catza*ozone	0.08961933
cldfrc*aerssa	0.08102086
catza*cldrad	-0.0772305
aerssa*aerssa	-0.2499258
cldfrc*aertau	0.07363462

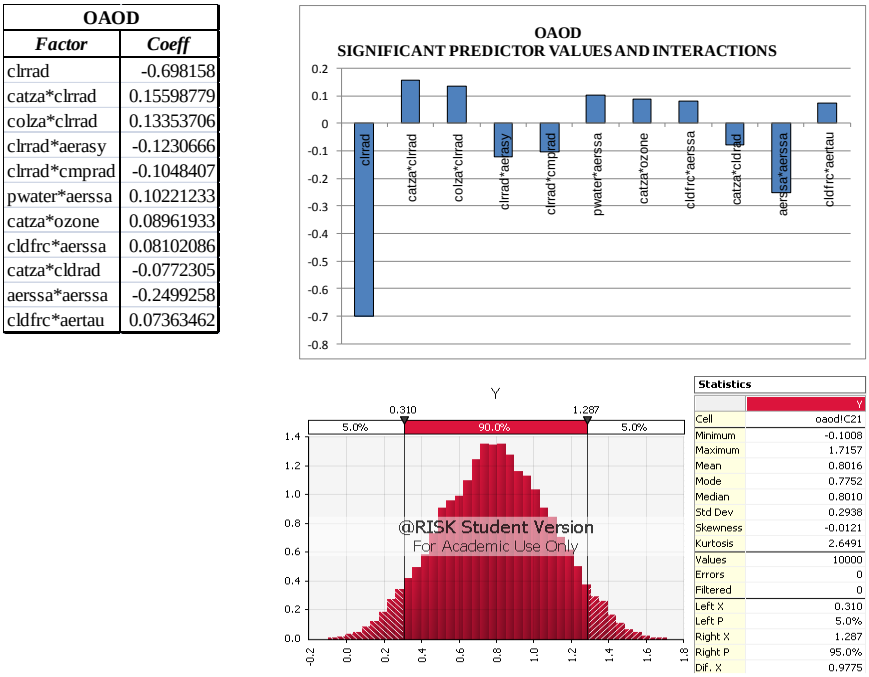

Figure 62. Sahara Region Uncertainty Analysis – OAOD

Sahara Region Uncertainty Analysis – OCOD

OCOD	
Factor	***Coeff***
colza*cldrad	-78.75440927
colza*pwater	45.06836112
catza*cldrad	33.2074559
azi*cldfrc	31.81527529
colza	-41.8621949
colza*colza	102.3657803
cldrad*cmprad	26.7863888
colza*clrrad	-27.03889742
aerssa	-39.66527272
aerasy	-31.43605328
cmprad*aerssa	23.66797602
pwater	-29.58478322
cldfrc*ozone	20.98220286
aerssa*aerssa	-68.43263971
cldfrc*cmprad	20.17258347
pwater*aertau	-20.74541053
colza*catza	19.41752766
pwater*pshcld	-35.61526734
cldrad*ozone	16.22640896
azi*clrrad	-18.05678151
colza*pshcld	-31.08132355

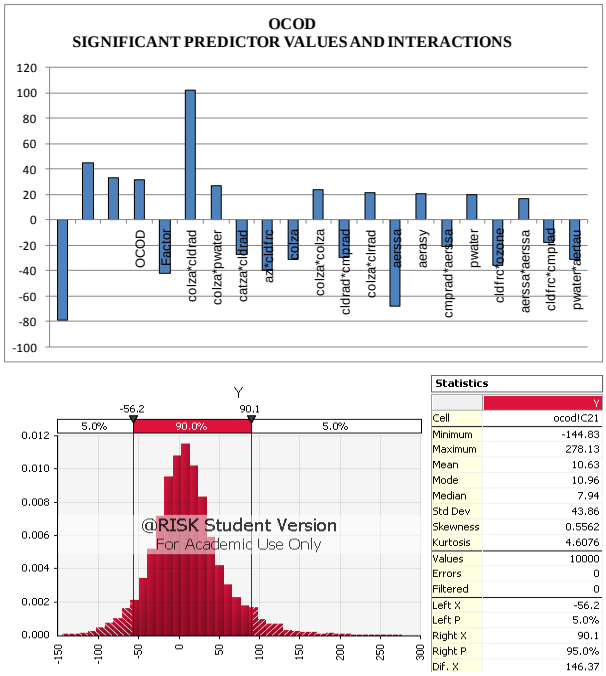

Figure 63. Sahara Region Uncertainty Analysis – OCOD

Sahara Region Uncertainty Analysis – SRFDWNPRS

SRFDWNPRS	
Factor	***Coeff***
colza	476.4209807
pwater	-40.28675512
colza*pwater	-22.98679254
pwater*pwater	17.52213564
colza*colza	7.636701048
cmprad	1.980448098
ozone	-1.751331696
pshcld*aerasy	1.82644355
aerasy	-1.150494451
cmprad*aerssa	-0.859999452
colza*cmprad	0.910177921
colza*catza	-0.888353295
cldfrc*ozone	-0.896823924
aertau	1.152680343
cldfrc*cldfrc	2.500101323
colza*ozone	-0.751566679
aerssa*aerasy	-0.661628654
cldfrc*aerssa	-0.612597382
cldfrc*pshcld	1.219399108
cldfrc*clrrad	-0.663068517
ozone*aertau	0.607323397
cldrad	-0.803732392
clrrad*aerssa	-0.58682963
pwater*aerssa	0.581852338
cldrad*cldrad	-2.184902192
cldfrc*aertau	-0.601238959
catza	0.76435898
catza*cldrad	-0.547098387

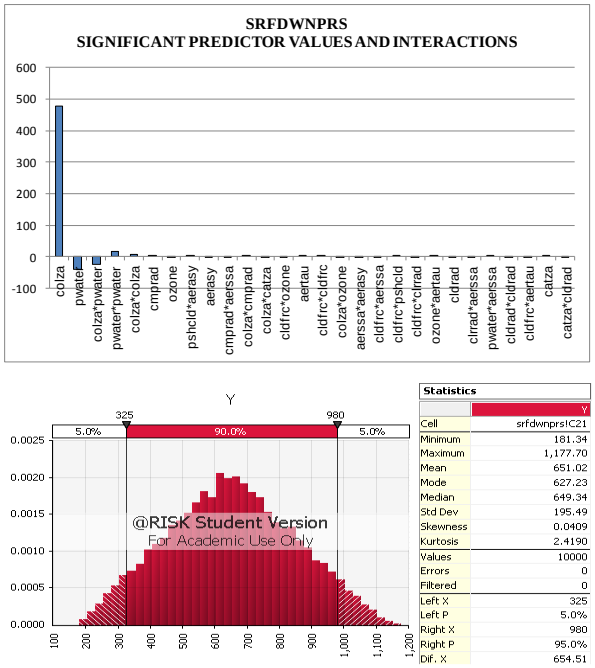

Figure 64. Sahara Region Uncertainty Analysis – SRFDWNPRS

Sahara Region Uncertainty Analysis – TOAUPPRS

TOAUPPRS	
Factor	***Coeff***
cmprad	69.83403216
colza*cmprad	52.07710442
colza	58.43191222
colza*colza	-80.773844
colza*catza	-20.213591
pwater*aerssa	10.78433038
colza*pwater	9.366714724
catza*azi	-8.90294332
cldrad*ozone	8.119839882
colza*aertau	8.066928245
aertau	10.40494033
catza*pwater	-7.48995828
azi*azi	-22.5316049
cmprad*aertau	7.336534485
catza*aertau	-7.1247751

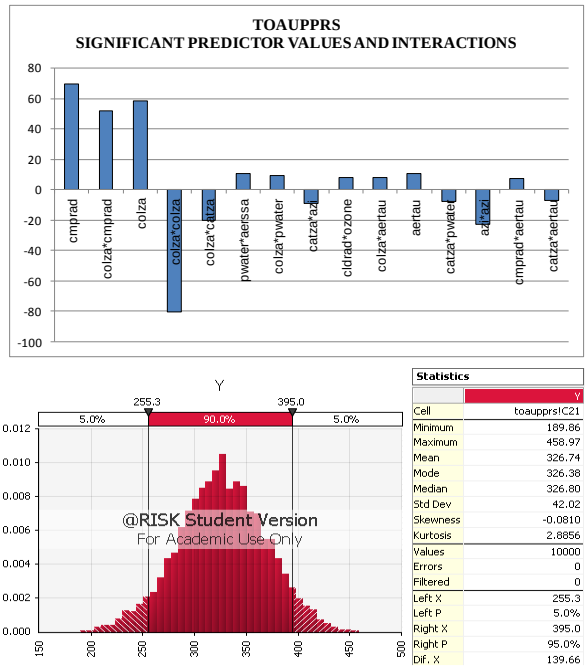

Figure 65. Sahara Region Uncertainty Analysis - TOAUPPRS

VITA

PATRICIA A. QUIGLEY
613 Carlton Drive
Hampton, VA 23666
(757) 864-7418

EDUCATION:

Old Dominion University – Department of Engineering Management, 5115 Hampton Boulevard, Norfolk, VA 23529

Old Dominion University – M.S Engineering Management (12/12)

Strayer University – B.S. Computer Information Systems (3/07)

Community College Air Force - A.A.S. Aerospace Control & Warning Systems (5/85)

Thomas Nelson Community College - A.A.S. Mechanical Engineering (5/92)

Community College of the Air Force - A.A.S. Avionics Systems (7/11)

EMPLOYMENT HISTORY:

Company: NASA/CSC/SAIC/SSAI - FEB 1998 to present
Position: Functional Test Engineer/Senior Software Engineer/Analyst/System Administrator

Company: NASA/Analytical Services and Materials - SEP 1995 to FEB 1998
Position: Assistant Research Scientist

Company: Lockheed Engineering and Science Corporation - OCT 1992 to SEP 1995
Position: Engineer Aide

MILITARY EXPERIENCE:

Active duty Air Force – 1979 – 1987 – Aerospace Control and Warning Systems
Army National Guard – JAN 87 – JAN 90 – Artillery Unit
Air National Guard – 19 FEB 08 – PRESENT (F22 Avionics)